NASA TECHNICAL NOTE

NASA TN D-3177

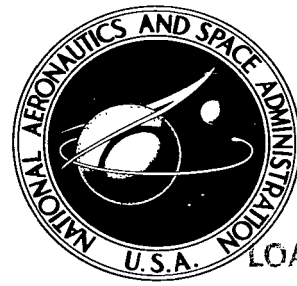

EXPERIMENTAL AND ANALYTICAL STUDIES OF CRYOGENIC PROPELLANT TANK PRESSURANT REQUIREMENTS

by M. E. Nein and J. F. Thompson

George C. Marshall Space Flight Center
Huntsville, Ala.

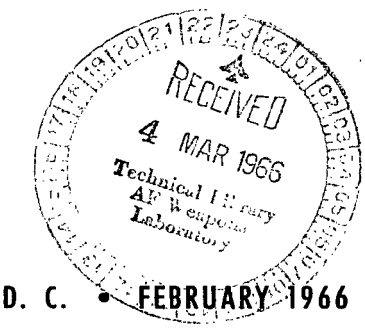

NATIONAL AERONAUTICS AND SPACE ADMINISTRATION • WASHINGTON, D. C. • FEBRUARY 1966

NASA TN D-3177

EXPERIMENTAL AND ANALYTICAL STUDIES OF CRYOGENIC PROPELLANT TANK PRESSURANT REQUIREMENTS

By M. E. Nein and J. F. Thompson

George C. Marshall Space Flight Center
Huntsville, Ala.

NATIONAL AERONAUTICS AND SPACE ADMINISTRATION

For sale by the Clearinghouse for Federal Scientific and Technical Information
Springfield, Virginia 22151 – Price $4.00

TABLE OF CONTENTS

LIST OF ILLUSTRATIONS

LIST OF ILLUSTRATIONS (Cont'd)

LIST OF ILLUSTRATIONS (Cont'd)

LIST OF ILLUSTRATIONS (Cont'd)

LIST OF ILLUSTRATIONS (Cont'd)

LIST OF ILLUSTRATIONS (Concluded)

LIST OF TABLES

DEFINITION OF SYMBOLS

Symbol	Definition	
A	Tank total surface area	(ft^2)
A_D	Pressurant distributor area	(ft^2)
b_1, b_2, b_3	Constants used in calculation of gas to wall forced coefficients (Table III)	(-)
c_1, c_4, c_6, c_8	Constants used in calculation of free convection heat and mass transfer Coefficients (Table III & Computer Program)	(-)
c_7	$g/_{gc}$	(-)
δ	Tank wall thickness	(ft)
d_1, d_2, d_3	Constants used in calculations of gas to liquid forced convection heat and mass transfer coefficients	(-)
D	Tank diameter	(ft)
$\overline{D}$	Diffusion coefficient	(ft^2/hr)
EK	Modification factor for thermal conductivity caused by mixing of fluid	(Btu/hr ft °R)
ED	Modification of diffusion coefficient caused by mixing of gas	(ft^2/hr)
g_c	Constant = 32.17	(lb_m ft/lb_f sec^2)

DEFINITION OF SYMBOLS (Cont'd)

Symbol	Definition	
h_{gw}	Ullage gas-to-wall heat transfer coefficient	(Btu/hr ft^2 °R)
h_c	Ullage gas-to-wall free convection heat transfer coefficient	(Btu/hr ft^2 °R)
h_o	Ullage gas-to-wall forced convection heat transfer coefficient at tank top	(Btu/hr ft^2 °R)
h_s	Gas-to-liquid heat transfer coefficient	(Btu/hr ft^2 °R)
h_{sc}	Gas-to-liquid free convection heat transfer coefficient	(Btu/hr ft^2 °R)
h_L	Liquid-to-wall heat transfer coefficient	(Btu/hr ft^2 °R)
K	Gas thermal conductivity	(Btu/hr ft °R)
L/D	Tank length to diameter ratio	(-)
$\dot{M}$	Pressurant flowrate	(lb_m/sec)
M_t	Mass transfer	(lb_m)
Δm	Pressurant mass accumulated	(lb_m)
P	Ullage pressure	(psia)
r	Tank radius	(ft)
t	Time	(sec)
T	Temperature	(°R)
Th	Vehicle thrust	(lb_f)
v	Gas velocity	(ft/sec)
V	Tank volume	(ft^3)

DEFINITION OF SYMBOLS (Cont'd)

Symbol	Definition	
V_d	Volumetric pressurant flowrate at distributor	(ft^3/sec)
V_{o_d}	Reference volumetric pressurant flowrate	(ft^3/sec)
X	Radial distance from tank wall	(ft)
Y_s	Gas-to-liquid mass transfer coefficient	(ft/hr)
Y_{sc}	Gas-to-liquid free convection mass transfer	(ft/hr)
Y_{so}	Gas-to-liquid forced correction mass transfer coefficient at tank top	(ft/hr)
Z	Axial distance from tank top	(ft)
Z_i	Axial distance of gas-liquid interface from tank top	(ft)
β_w, β_s, β_L	Dimensional decay coefficient of ullage forced heat transfer coefficients (Table III)	(ft^{-1})
β_{LP}	Thermal expansion coefficient of liquid	(R^{-1})
θ_T	Total time of pressurization	(sec)
μ	Gas viscosity	(lb_m/ft hr)
ρ	Gas density	(lb_m/ft^3)
ϕ	Molefraction	(-)

DEFINITION OF SYMBOLS (Concluded)

Symbol	Definition
Subscripts	
a	Ambient
c	Calorimeter
f	Free convection
g	Ullage gas
i	Interface
L	Liquid
m	Mean
o	Reference, pressurant inlet
u	Ullage
w	Wall

ACKNOWLEDGEMENT

The contribution of the MSFC Test Laboratory in providing the test facilities and complex instrumentation and obtaining the experimental data is gratefully acknowledged. Invaluable contributions in program definition and analysis of experimental results were made by J. Moses, T. Stokes, L. Worlund, and G. Platt of the Fluid Mechanics and Thermodynamics Branch.

NOTE:

Mr. J. F. Thompson is currently Assistant Professor, Mississippi State University, Aeronautical Engineering Department. He was formerly associated with Propulsion Division, MSFC.

EXPERIMENTAL AND ANALYTICAL STUDIES OF CRYOGENIC PROPELLANT TANK PRESSURANT REQUIREMENTS

SUMMARY

The extensive requirement for pressurization of cryogenic propellant tanks of launch and space vehicles has directed attention to the need for accurate methods of analysis of propellant tank thermodynamics. This paper presents the results of experimental and analytical studies of pressurization gas requirements for cryogenic liquids. Experimental results are analyzed for cylindrical and spheroidal tanks ranging in size over four orders of magnitude. A parameter study of the controllable variables of a pressurization system design illustrates their effect on ullage gas temperature.

Pressurization data are provided for use in the development or checkout of analytical pressurization models and for design of pressurization systems for future launch and space vehicles. A tank pressurization computer program, using recommended coefficients, can be used to predict total and transient pressurant requirements and ullage temperature gradients within 10 percent accuracy.

INTRODUCTION

Determination of the pressurant gas weight for cryogenic propellant tanks is complex and defies exact analytical treatment because of the interdependent transient phenomena of heat and mass transfer that occur simultaneously in a propellant tank. Mathematical models describing the internal thermodynamics of tank pressurization have been developed by various investigators.

The analysis by Clark [1] represents an analytical solution of the governing equations that predict the transient temperature, the response of the pressurant gas, and container wall. However, the solution requires assumptions, such as constant tank pressure and zero initial ullage, that are not always met with real systems. The studies by Coxe and Tatum [2] are based on analysis of a system in which the ullage is thermally mixed and heat transfer between the gas and the wall is independent of time and space. Gluck and Kline [3] used dimensional analysis to express gas requirements as a function of known system parameters; they determined, experimentally, quantities of interfacial mass transfer and gas phase heat transfer.

Epstein [4] presented a numerical method for calculation of pressurant gas requirements that contains a number of phenomena absent from previous analytical methods. However, empirical data are required to evaluate many constants and physical parameters.

To provide a reliable method for determination of pressurant gas requirements, the experimental data on pressurization obtained by the Marshall Space Flight Center during the Saturn launch vehicle development were applied to the method of Epstein. The physical parameters and the previously indeterminate constants were developed. After modification, this numerical method is capable of accurate prediction of pressurization gas requirements for cryogenic propellant tanks.

PRESSURIZATION REQUIREMENTS AND LAUNCH VEHICLE DESIGN

The increasing size and complexity of space launch vehicles necessitates optimization studies of the many subsystems involved in launch vehicle design. The propellant tank pressurization system is of particular importance because its weight is large in comparison to the weight of other subsystems. Weight optimization studies of propellant tank pressurization systems for the Saturn V, S-IC stage, were used to establish the location of the oxidizer and fuel tanks within the over-all vehicle configuration (Fig. 1 and Ref. 5). Even the pressurization system components such as heat exchangers, pressurant lines, and controls, weigh considerably less than the pressurizing gas.

A further indication of the need for optimization of pressurant requirements is illustrated in Figure 2. The pressurant-mass/tank-pressure ratios of typical launch vehicles is given as a function of vehicle thrust, thrust being representative of vehicle size. Although there is a great deal of difference between the propellant tank configurations of tactical missiles and space launch vehicles, a near linear increase occurs in pressurant-mass/tank-pressure as vehicle size increases. Considering only pressurant gas weight, it appears advantageous to use helium as a pressurant. If, however, the weight of the pressurant storage containers is included in the weight of the pressurization system, the use of helium as a pressurant in most instances results in a weight penalty.

For vehicles with high acceleration and low turbo-pump NPSH requirements, it is possible to eliminate the pressurization system, relying only on the self pressurization of the saturated propellant (flash boiling). Flash boiling pressurization, however, results in high pressurant weight and can only be justified if it significantly simplifies vehicle design. Because of the infant knowledge of cryogenic tank pressurization at the initiation of the Saturn launch vehicle development program, a long series of pressurization experiments was conducted at MSFC to obtain system design information and scaling laws for the large propellant tanks of the Saturn I vehicle. Results of this experimental program and correlations with analytical studies are presented in the following sections of this report.

EXPERIMENTAL PROGRAM

Test Facilities

The experimental work was conducted on five tank configurations at the Marshall Space Flight Center:

A. Saturn I, S-I Stage, Multiple Interconnected LOX Tanks (Fig. 3a)

B. Saturn I, S-IV Stage (Fig. 3b) LOX and LH_2 Tanks

C. A 6.5 by 39-ft (DxL) cylindrical LOX tank (Fig. 4)

D. A 13 by 26-ft (DxL) cylindrical LOX tank (Fig. 5a, Fig. 5b)

E. A 1 by 3-ft (DxL) cylindrical LOX tank.

The test parameters for these tank configurations are compared in Table I. Configurations A and B were flight vehicles and thus contained the standard test instrumentation of the Saturn propellant feed system, including continuous liquid level sensors, tank pressure, pressurant flowrates, and supply temperature measurements. Configurations C, D, and E were equipped with many thermocouples along the tank axis. Thermocouples, mounted at several radii at three elevations in these tanks, allowed measurement of radial temperature gradients. Wall temperatures were measured in Configurations C and D by thermocouples on the inside and outside surfaces of the tank at several locations. The locations of the temperature sensors in these tanks are shown in Figures 6a and 6b. Special calorimeter plates were mounted in both tanks for determination of gas-to-wall heat transfer coefficients. Finally, gas sampling devices were placed at several locations to measure ullage gas concentration gradients.

Configurations C, D, and E were equipped with heat exchangers that provide a variable pressurant inlet temperature up to 1000 °R. The pressurant gas was introduced at the top of the container through a distributor (either a deflector plate-Configuration C and E, or a screen arrangement-Configuration D) to minimize inlet velocities and disturbances of the liquid surface by impinging gas jets. Figure 7 shows a typical distributor configuration. Pressurant velocities at the distributor periphery are given in Table I for the five test configurations.

The tank Configurations C, D, and E could be sloshed at rotational or translatory oscillation in excess of the first critical frequency of the tank. Configurations A, C, and D were equipped with cameras so that the conditions inside the tank could be observed. The results of tests conducted with the five tank configurations are presented in Figures 13 through 38. The conditions of these tests are summarized in Table II.

Instrumentation

Analysis of ullage gas temperature history required a temperature probe with fast response characteristics and good accuracy. A fast response temperature probe (Fig. 8a) consisting of a fork-like support with a 30 gage CuCo welded thermojunction was designed at MSFC. The length-to-diameter ratio of the thermocouple wire and its distance from the fork base were determined using an analog computer representation of the heat transfer conditions around the probe assembly. Figure 9a shows the response time; 63.2 percent of the total temperature change was attained in eight seconds when the probe was extracted from liquid oxygen into a gas circulating at a velocity of about three feet per second [6]. The response of the probes during a pressurization test was also determined (Fig. 9b); the fork-type thermocouple has a good response characteristic.

A thermocouple mounted on a long, rod-like support (Fig. 8b), which was designed for liquid measurement in the high vibration environment of static and flight testing, exhibited an extremely poor response in the gas phase as indicated in Figure 9a. Response time to 63.2 percent of total temperature change was in excess of 10 minutes. Commercial temperature probes of the resistance thermometer type (Fig. 8c) were also investigated under these conditions. Although their response was considerably better than the flight type thermocouple (63.2 percent temperature change in approximately 50 seconds), it was too slow for the pressurization studies.

Pressure measurements in the ullage space, pressurant supply lines, and liquid discharge lines were made with close-coupled pressure transducers to assure good response characteristics. The pressurant flowrate and liquid discharge flowrate measurements were obtained with turbine type flowmeters. Liquid level before and during the tests was measured by capacitance discrete level probes and continuous delta P measurement of the liquid column.

Test Results

Heat Transfer Coefficients. Heat transfer between pressurant and tank side walls was measured during pressurization tests in Configuration C by two plate calorimeters. Each calorimeter was a 12 by 12-inch, 30-gage copper plate mounted from teflon spacers parallel to and at a distance of four inches from the tank wall (Fig. 10). Three thermocouples, spaced to represent equal calorimeter areas and connected as a thermo-pile, provided a temperature/time history of the copper plate before and during the tests. The local ullage gas temperature was measured in the vicinity of the calorimeter (Fig. 11). The calorimeters were located 11 and 30 feet from the top of the test tank.

For determination of heat transfer coefficients, it was assumed that heat transfer to the back side of the plate (toward tank wall) was by free convection because of the shielding effect of the plate-to-wall arrangement. The free convection coefficients for a one component gas were evaluated by the equation of Jackson and Eckert [7]; the results are plotted in Figure 12. The free convection heat transfer coefficient was also

calculated for two component mixtures based on the time and space dependent helium-oxygen concentration in the tank. The total heat transfer to the calorimeters was then corrected using the calculated free convection effect on the back side. The heat transfer coefficients to the front of the calorimeter plates measured in Tests 130-9, -10, -15 are presented in Figures 13 and 14 using gaseous oxygen and helium as pressurants. Ullage gas-to-wall heat transfer was also evaluated from wall temperature measurements at a location 3.5 feet from the top to the tank. Wall measurements at locations initially below the liquid surface produced erroneous readings and were discarded. These coefficients were corrected by subtracting the effect of external heat flux from the measured wall temperature rise. During a flash-boiling test, which did not require pressurant flow, the wall temperature rise indicated an external heat flux of 13 Btu/min ft^2; this compares very favorably with a calculated flux of 15 Btu/min ft^2 [8] and confirms the method used for correcting wall measurements.

Inspection of Figures 13 and 14 shows very good agreement between measured and calculated heat transfer coefficients. It is noted that the gas-to-wall heat transfer coefficient is definitely within the forced convection regime for the oxygen tests, but in the free convection regime for the helium test. Although the heat transfer coefficient by forced convection diminishes with increasing distance from the pressurant distributor, the free convection contribution (Eq. 1) compensates for this decay to such a degree that a nearly constant heat transfer coefficient is obtained along the tank bulkhead and side wall.

Sloshing Effects. Pressurization studies conducted at MSFC have shown that there is little benefit derived from the use of helium as a main pressurant for cryogenic propellants. However, it was determined experimentally that prepressurization with helium reduces pressure decay during liquid sloshing near the critical frequency. It is assumed that the helium acts as a buffer zone between the splashing cryogenic liquid and the condensable pressurant, suppressing excessive mass transfer.

Figure 15 shows a typical tank pressure history for a stationary liquid oxygen test tank as compared to a pressure history in which the liquid sloshes near the first critical mode of oscillation [9]. The tank was prepressurized, with either helium or nitrogen, followed by main pressurization during liquid expulsion with super-heated oxygen. The tank pressure history during the slosh test (using helium as a prepressurant) is nearly identical to the pressure history of the nonsloshing expulsion test. In contrast, prepressurization with gaseous nitrogen resulted in a marked pressure decay during the sloshing of the liquid, which was not evident during a nonsloshing expulsion test with gaseous nitrogen prepressurization.

Ullage Gas Concentration Gradients. Gas flow conditions and the concentration of helium gas in a cryogenic propellant tank during pressurization discharge were studied in test Configurations C and D. Spectrographic analyses were made of gas samples taken at various positions in the tanks. Samples taken at various elevations in tank Configuration C just before the end of the tests yielded the results shown in Figure 16. In the test

in which helium was used for prepressurization and oxygen as the main pressurant, the helium concentration is maximum at 12 feet above the liquid, and gradually decreases in both directions.

The concentration of oxygen near the liquid surface is probably caused by accumulation of the gaseous oxygen that is initially in the ullage before prepressurization. For comparison, Figure 16 also shows the concentration of helium above the liquid oxygen for the case in which helium prepressurization is followed by pressurization with helium during liquid expulsion. The oxygen concentration at 10 feet above the liquid interface was only six percent by volume. The total amount of gaseous oxygen in the ullage was only slightly larger than the amount of oxygen in the ullage before prepressurization (0.77 moles versus 0.73 moles). This indicates that interfacial mass transfer, although small under these conditions, was in the form of evaporation.

Mass Transfer. A comparison of mass transfer results obtained in Configuration C with results obtained by Clark [1] is shown in Figure 17. Condensation in excess of 30 percent of the pressurant flow was found by Clark during liquid nitrogen expulsion tests with a 1 by 3-foot cylindrical tank. Similar results were obtained with the MSFC test Configuration E, also shown in Figure 17. The mass transfer measured in test Configuration C indicates that condensation was 5 to 10 percent. Condensation in the larger facility is less because of the smaller wall-area/volume ratio of a larger tank.

Comparing the condensation in the small tank with that in the large tank on the basis of wall-area/volume ratio, the values are approximately equal. During tests at high pressurant inlet temperature, initial evaporation noted in Configuration C diminished as the test proceeded. However, Clark had found increased condensation at higher pressurant inlet temperatures in small tanks. These conflicting results point out the incomplete knowledge of mass transfer.

Condition of Liquid Interface. The condition of the liquid interface in Configuration C and during the launch and flight of SA-5, are shown in several frames from a movie taken inside these tanks (Figs. 18 and 19). Violent boiling occurred during venting of the tank before prepressurization. As the vents were closed and prepressurization proceeded, the liquid surface became nearly quiescent before discharge. After discharge began, disturbance of the liquid surface caused by pressurant flow and acceleration of the liquid surface were observed; the disturbance diminished as time and distance between the surface and the pressurant inlet increased.

Radial Ullage Temperature Gradients. Radial temperature gradients obtained with Configurations C and D are shown in Figure 20. In both cases the radial gradients were small, and there apparently exists little difference between the gas flow conditions in the two tanks, even though the gas distributors, baffling, and tank diameters are not comparable.

The temperature probes at X/D - 0.025 in Configuration D, which are located between the antislosh baffles (Fig. 5a), recorded virtually the same temperature as probes at smaller radii. It was concluded that the gas circulation in the tank is not appreciably affected by the antislosh baffles, and subdivision of the tank into volume elements perpendicular to the tank axis is permissable for the pressurization analysis.

Axial Ullage Temperature Gradients. The axial ullage temperature gradients obtained in tests 130-6 and 130-7 with Configuration C (Fig. 21a, 21b, 22a, and 22b) became approximately linear as the test proceeded. These two tests were conducted with oxygen as pressurant at about 550°R. There was a rapid increase in temperature of about 30°R immediately above the liquid interface in these tests, indicating that mass transfer was small. In tests 130-9 and 130-10 (Figs. 23a, 23b, 24a, and 24b) with the same Configuration with oxygen pressurant at a lower temperature, the ullage temperature gradients are much flatter; the rapid increase in temperature immediately above the liquid interface is still in evidence. The ullage temperature gradients in this same configuration with helium as pressurant (Test 130-15; Fig. 25a, and 25b) are concave, rather than linear as in the tests with oxygen as pressurant, and the increase in temperature just above the liquid interface is very gradual. The concave shape is to be expected in this case because the mass transfer is in the form of evaporation with an ullage that is predominately helium. The linear ullage temperature gradients in tests with oxygen as pressurant indicate that the mass transfer is very small with an ullage that is predominantly oxygen.

Other Test Results. Tests are being performed with Configuration D, but so far only three tests have been completed. The pressurant distributor in this configuration was designed to minimize the gas circulation in the tank, reducing forced convection heat transfer. While this is the desired condition for optimum pressurization system operation, it is detrimental to the response time of the temperature probes as the liquid interface passes. Precise ullage temperature gradients will not be available until this instrumentation is improved. However, preliminary data, with very hot GOX used as pressurant, indicate that the temperature gradients are concave rather than linear as was the case in the tests with Configuration C using colder GOX as pressurant. The concave temperature gradients found in the helium pressurant tests with Configuration C were also in evidence with Configuration D. Pressurant flowrates and wall temperature gradients from these tests are presented in Figures 26a, 26b, 26c, 27a, 27b, 27c, 28a, 28b and 28c.

Pressurant flowrates in the LOX tanks of the Saturn I, S-I stage, during static test and flight are presented in Figures 29a and 30. Figures 31a and 32a show pressurant flowrates in the LOX and LH_2 tanks of the Saturn I, S-IV stage, during static test. Finally, ullage temperature histories obtained in a very small tank, Configuration E, containing LN_2 pressurized with nitrogen are given in Figure 33.

PRESSURIZATION ANALYSES

Previous Work

Pressurized discharge from cryogenic liquid containers was studied analytically and experimentally by Clark [1] under sponsorship of the Army Ballistic Missile Agency and later MSFC. The analytical solutions obtained by Clark were applied to test data obtained for Configuration C. In Figure 34 the axial temperature gradient through the ullage gas is shown as a function of distance from the tank top or gas distributor. Excellent agreement with test results was obtained for an assumed gas-to-wall forced convection heat transfer coefficient of 10 Btu/hr $ft^{2o}R$. Agreement for a coefficient of 2 Btu/hr $ft^{2o}R$, approximately in the range of free convection, was poor. This illustrates one limitation of analytical solutions in which the gas-to-wall heat transfer coefficient enters as an independent variable.

In spite of this restriction and the assumption of initial zero ullage volume, the method by Clark was successfully applied in design analyses of the Saturn I pressurization system. While Clark's analysis assumed stratification of the ullage gas and constant heat transfer coefficient, the analysis by Coxe and Tatum [2] was based on the assumption of a complete thermally mixed ullage gas and constant heat transfer coefficient. Figures 35 and 36 compare test results obtained with MSFC Configuration C with the analytical predictions by the method of Coxe and Tatum. Toward the end of the test, agreement is good possibly because the conditions of constant heat transfer coefficients are approached in the large ullage near the end of the run.

A comparison of the pressurant flow requirements with predictions by an analog computer simulation developed by MSFC, is shown in Figure 37. Representation of the pressurization thermodynamics by analog method was difficult because of scaling problems and the extreme sensitivity of the equations to tank pressure fluctuation. In Figure 35, 36, and 37 pressurant flow requirements are also compared with a digital computer program developed by Rocketdyne [4] and modified by MSFC [10]. This program closely matches test data. However, the program insufficiently describes mass transfer and is sensitive to fluctuations of ullage pressure. These fluctuations do not appear in the measured flowrates because they are apparently counteracted by the effects of evaporation and condensation [11].

Summary of Analytical Program

Since the Rocketdyne program makes maximum use of the techniques of digital computer calculations and is not subject to the restrictive assumptions that are made in other programs, this method was chosen by MSFC for pressurization system analyses. However, extensive comparisons of the program with test data were required to evaluate the physical parameters and constants initially contained in the program as indeterminate identities. The equations were modified when necessary.

This program includes in its calculations a pressurant gas storage tank, heat exchanger, and flow control valve. It considers a propellant tank with or without outside insulation and pressurized with either evaporated propellant or with a gas stored under pressure in a storage tank in which the gas expands nonadiabatically. The ullage pressure is controlled by a pressurant flow control valve that has finite maximum and minimum areas and may be either the on-off or the continuously regulating type. In the propellant tank the ullage gas may be a two component mixture of evaporated propellant and another gas. The ullage gas temperature, composition, and properties are considered functions of time and of axial, but not radial or circumferential, distance. Liquid and wall temperature and properties are treated in the same manner. The heat transfer modes considered are shown in Figure 38. Mass transfer within the ullage and at the gas-liquid interface is considered. The effects on heat and mass transfer caused by gas circulation, as influenced by pressurant gas inlet velocity, is also taken into account.

Modifications in the Program

In the course of the comparisons with test data, it was necessary to make several modifications in the program to obtain good data correlations. These modifications are discussed in reference 10. The ullage gas-to-wall heat transfer coefficient, which decreases exponentially from the tank top, is written as the sum of a free convection coefficient and a forced convection coefficient.*

$$h_{gw} = h_c + h_o \left(\frac{\dot{V}_d}{\dot{V}_{od}} \right) e^{-\beta_w Z} \tag{1}$$

where h_o is an input constant.

Thus the forced convection coefficient at the tank top is a linear function of the pressurant volumetric flowrate ($\dot{V}_d$) from the distributor. The free convection coefficient (h_c) is calculated by the free convection equation,

$$h_c = c_1 k \left[\frac{g_c c_7 c_p \rho^2 \left(|T_g - T_w| \right)}{T_g \mu k} \right]^{c_4} . \tag{2}$$

In the same manner the gas-to-liquid heat transfer coefficient at the gas-liquid interface is written

* Schmidt [12] also writes the total heat transfer coefficient as the sum of the free and forced convection coefficients.

$$h_s = h_{sc} + h_{so} \left(\frac{\dot{V}_d}{\dot{V}_{o_d}} \right) e^{-\beta_s Z_i} \tag{3}$$

where h_{so} is an input constant.

The free convection coefficient h_{sc} is calculated by the equation

$$h_{sc} = c_1 k \left[\frac{g_c c_7 c_p \rho^2 \left(|T_g - T_L| \right)}{T_g \mu k} \right]^{c_4} \qquad T_g \tag{4}$$

It was found that both forced convection coefficients at the tank top could be calculated more accurately by a forced convection equation of the standard form expressing the Nusselt number as a function of the Reynolds and Prandtl numbers:

$$\frac{h_o r}{k} = b_1 \left(\frac{r\dot{M}}{A_D \mu} \right)^{b_2} \left(\frac{\mu c_p}{k} \right)^{b_3} \tag{5}$$

$$\frac{h_{so} r}{k} = d_1 \left(\frac{r\dot{M}}{A_D \mu} \right)^{d_2} \left(\frac{\mu c_p}{k} \right)^{d_3} \tag{6}$$

Thus, the ullage gas-to-wall heat transfer coefficient and the gas-to-liquid heat transfer coefficient at the gas-liquid interface are better calculated to equations (7) and (8).

$$h_{gw} = h_c + h_o e^{-\beta_w Z} \tag{7}$$

$$h_s = h_{sc} + h_{so} e^{-\beta_s Z_i}, \tag{8}$$

where h_o and h_{so} are calculated by equations (5) and (6), rather than being input as constants, and h_c and h_{sc} are calculated by equations (2) and (4).

It was also found that the liquid-to-wall heat transfer coefficients could be better calculated according to a free convection equation rather than being taken as constant:

$$h_L = c_1 k \left[\frac{g_c c_7 \beta_{LP} c_p \rho^2 (T_L - T_w)}{\mu k} \right]^{c_4} . \tag{9}$$

As in the case of gas-to-liquid heat transfer coefficient at the gas-liquid interface, the mass transfer coefficient at the interface was written

$$Y_s = Y_{sc} + Y_{so} \left(\frac{\dot{V}_d}{\dot{V}_{od}} \right) e^{-\beta_s Z_i} , \tag{10}$$

where Y_{so} is an input constant.

The free convection coefficient (Y_{sc}) is calculated by the equation

$$Y_{sc} = c_1 \overline{D} \left[\frac{g_c \, c_7 \, \rho \, (|\phi_g - \phi_i|)}{\mu \, \overline{D}} \right]^{c_4} . \tag{11}$$

The forced convection mass transfer coefficient at the tank top can be better calculated by a forced convection equation expressing the Sherwood number as a function of the Reynolds and Schmidt numbers:

$$\frac{Y_{so} r}{\overline{D}} = d_1 \left(\frac{r\dot{M}}{A_D \mu} \right)^{d_2} \left(\frac{\mu}{\rho \overline{D}} \right)^{d_3} . \tag{12}$$

Thus, the mass transfer coefficient at the gas-liquid interface is calculated by

$$Y_s = Y_{sc} + Y_{so} \, e^{-\beta_s Z_i} , \tag{13}$$

where Y_{so} is calculated according to equation (12), rather than being input as a constant, and Y_{sc} is calculated by equation (11).

Evaluation of Program Parameters

All pressurization analyses contain numerous parameters that must be known before pressurization requirements can be predicted. These parameters determine the heat and mass transfer coefficients and the distribution of these coefficients over the tank. Therefore, studies were conducted to determine the relative importance of each of the parameters involved in the program, and extensive comparisons with the results of the tests were made to obtain numerical values for these parameters.

A summary of the test conditions is given in Table II, and the values of the important parameters are given in Table III. The exponential decay coefficients β_w and β_s in equations (7), (8), and (13) are scaled by the equation:

$$\beta = 0.00117\ r^2 . \qquad (14)$$

The parameters not listed in this table are of small importance and may be taken as zero.

Comparison with Test Data

The pressurant flowrate and ullage and wall temperature gradients predicted by the computer program using the calculated constants from Table III are compared with test data [13, 14, 15, 16, and 17] in Figures 21 through 30. In all comparisons the ullage pressure, liquid drain rate, ambient heat transfer coefficients, and ambient temperature were input to the computer as functions of time. Either the pressurant inlet temperature or the heat exchanger performance curve was also input.

Figures 21 through 25 show comparisons with test data obtained with Configuration C described in Table I and shown in Figure 4. As can be seen from these figures, the agreement between the computer predictions and the test data is generally good. The irregularities in the computed pressurant flowrate, particularly marked in Tests 130-6 and 130-7 (Fig. 21 and 22), are caused by the over-sensitivity of the program to changes in the slope of the ullage pressure curve. Both ullage pressure curves of Test 130-6 and 130-7 have depressions in the latter half of the runs, while the slopes of the ullage pressure curves of the other tests were nearly constant. The agreement between the computed and measured ullage temperature gradients was good throughout the run for all the tests using oxygen as pressurant. In the test with helium as pressurant (130-15, Fig. 25) the pressurant flowmeter failed. Storage bottle pressure and temperature history were used for calculation of an average flowrate. Therefore, it was not unexpected that the computed flowrate was somewhat below this value. However, the agreement between computed and measured ullage temperature gradients was not as good in this test as in the test with oxygen as pressurant. This was probably caused by deficiencies in the program's mass transfer calculations from the assumption that all heat transfer from the ambient to the propellant is converted to sensible heat rather than latent heat. In Tests 130-9 and 130-10 the ullage heat transfer coefficients were calculated from calorimeter measurements and were compared with those calculated by the computer. Although the assumption of exponential decay of the ullage heat transfer coefficient with distance from the tank top (Eq. 7) seems arbitrary, the results were in excellent agreement with the measured heat transfer coefficients (Figs. 13 and 14).

In comparing the velocity decay of a free jet (Fig. 39, discussed in Ref. 18) it was found that the exponential decay of the forced convection heat transfer coefficient expressed as a velocity decay $(v_Z/v_o)^{0.8}$ is bracketed by the velocity decay of a free jet discharging from a circular opening and that of a free jet discharging from an infinite slit. This is analogous to the pressurant entering the tank through the gas distributor.

Comparisons with data from the LOX tanks of the Saturn I, S-I stage during static test and flight are presented in Figures 29 and 30. The agreement between computed and

measured pressurant flowrate and pressurant inlet temperature is excellent. Ullage temperature measurements were not available in these tests because instrumentation on flight vehicles is limited. Figure 29 shows a comparison of the computed and measured flowrate from the flight of SA-5. The agreement was generally good, though not as good as in the static test of SA-6. Evaluation of SA-5 pressurant requirements was complicated by the complex air flow pattern around and between the propellant tanks of the Saturn I, S-I stage during flight. The aerodynamic heating was difficult to evaluate; the only possible approach was to use average values for all propellant tanks. Figures 31 and 32 show comparisons with data from the LOX and LH_2 tanks of the Saturn I, S-IV stage during static test. These tanks are not of ordinary cylindrical shape, as can be seen in Table I; the LOX tank is an oblate spheroid and the LH_2 tank contains a convex inward lower bulkhead. By computer variation of the characteristic tank radius used in equations (5), (6), and (12), it was determined that the proper characteristic value should be about two-thirds of the maximum radius for the LOX tank. This assumption is theoretically justified because a cylinder having the same volume and surface area as an oblate spheroid has a radius equal to 0.63 times the maximum radius of the oblate spheroid. The agreement between computed and measured pressurant flowrate in the LOX tank is excellent, as shown in Figure 31. Because the pressurant flowrate in the LH_2 tank was a step function, it could not be matched at all times. However, the general range of flowrate, as computed and measured, is the same, and there is excellent agreement between the computed and measured total pressurant weight.

Test results with Configuration D are shown in Figures 26 through 28. This tank is an approximate one-third scale model of the Saturn V, S-IC stage, LOX tank. It is the largest single cylindrical LOX tank from which test data is currently available. Comparisons of the computer predictions with data obtained from three tests with this configuration is good for pressurant flowrates and tank wall temperatures.

The final comparison presented is with data from a very small cylindrical tank (one foot in diameter and three feet long) with flat bulkheads (Configuration E). Although pressurant flowrate measurements were not available in this test, the computed and measured ullage temperature histories are compared in Figure 33. The agreement is not as good as obtained in Configuration C, probably because equation (14) for the scaling of the exponential decay coefficients was developed for tanks with rounded rather than flat bulkheads.

Conclusions from Comparisons with Test Data

These comparisons with test data cover a range of conditions, using oxygen, helium, and nitrogen as pressurants and liquid oxygen, liquid hydrogen, and liquid nitrogen as propellants in tanks ranging in size over four orders of magnitude. The tank shapes were representative of those commonly used in space vehicles, namely cylinders with various bulkhead shapes and oblate spheroids. As a result of the evaluation of the many physical parameters and constants involved in the equations, this program can be used to predict total and transient pressurant flow requirements, ullage and wall

temperature gradients, and gas-to-wall heat transfer coefficients with an accuracy of ±5 percent. The numerical values of parameters recommended by MSFC for use in the program are given in Table III. There are presently no other values available in the literature. The characteristic dimension used in the calculation of the exponential decay coefficients was taken as the radius of the cylindrical section for cylindrical tanks. For tanks of other shapes, some comparison with test data was necessary to determine the proper choice for the characteristic radius. A value of two-thirds of the maximum radius appears acceptable for oblate spheroids.

The comparison with test data indicates a sensitivity of the program to sudden changes in ullage pressure. However, in most cases vehicle design pressures are either constant or vary in a monotonic manner. It was further found that considerable experimental experience with pressurization systems is required before this method of analysis can be applied reliably to evaluate a new system.

THE EFFECTS OF SYSTEM PARAMETERS ON PRESSURANT REQUIREMENT

Weight optimization of propellant tank pressurization systems demands that a low pressurant density be maintained in the ullage space; this is analogous to using a gas of low molecular weight and maintaining a high ullage mean temperature. Therefore, 30 pressurization tests and 120 computer predictions were used to separate the relative significance of various controllable parameters of pressurization systems and to determine their influence on mean ullage temperature. Figure 40 presents a graphical illustration of the relative influence of these parameters.

From a central origin, representing a reference condition (Saturn V, S-IC Stage) for all parameters, the increase (+Y) and decrease (-Y), of the ullage mean temperature at cutoff is shown as a function of variation of the parameters on the abscissa. The parameters were varied over a range expected for vehicle design. Thus, pressurant inlet temperature can increase or decrease by a factor of two from the reference condition, pressure by a factor of three, tank radius by a factor of two, expulsion time by a factor of three, etc. It was indicated that the pressurant inlet temperature exerts the greatest influence on the ullage mean temperature. Diminishing return of this effect did not exist within the range of investigation (530°R to 1200°R). The mean temperature increased as the ullage pressure was increased and also as the tank radius was increased. Increasing the tank wall thickness, heat capacity, or density caused a decrease in the mean temperature. The pressurant distributor flow area (A_D) that controls the gas-to-wall forced convection heat transfer coefficient had a significant effect on the mean temperature when the area was reduced, but no effect at all when flow area was increased. This indicates that the pressurant inlet velocity for the reference systems was chosen at an optimum point. Figure 40 also indicates that helium pressurant must be introduced into a tank at a temperature 1.1 times higher than oxygen pressurant to obtain the same

ullage mean temperature. This confirms the results of other studies (Fig. 2) indicating that the benefits derived from a helium pressurization system are not based on weight optimization.

CONCLUSIONS AND RECOMMENDATIONS

a. Pressurization data from cylindrical and spheroidal tanks ranging in size over four orders of magnitude are available for development or checkout of analytical pressurization models and for design of pressurization systems for future launch and space vehicles.

b. The Rocketdyne tank pressurization program, modified as described herein and utilizing recommended coefficients, can be used to predict total and transient pressurant requirements and ullage temperature gradients with an accuracy of ±5 percent.

c. No significant radial ullage temperature gradient occurs, even in tanks with anti-slosh baffles. This permits the assumption of one-dimensional stratification of the ullage gas for analytical representation of pressurant requirements.

d. Heat transfer between pressurant and tank walls can differ significantly from free convection, depending on tank geometry and distributor design.

e. The strongest influence on pressurant weight is exerted by pressurant inlet temperature, for which no diminishing return occurs within a temperature range compatible with tank materials. Other important influencing factors are tank radius, distributor flow area, expulsion time and aerodynamic heating. The effect of wall heat capacity is not as significant as might be expected.

f. Mass transfer for large tanks is less than previously reported.

g. Additional work is necessary to develop better techniques for measuring gas concentration gradients and mass transfer.

George C. Marshall Space Flight Center,
National Aeronautics and Space Administration,
Huntsville, Alabama, July 12, 1965.

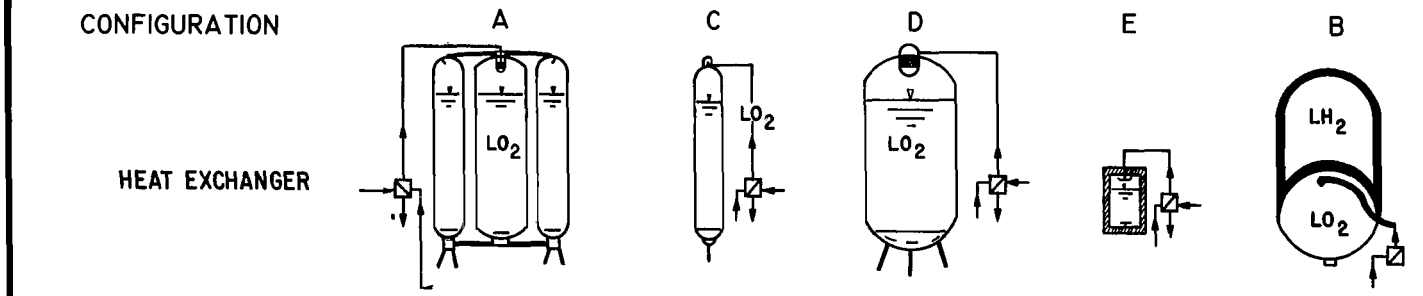

PARAMETER	SATURN I	CTL 114	SIC 1/3	1x3 MODEL	SIV (LOX)
TEST					
INITIAL ULLAGE VOLUME %	2 - 30	5 - 30	3 - 7	5	4.5
PREPRESSURANT	He	O_2, He	He	GN_2, He	He
PRESSURANT	O_2	O_2, He	O_2, He	GN_2	He
TANK PRESSURE (psia)	60	14.7 - 60	20 - 40	14.7 - 60	46
TIME OF DISCHARGE (sec.)	150	150	150 - 300	150 - 400	478
PRESSURANT TEMP (°R)	800	370 - 800	460 - 960	510	400 - 265
PRESS. INLET VELOCITY (FT/sec)	40 radial	35 down	13 radial	1 radial	50 up radial down
TANK					
TOTAL VOLUME FT^3	8980	1396	3058	2.36	1511
DIAMETER (in.)	1 @ 105 4 @ 70	78	156	12	260
L/D (APPROX.)	7	6	2	3	0.45
TANK MATERIAL	ALUM.	SS	SS	SS	ALUM.
INSULATION	NONE	NONE	NONE	ALL	COMMON BLKH.
DISTRIBUTOR FLOW AREA (FT^2)	2.92	2.1	2.5	0.0436	0.05

TABLE I. TANK CONFIGURATIONS AND TEST PARAMETERS

TABLE II. SUMMARY OF TEST CONDITIONS

TEST	FACILITY	ULLAGE PRESSURE (psia)	INLET TEMPERATURE (°R)	PRESSURANT	PRE-PRESSURANT	PROPELLANT
SA-15 [1]	A	60	800	GOX	He	
130-6 [1]	C	47	540	GOX	He	
130-7 [1]	C	30	560	GOX	He	
130-9 [1]	C	62	370	GOX	He	LO_2
130-10 [1]	C	65	450	GOX	He	
130-15 [1]	C	30	560	He	He	
SA-5 [2]	A	60	800	GOX	He	
S IV [1]	B	46.5	300	He	He	
187260 [1]	E	40	500	GN_2	Nz	LN_2
C-003 -7A [1]	D	20	750	GOX	He	LO_2
C-003 -12 [1]	D	20	900	GOX	He	LO_2
C-003 -10 [1]	D	40	530	He	He	LO_2

1) Tanks not sloshed
2) Sloshing during SA-5 flight unknown

PARAMETER	VALUE
b_1	0.06
b_2	0.8
b_3	0.333
d_1	0.06
d_2	0.8
d_3	0.333
C_1	0.13
C_4	0.333
C_6	0.13
C_8	0.333
EK_o	0
ED_o	0
$\beta_W = 0.00117\, r^2$ r IN FEET	
β_S , β_G , β_i	β_W
β_L	0

TABLE III. PARAMETERS FOR HEAT AND MASS TRANSFER CALCULATIONS

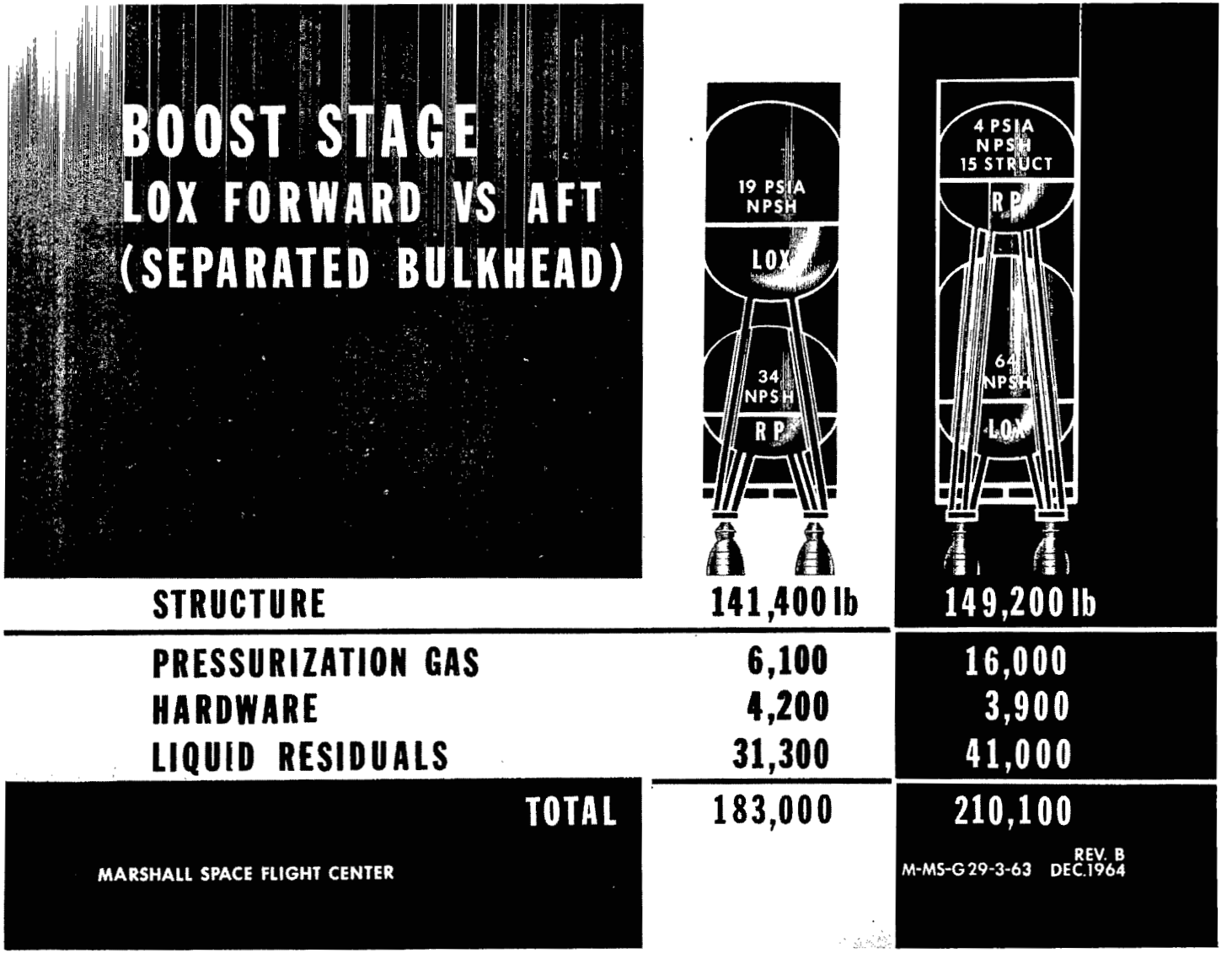

FIGURE 1. COMPARISON OF THE WEIGHTS OF THE PROPELLANT FEED SYSTEMS OF TWO FLIGHT VEHICLES

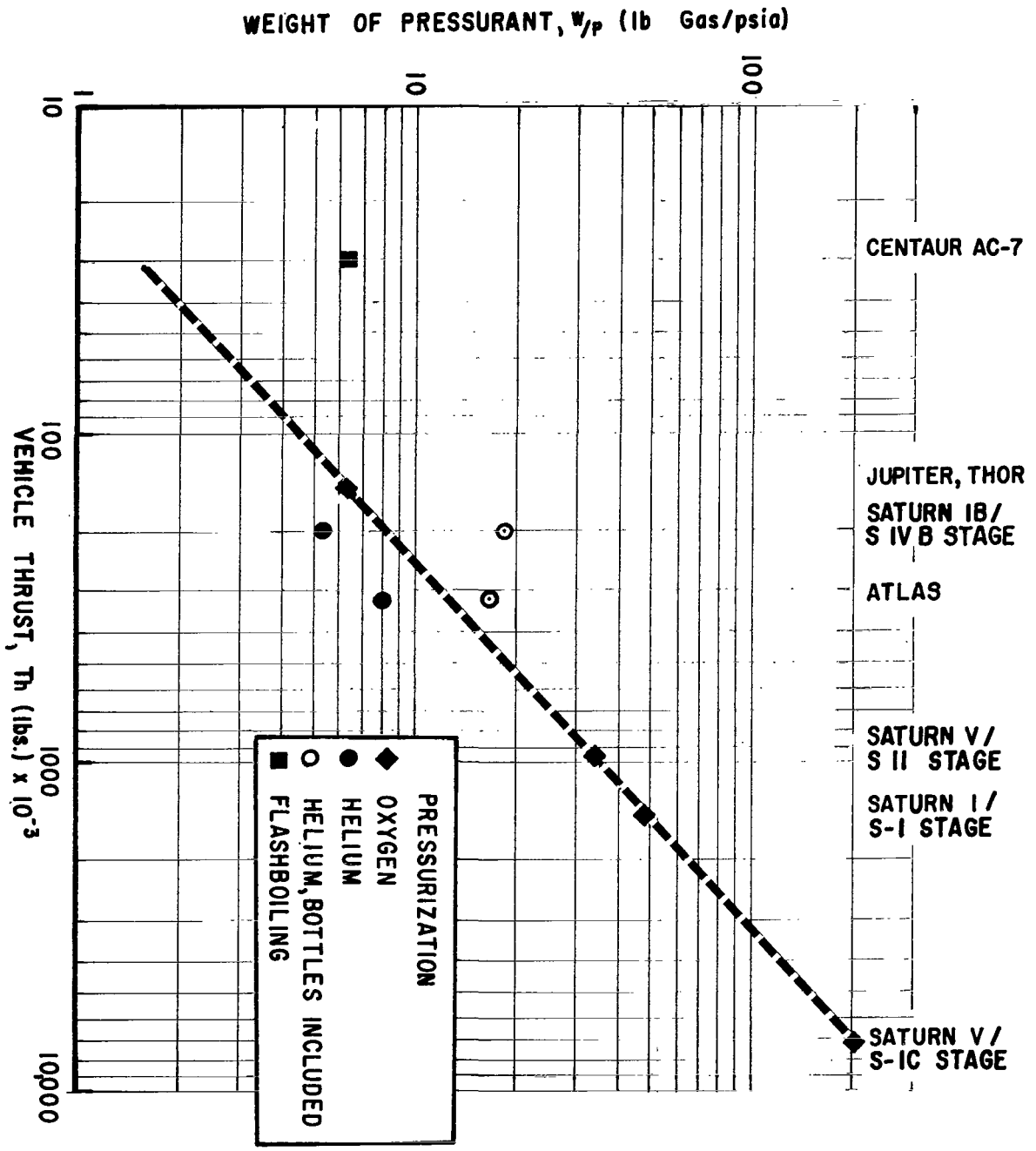

FIGURE 2. WEIGHT OF LOX TANK PRESSURANT VERSUS VEHICLE THRUST

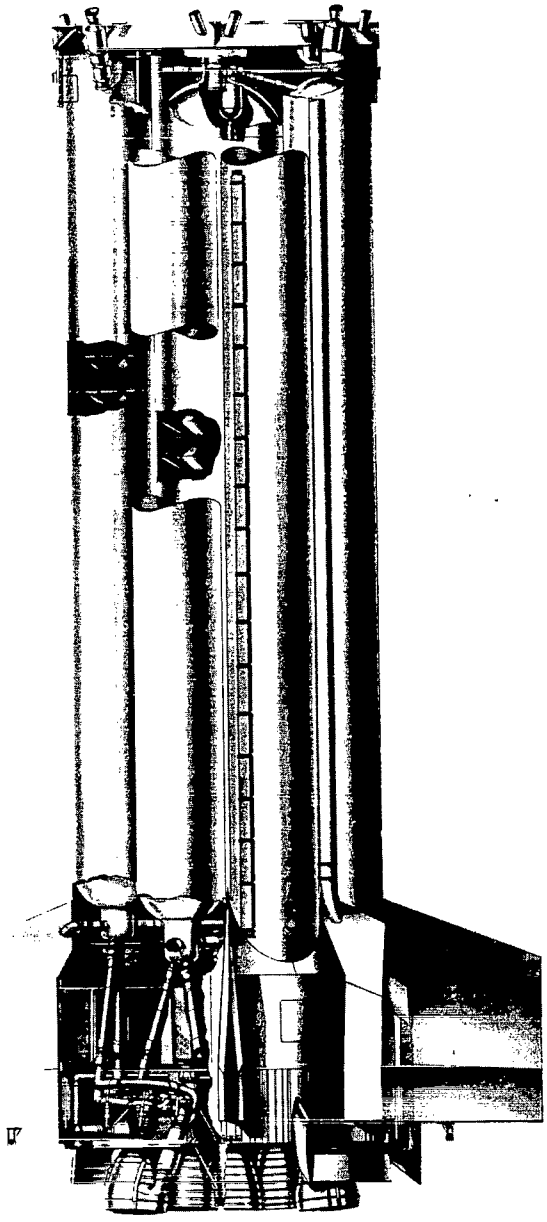

FIGURE 3A.

SATURN I, S-I STAGE

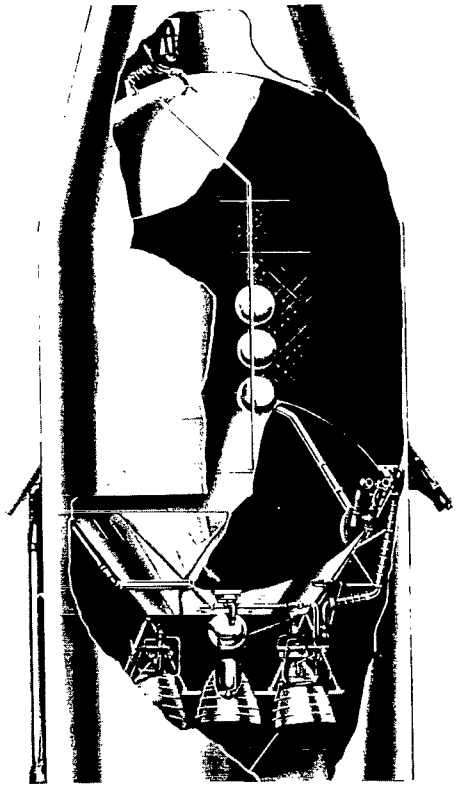

FIGURE 3B.

SATURN I, S-IV STAGE

FIGURE 3. SATURN I, S-I STAGE; SATURN I, S-IV STAGE

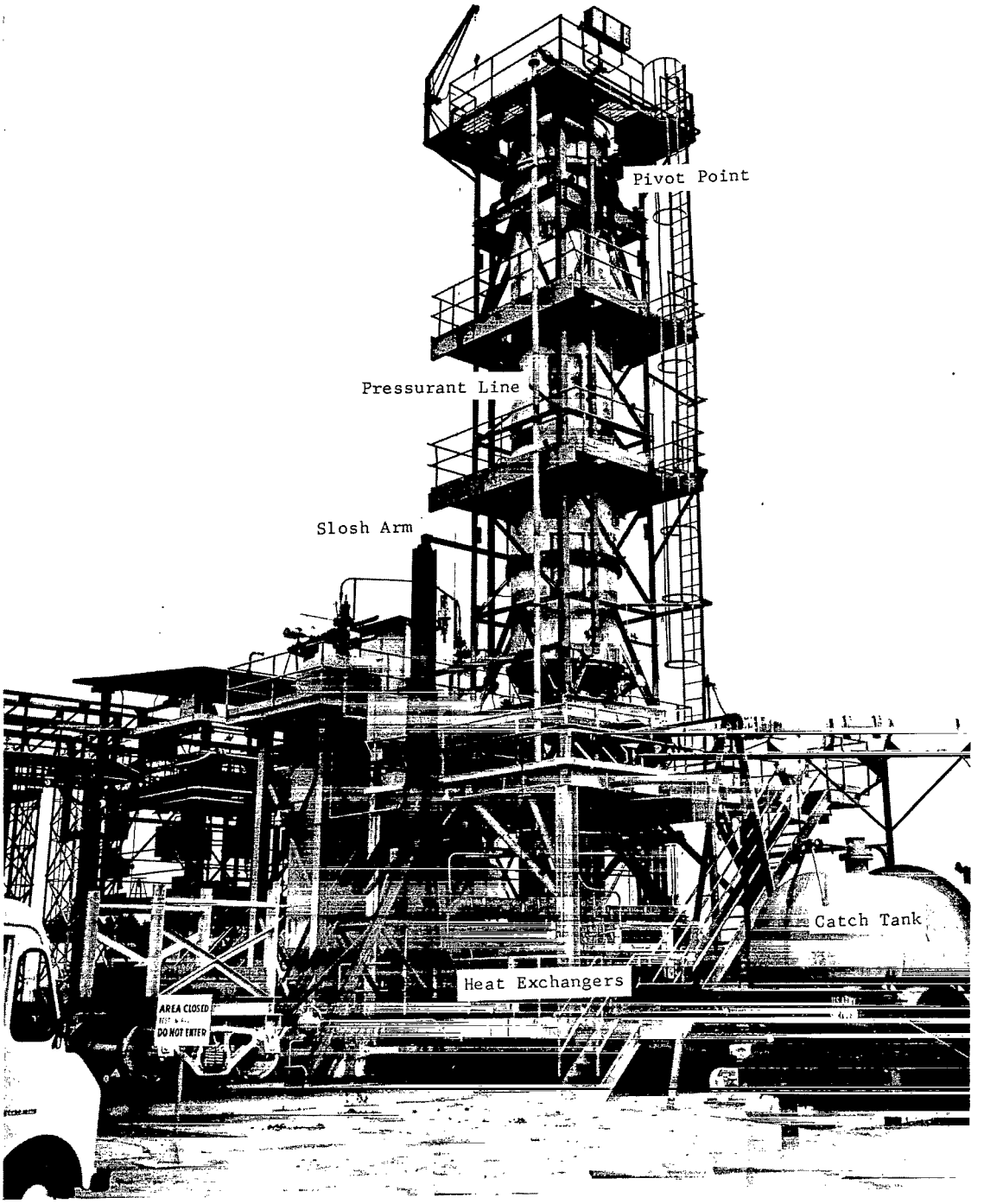

FIGURE 4. TEST FACILITY FOR TANK CONFIGURATION C

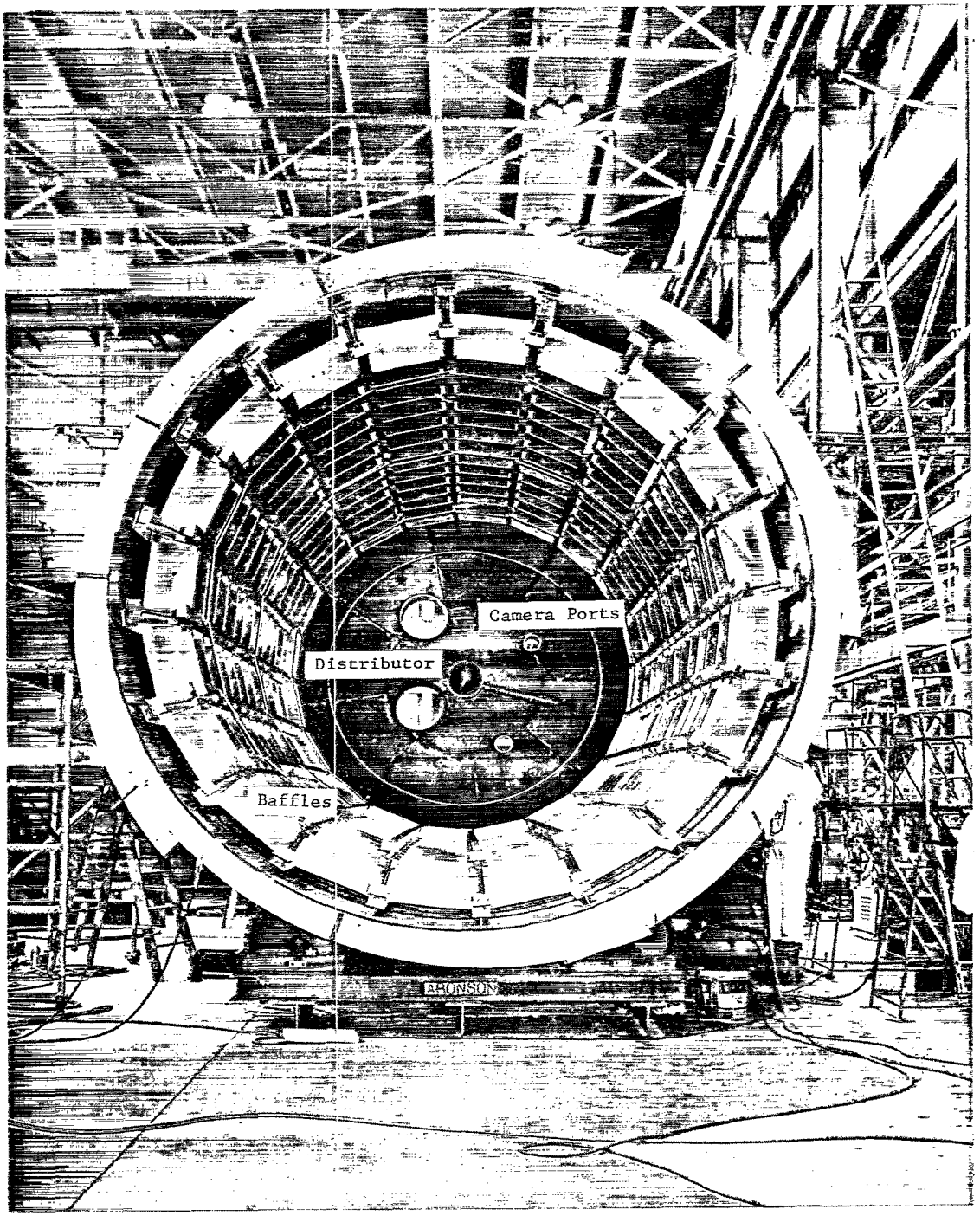

FIGURE 5a. INTERIOR OF TANK CONFIGURATION D

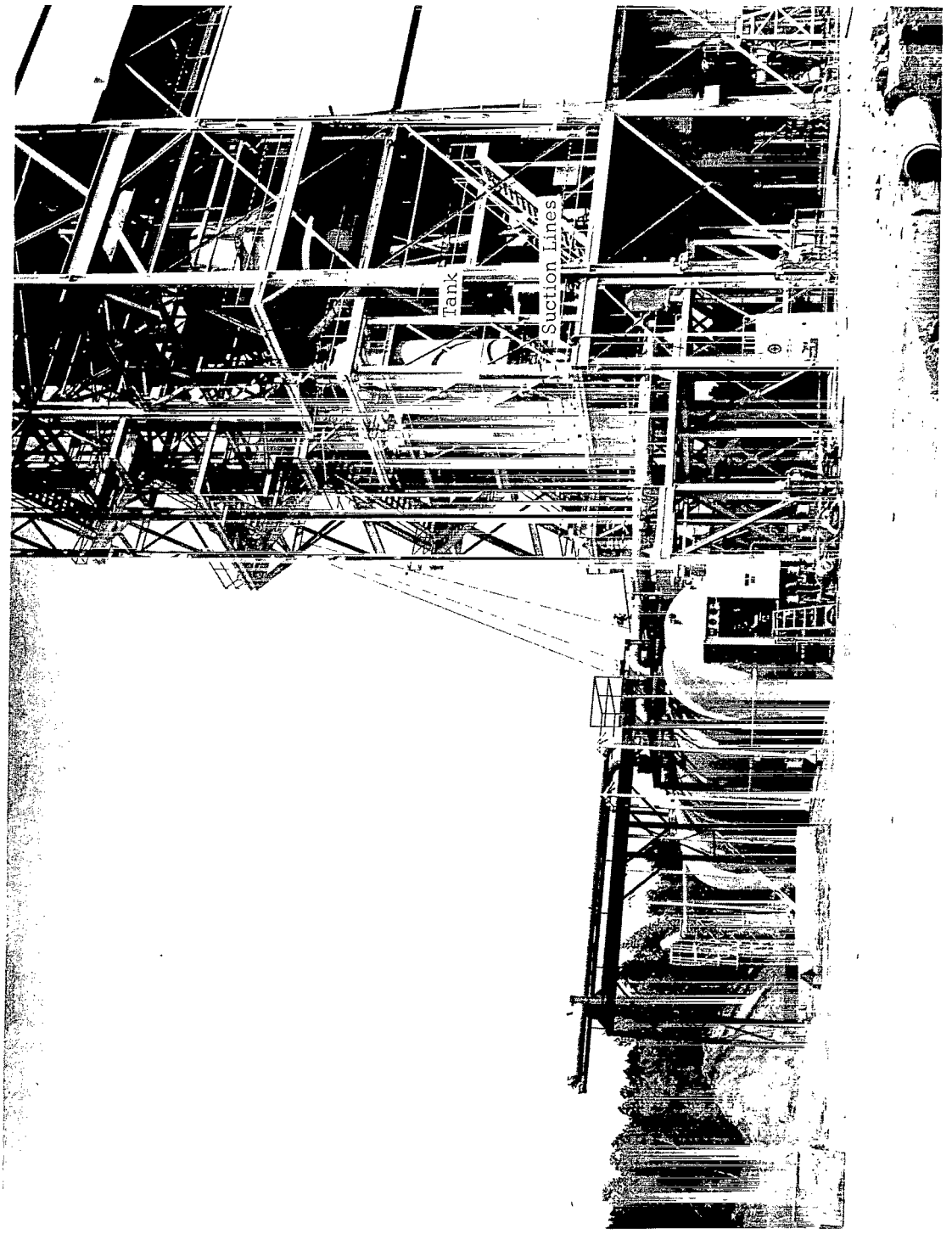

FIGURE 5b. TEST FACILITY FOR TANK CONFIGURATION D

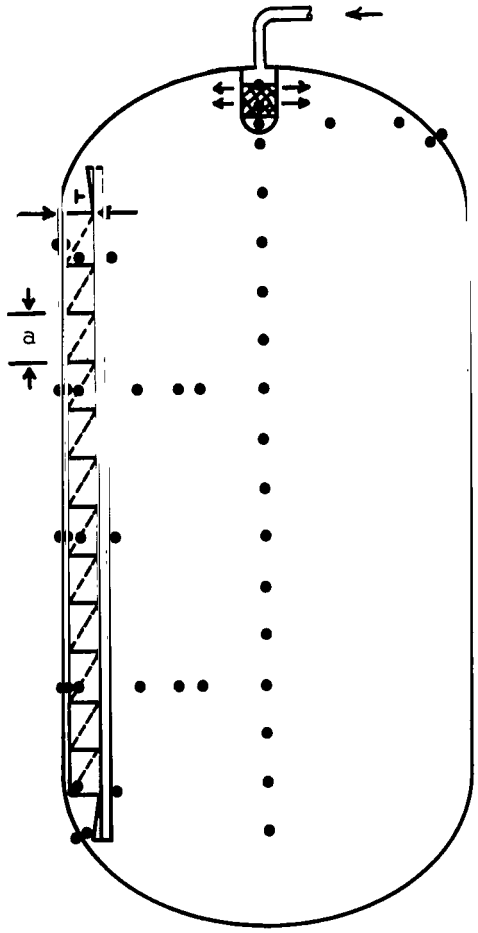

13	Tank Diameter (ft)	6.5
0.0442	Tank Wall Thickness (ft)	0.0312
13	Number of Baffles	8
1.64	Baffle Weight(lb/ft^2)	0.0357
1	Baffle Spacing a (ft)	2.42
1	Baffle Length r (ft)	2
Ring	Baffle Width (ft)	6 @ 1
0	Perforation %	25
16.65	Cylindrical Height (ft)	39.3
437	Top Bulkhead Volume (ft^3)	34.3
437	Bottom Bulkhead Volume (ft^3)	48.1

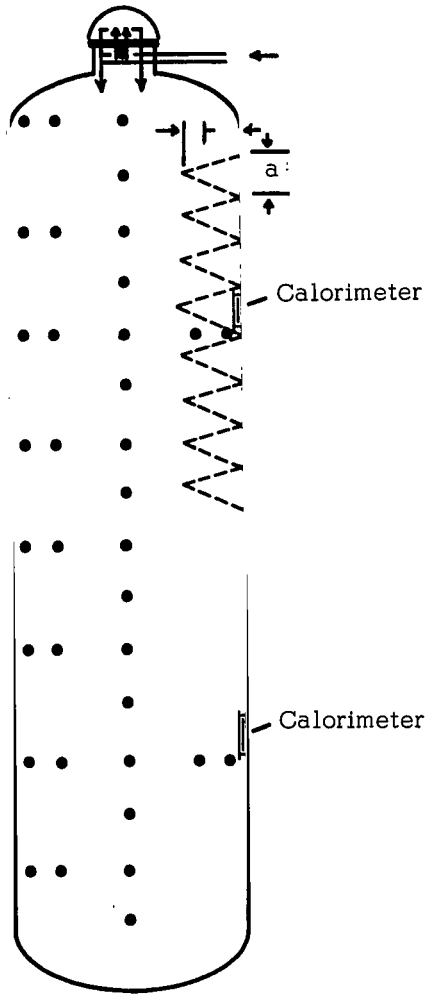

CONFIGURATION D
FIGURE 6A

CONFIGURATION C
FIGURE 6B

FIGURE 6. LOCATION OF TEMPERATURE PROBES

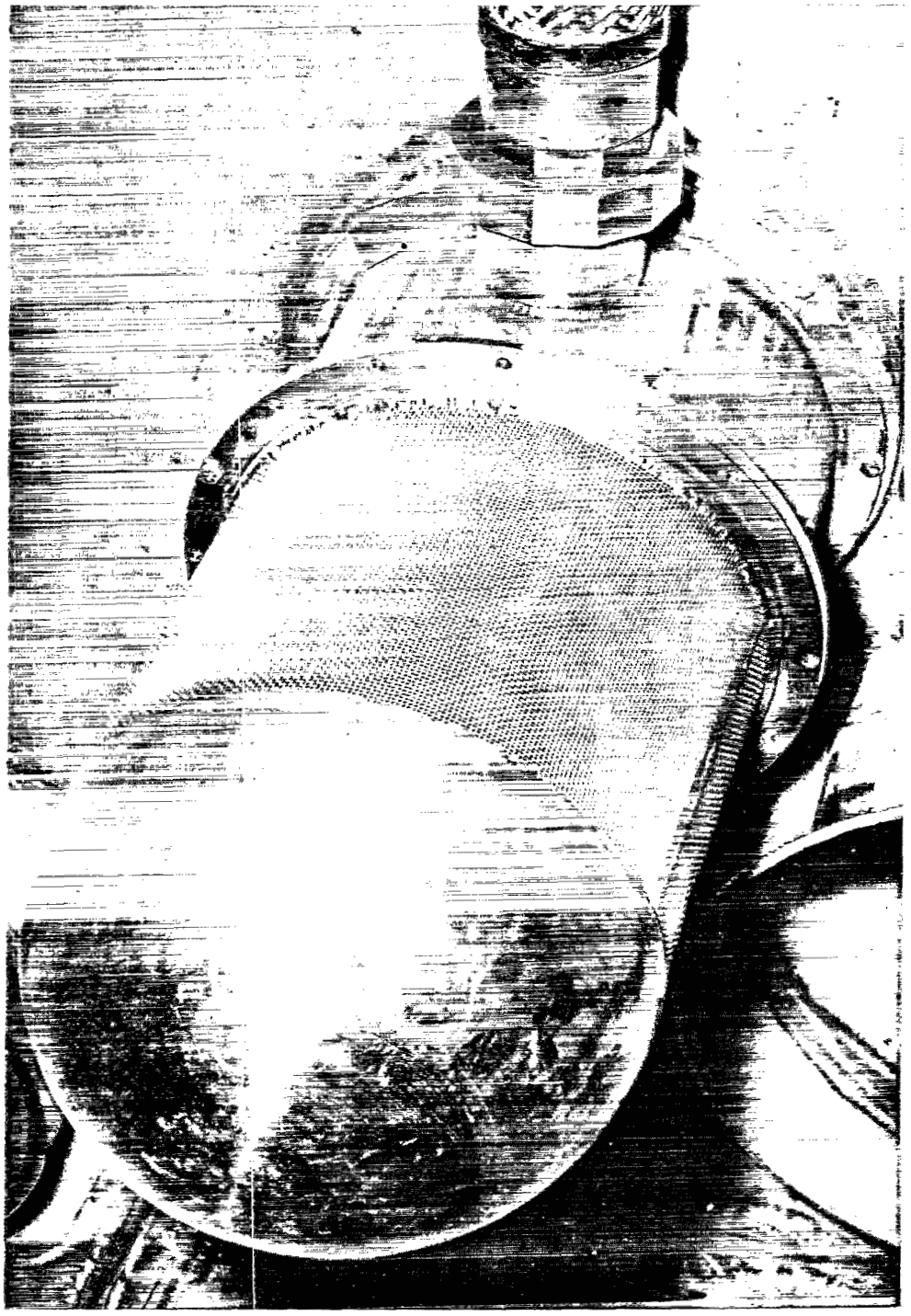

FIGURE 7. PRESSURANT DISTRIBUTOR, TANK CONFIGURATION D

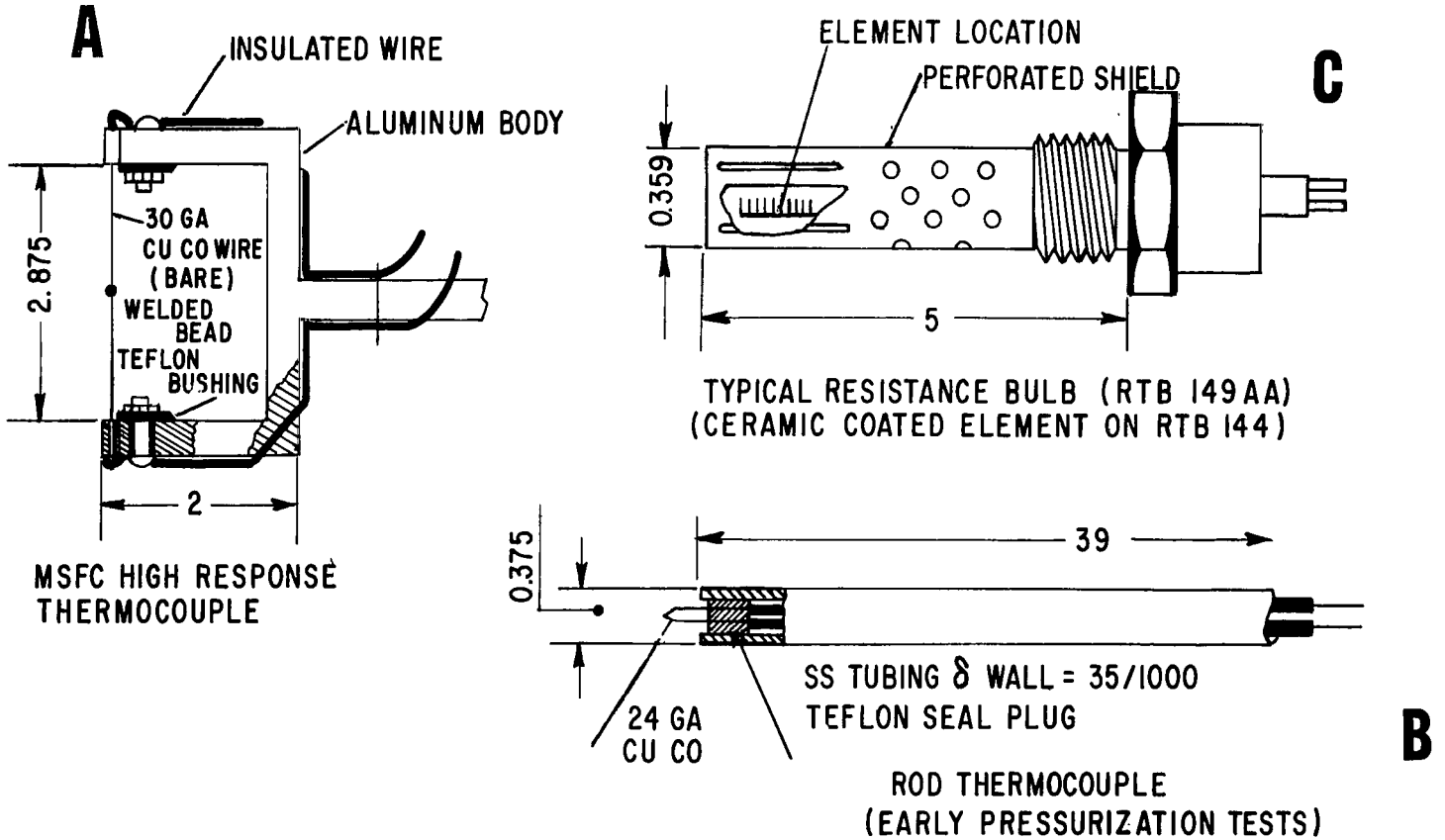

FIGURE 8. TEMPERATURE SENSORS

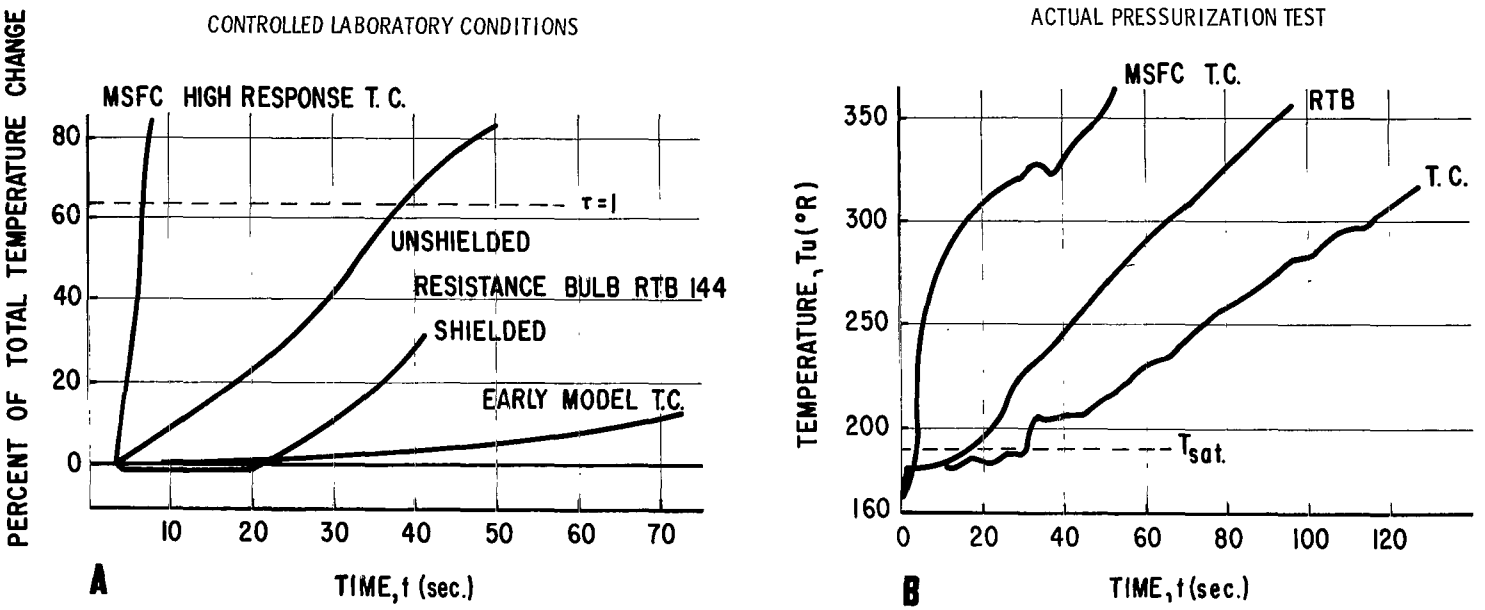

FIGURE 9. COMPARISON OF TEMPERATURE SENSOR RESPONSE TIME

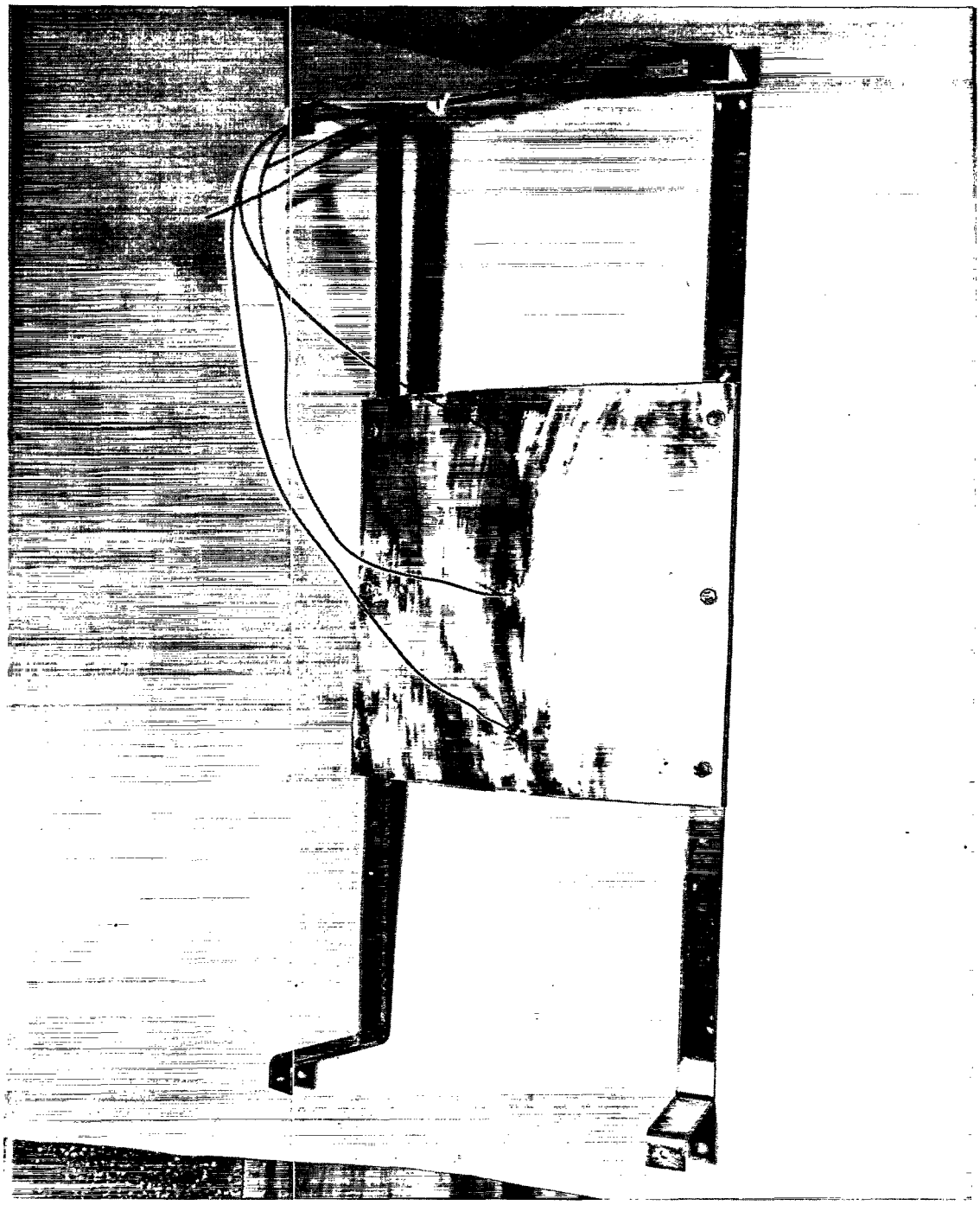

FIGURE 10. COPPER PLATE CALORIMETER

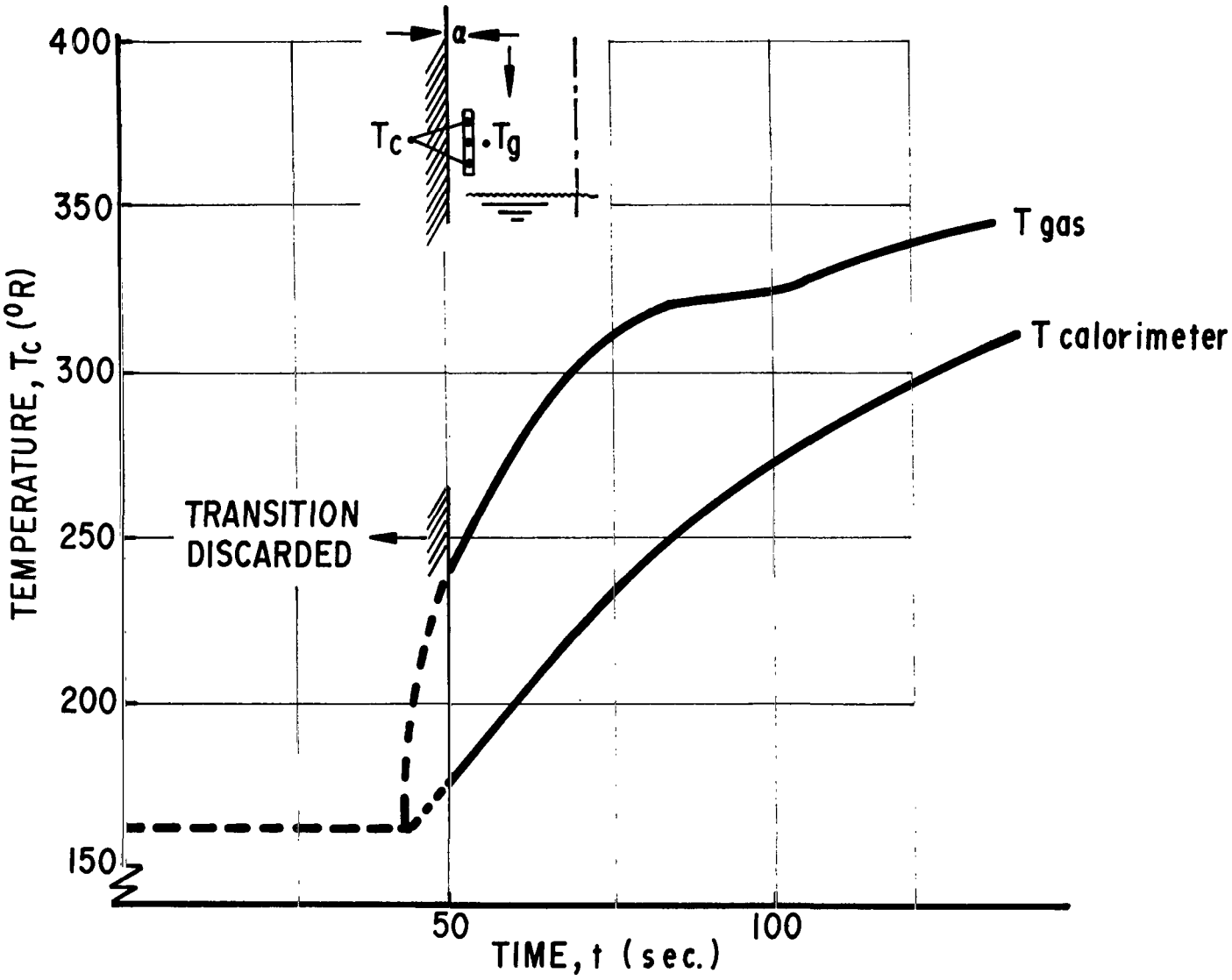

FIGURE 11. TEMPERATURE RESPONSE OF COPPER PLATE CALORIMETER

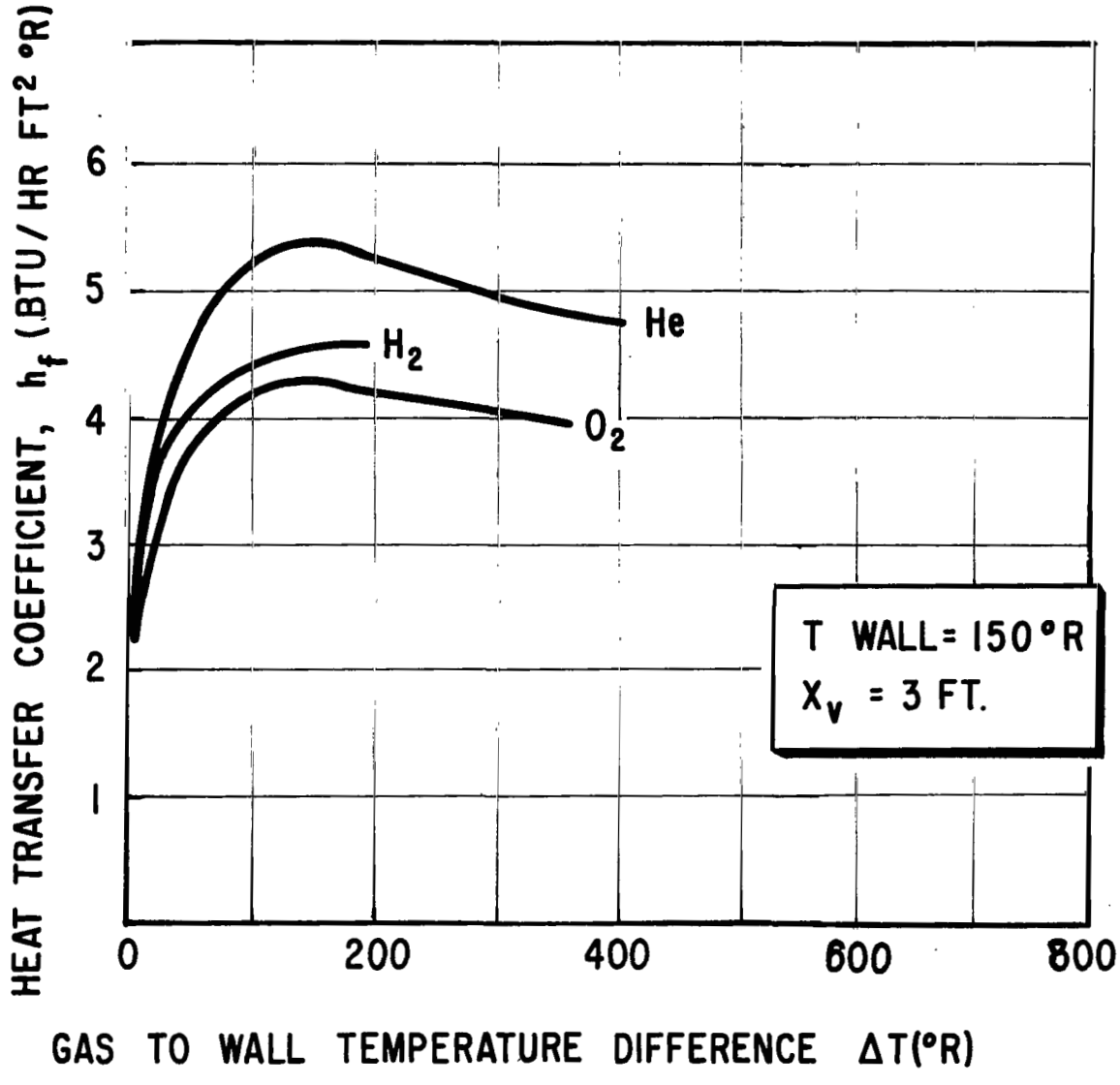

FIGURE 12. CALCULATED FREE CONVECTION HEAT TRANSFER COEFFICIENTS, h_f, ON VERTICAL WALL

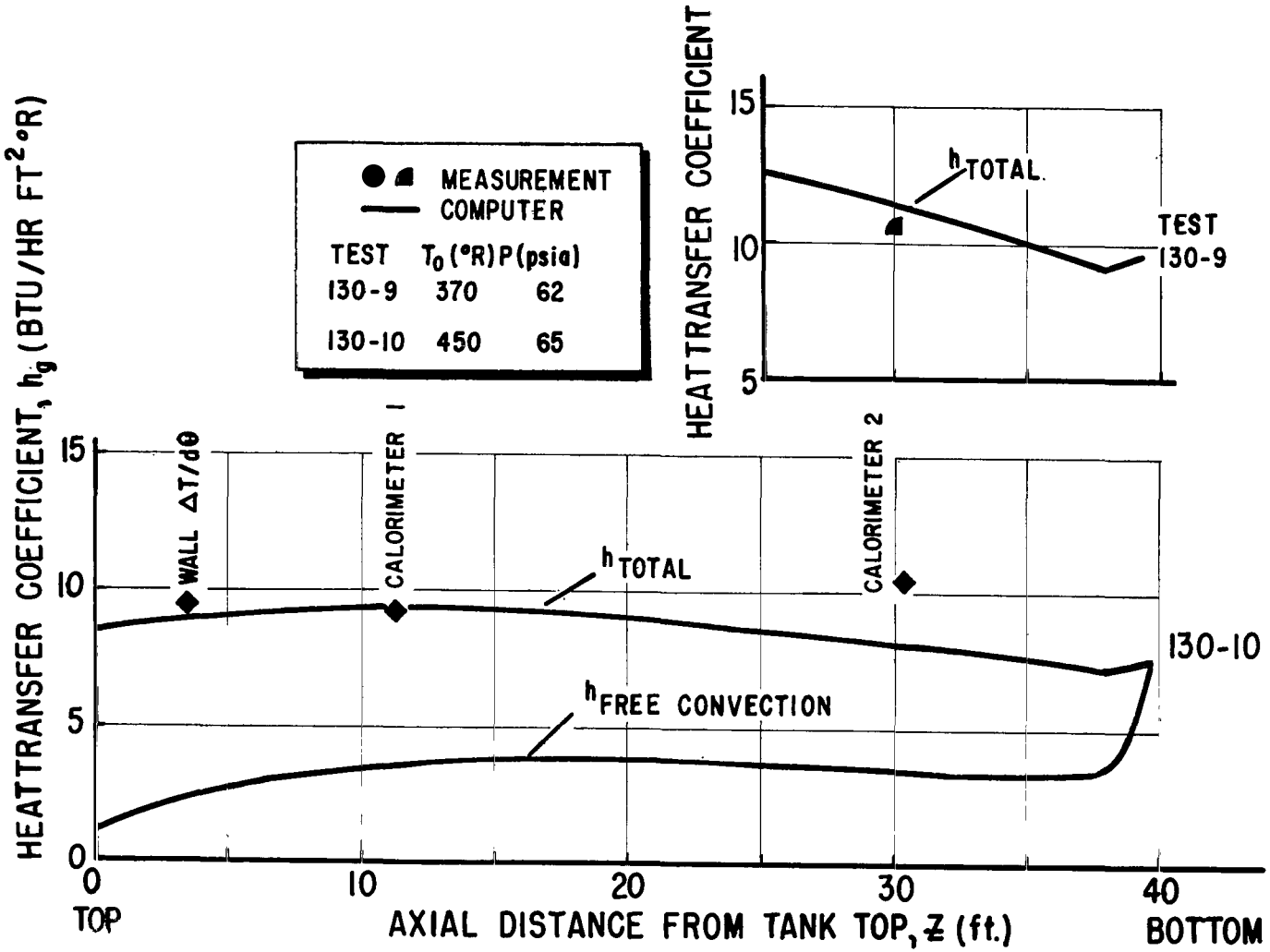

FIGURE 13. COMPARISON BETWEEN EXPERIMENTAL AND COMPUTED HEAT TRANSFER COEFFICIENTS, CONFIGURATION C, TESTS 130-9 AND 130-10, OXYGEN AS PRESSURANT

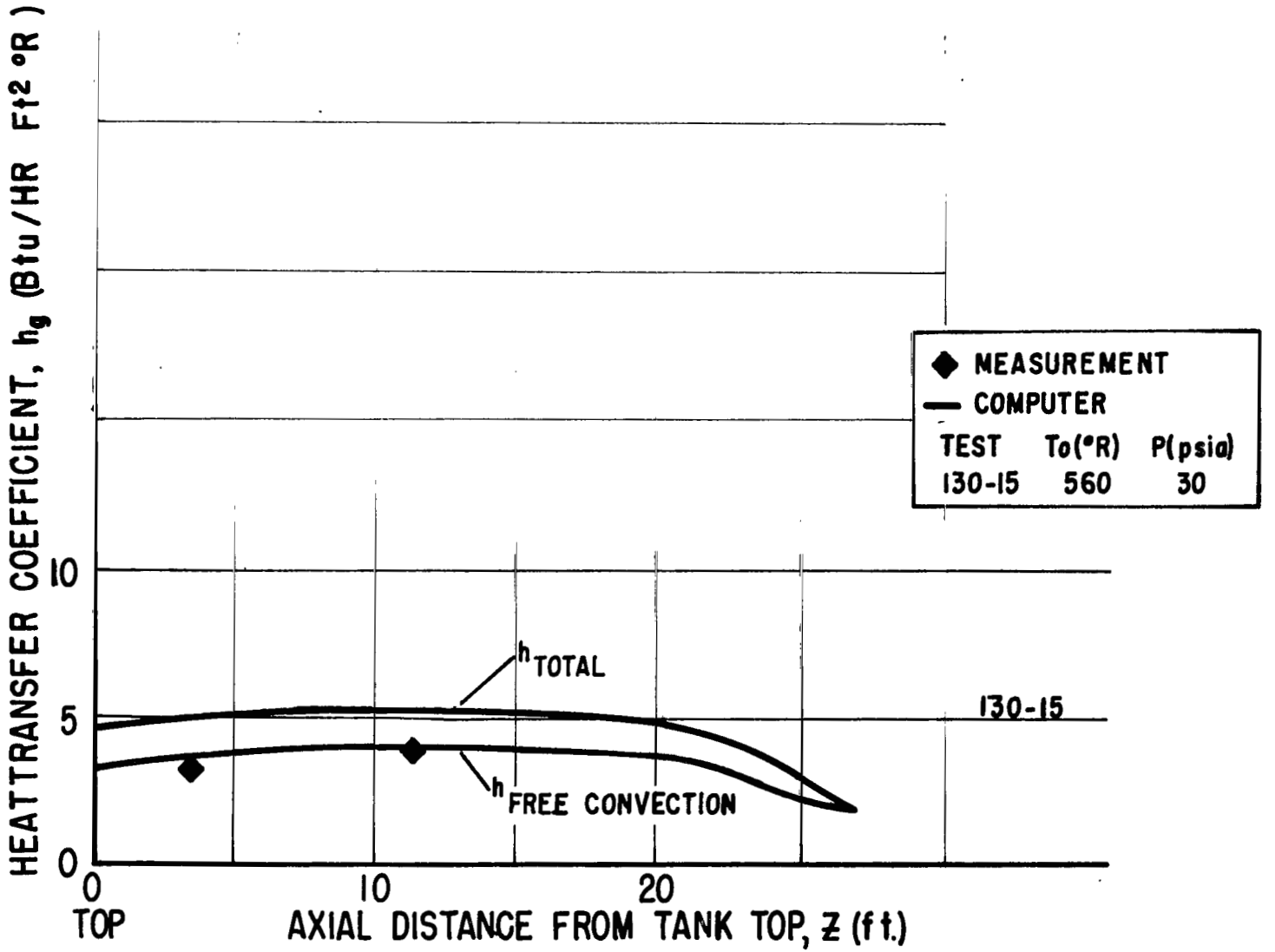

FIGURE 14. COMPARISON BETWEEN EXPERIMENTAL AND COMPUTED HEAT TRANSFER COEFFICIENTS, CONFIGURATION C, TEST 130-15, HELIUM AS PRESSURANT

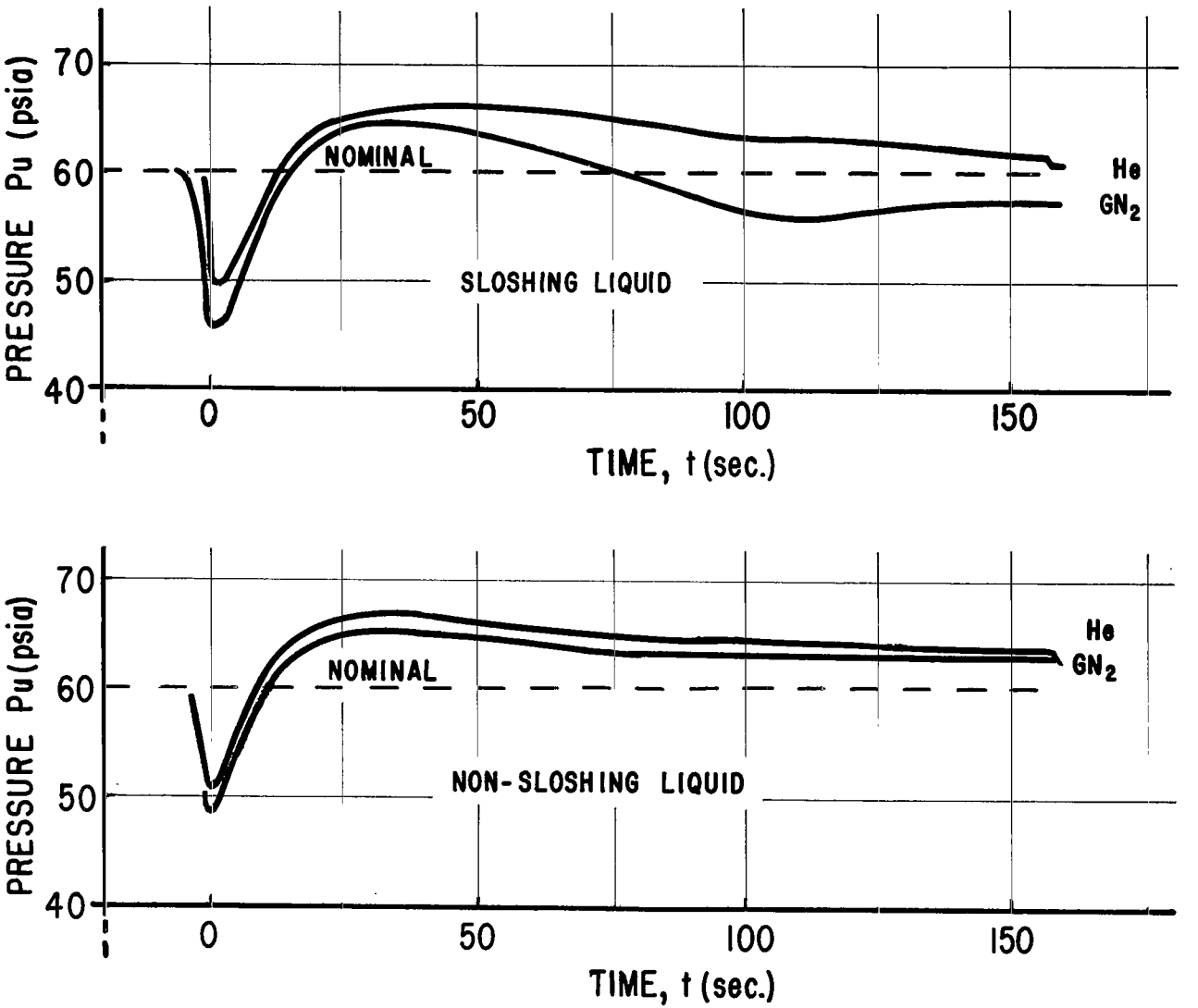

FIGURE 15. COMPARISON BETWEEN ULLAGE PRESSURE LOSS FOR He AND GN_2 PREPRESSURANTS UNDER LIQUID SLOSH AND NON-SLOSH CONDITIONS IN TANK CONFIGURATION C

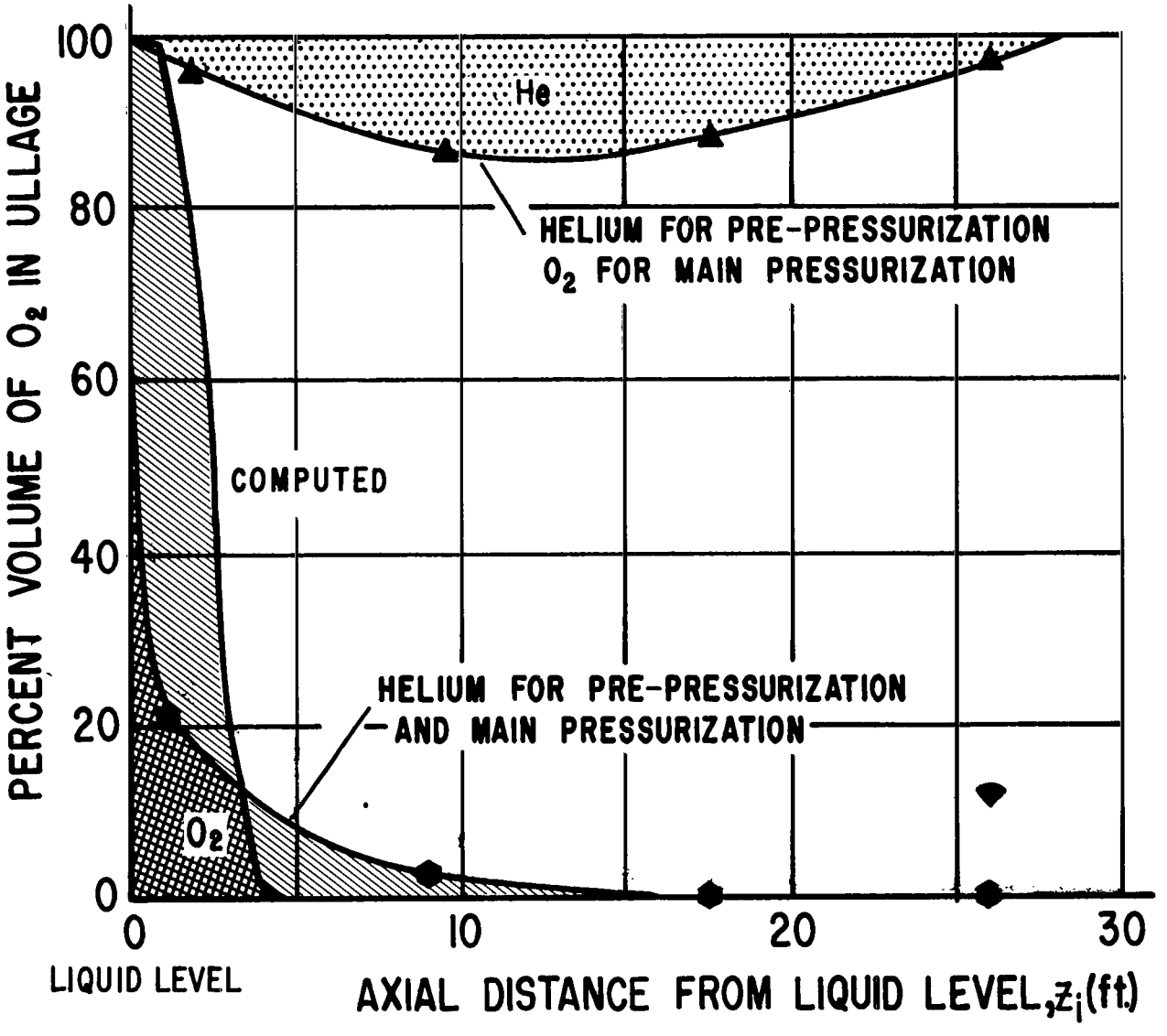

FIGURE 16. MEASURED AND COMPUTED ULLAGE GAS CONCENTRATION GRADIENTS IN TANK CONFIGURATION C

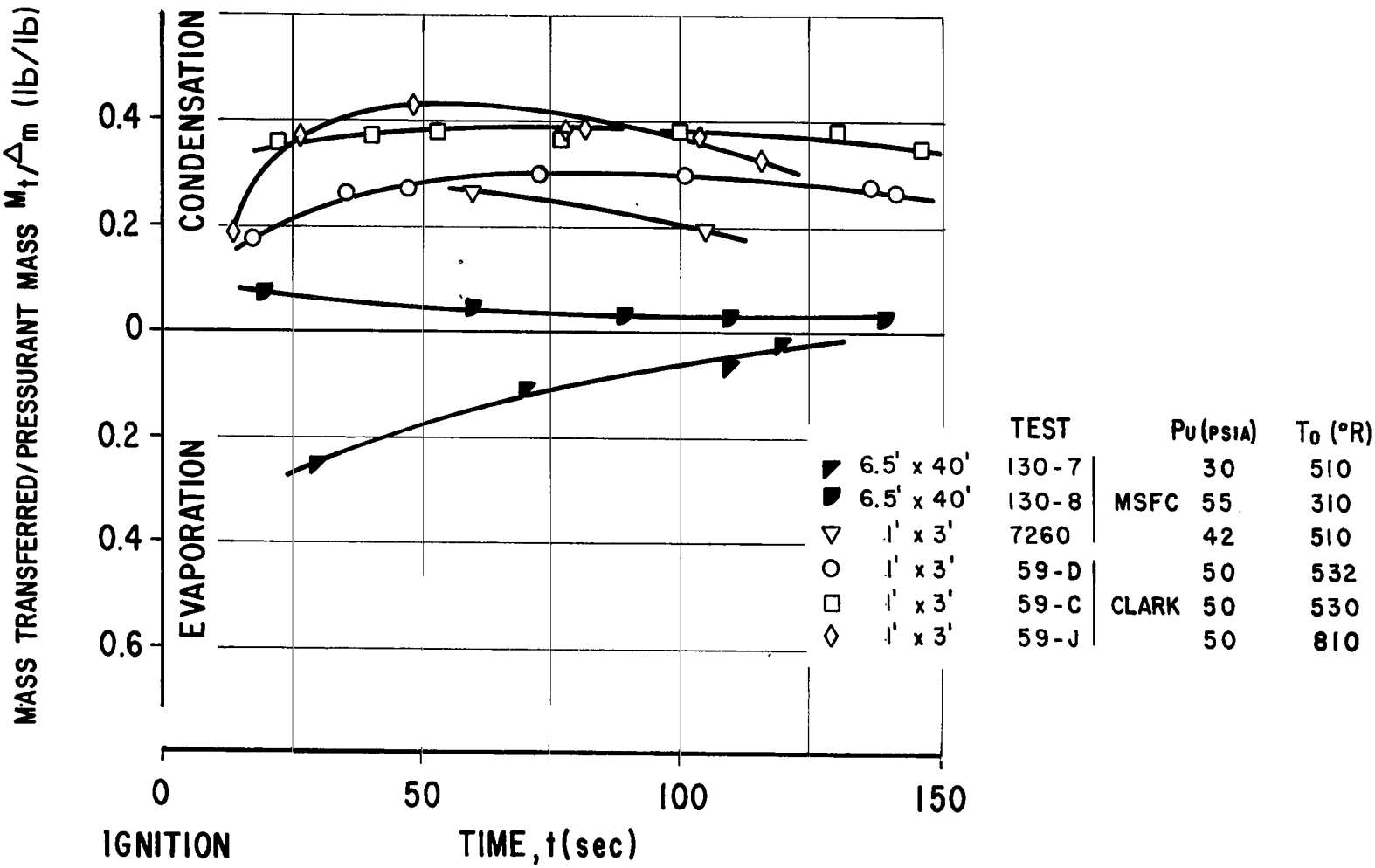

FIGURE 17. EXPERIMENTALLY DETERMINED MASS TRANSFER M_t/Δ_m (LB/LB) VERSUS TIME t (SEC)

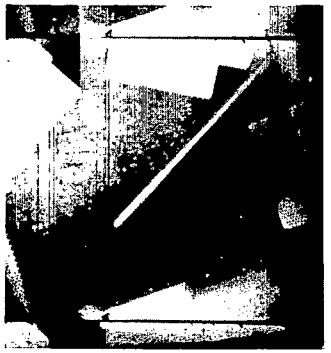

Violent Boiling During Venting

Vents Closed, Start of Prepressurization

End of Prepressurization

Start of Draining

During Draining

End of Draining

FIGURE 18. LIQUID SURFACE CONDITIONS DURING PRESSURIZATION TEST IN TANK CONFIGURATION C

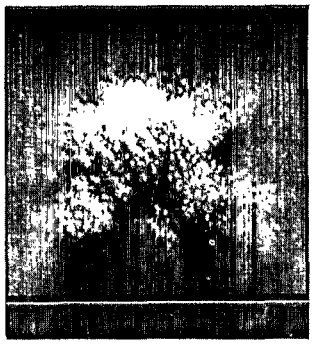

Ignition

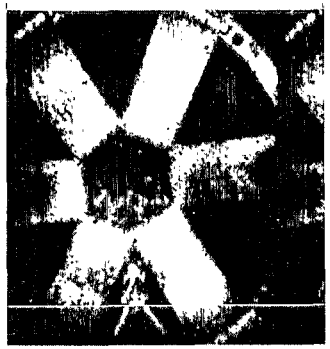

During Holddown

Cutoff

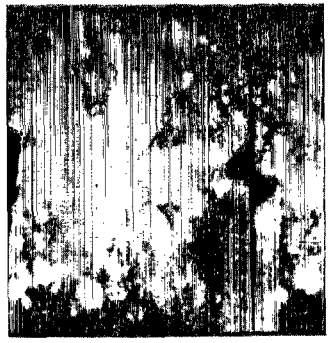

Residual Liquid Rising During The Firing of Retro Rockets
SA-5

FIGURE 19. LIQUID SURFACE AND ULLAGE CONDITIONS DURING SA-5 FLIGHT

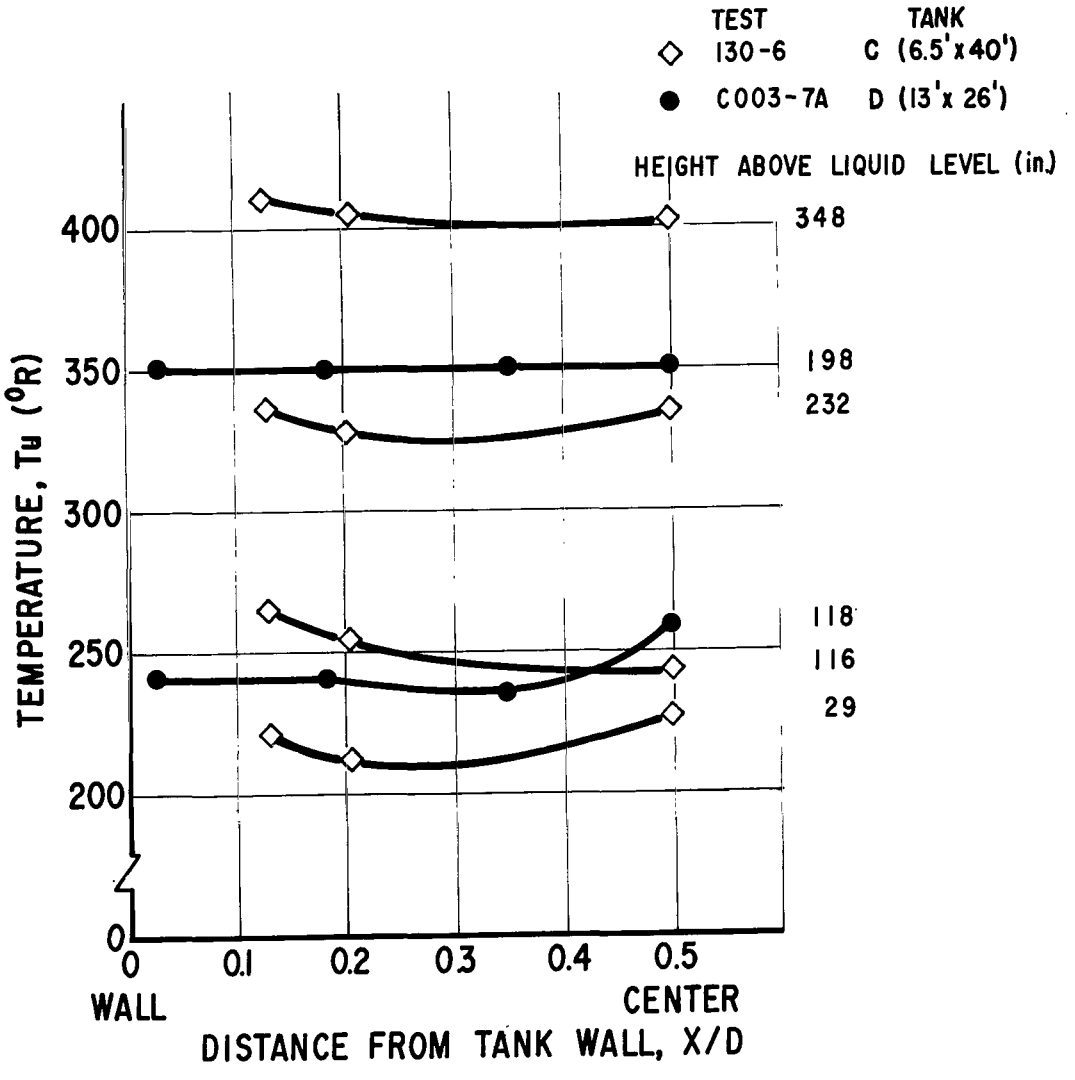

FIGURE 20. EXPERIMENTALLY DETERMINED RADIAL TEMPERATURE GRADIENTS

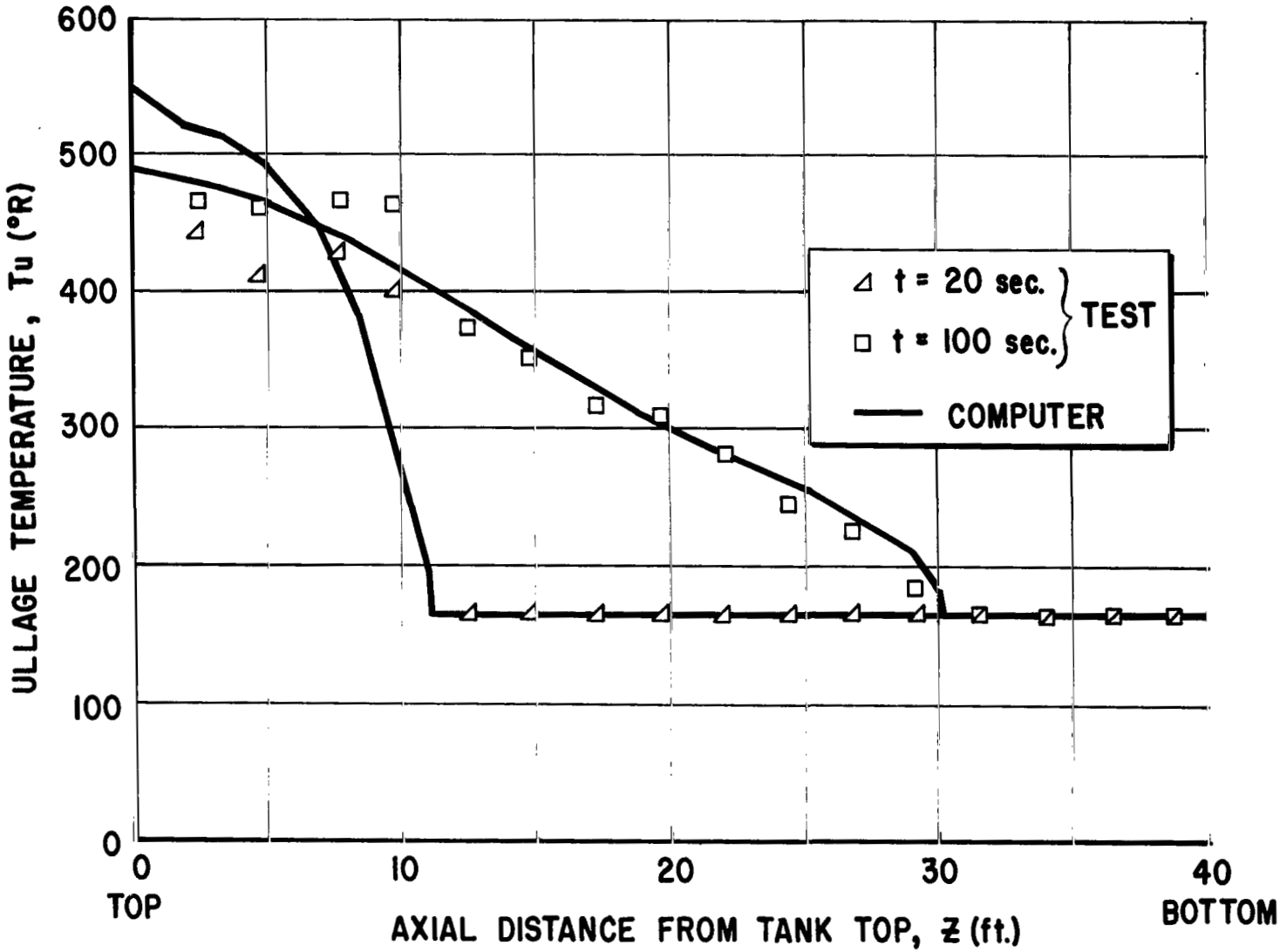

FIGURE 21a. COMPARISON BETWEEN EXPERIMENTAL AND COMPUTED ULLAGE TEMPERATURE GRADIENT, TANK CONFIGURATION C, TEST 130-6, OXYGEN AS PRESSURANT

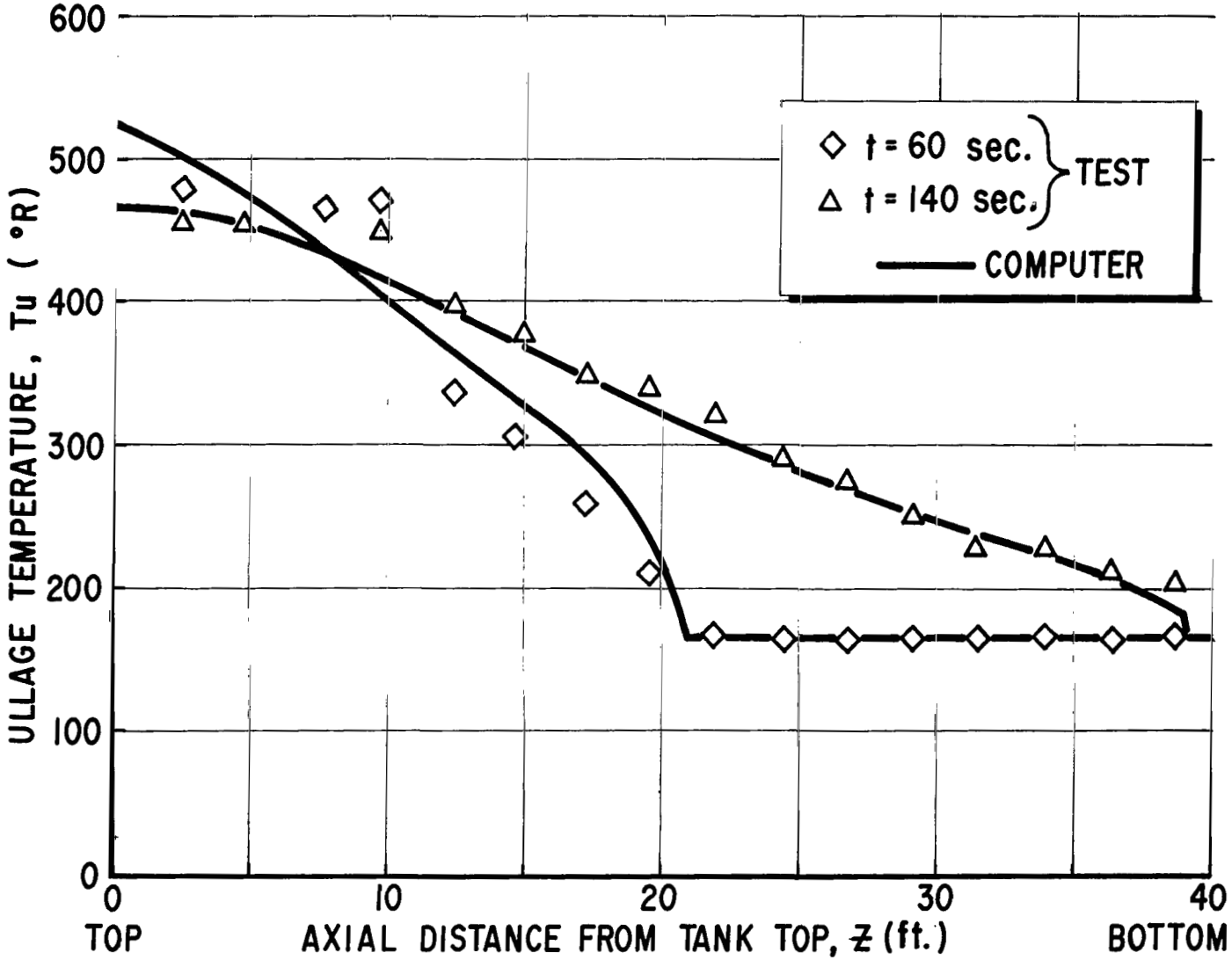

FIGURE 21b. COMPARISON BETWEEN EXPERIMENTAL AND COMPUTED ULLAGE TEMPERATURE GRADIENT, TANK CONFIGURATION C, TEST 130-6, OXYGEN AS PRESSURANT

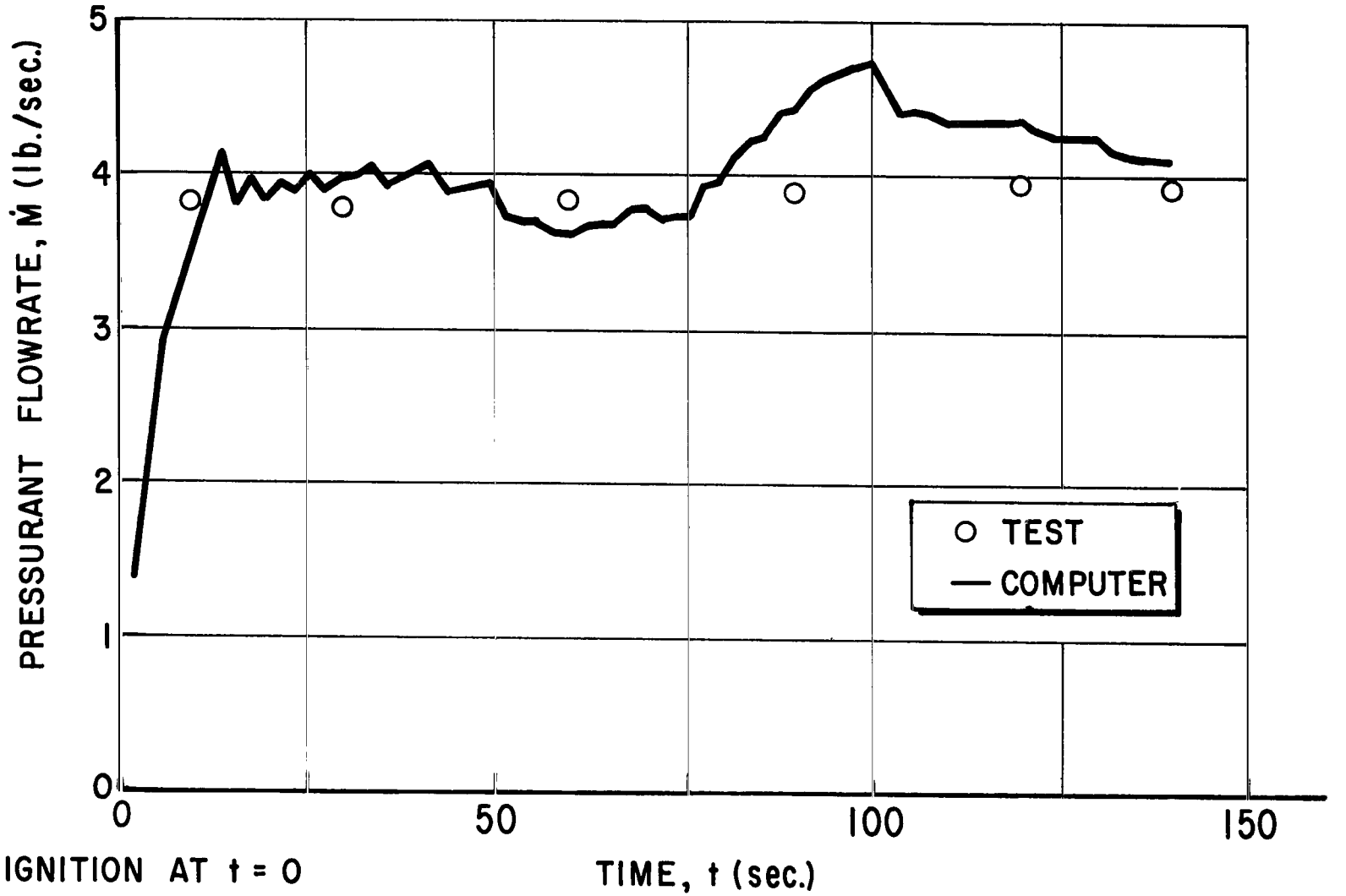

FIGURE 21c. COMPARISON BETWEEN EXPERIMENTAL AND COMPUTED PRESSURANT FLOWRATE, TANK CONFIGURATION C, TEST 130-6, OXYGEN AS PRESSURANT

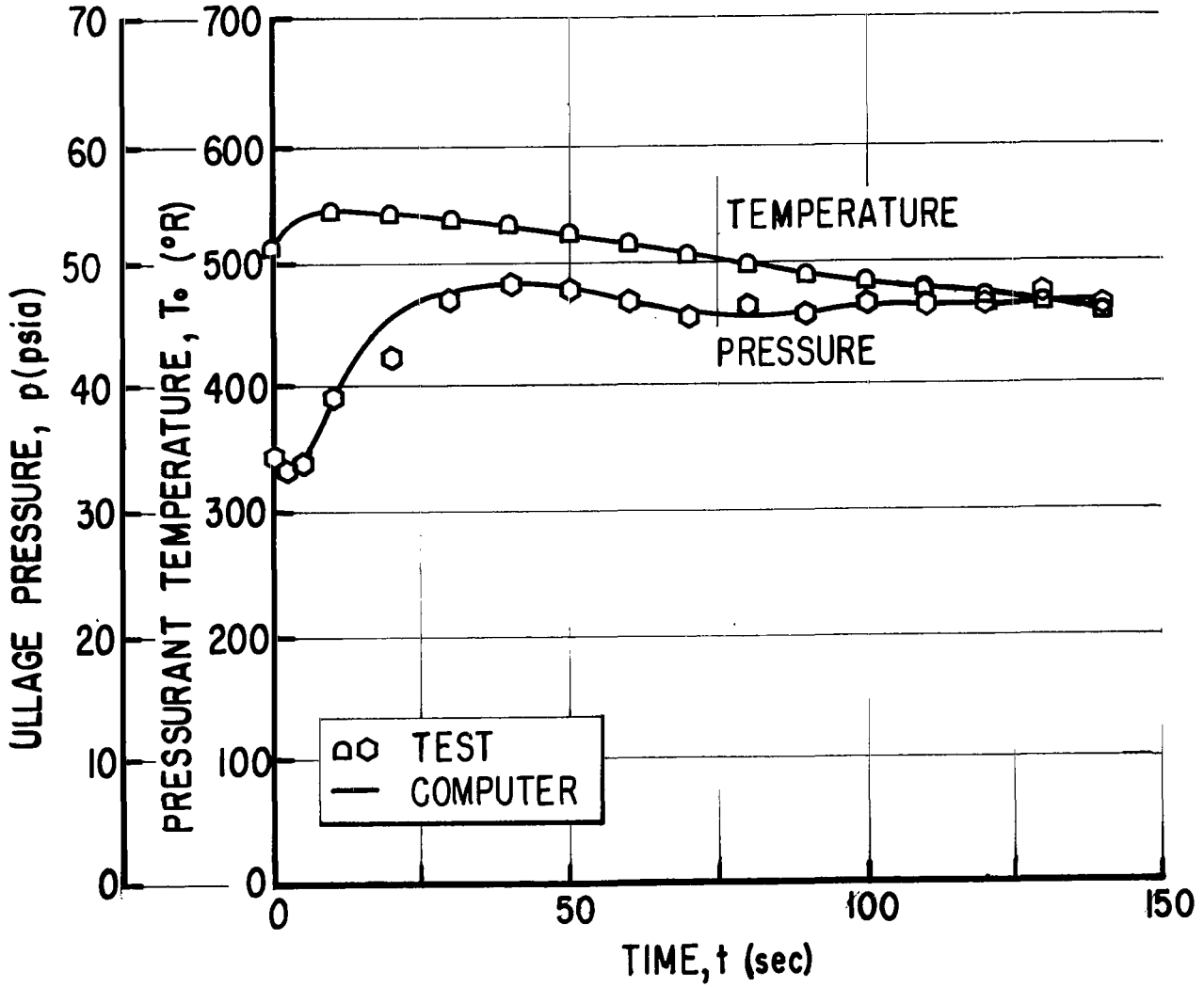

FIGURE 21d. ULLAGE PRESSURE AND PRESSURANT INLET TEMPERATURE HISTORIES, TANK CONFIGURATION C, TEST 130-6, OXYGEN AS PRESSURANT

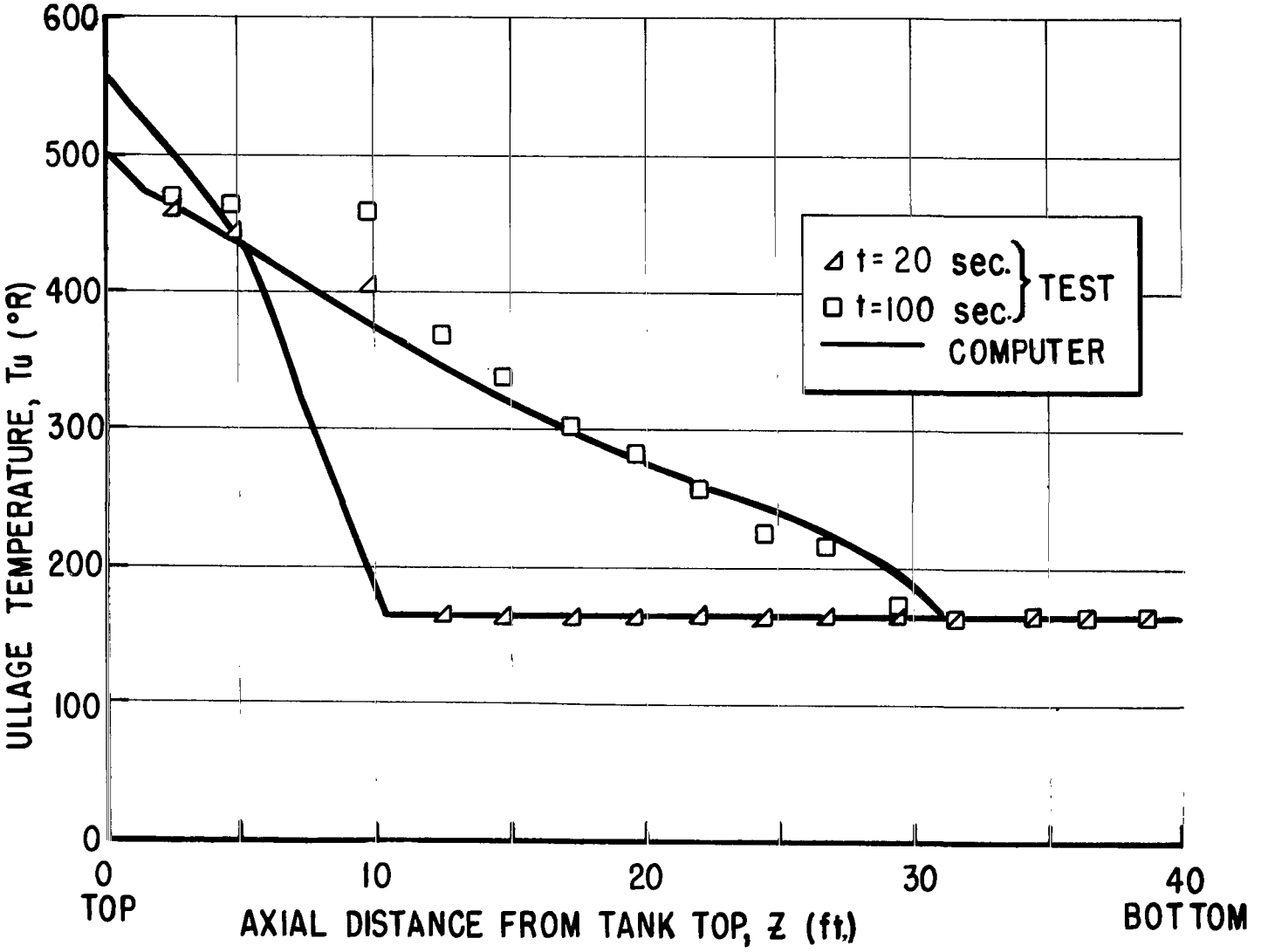

FIGURE 22a. COMPARISON BETWEEN EXPERIMENTAL AND COMPUTED ULLAGE TEMPERATURE GRADIENT, TANK CONFIGURATION C, TEST 130-7, OXYGEN AS PRESSURANT

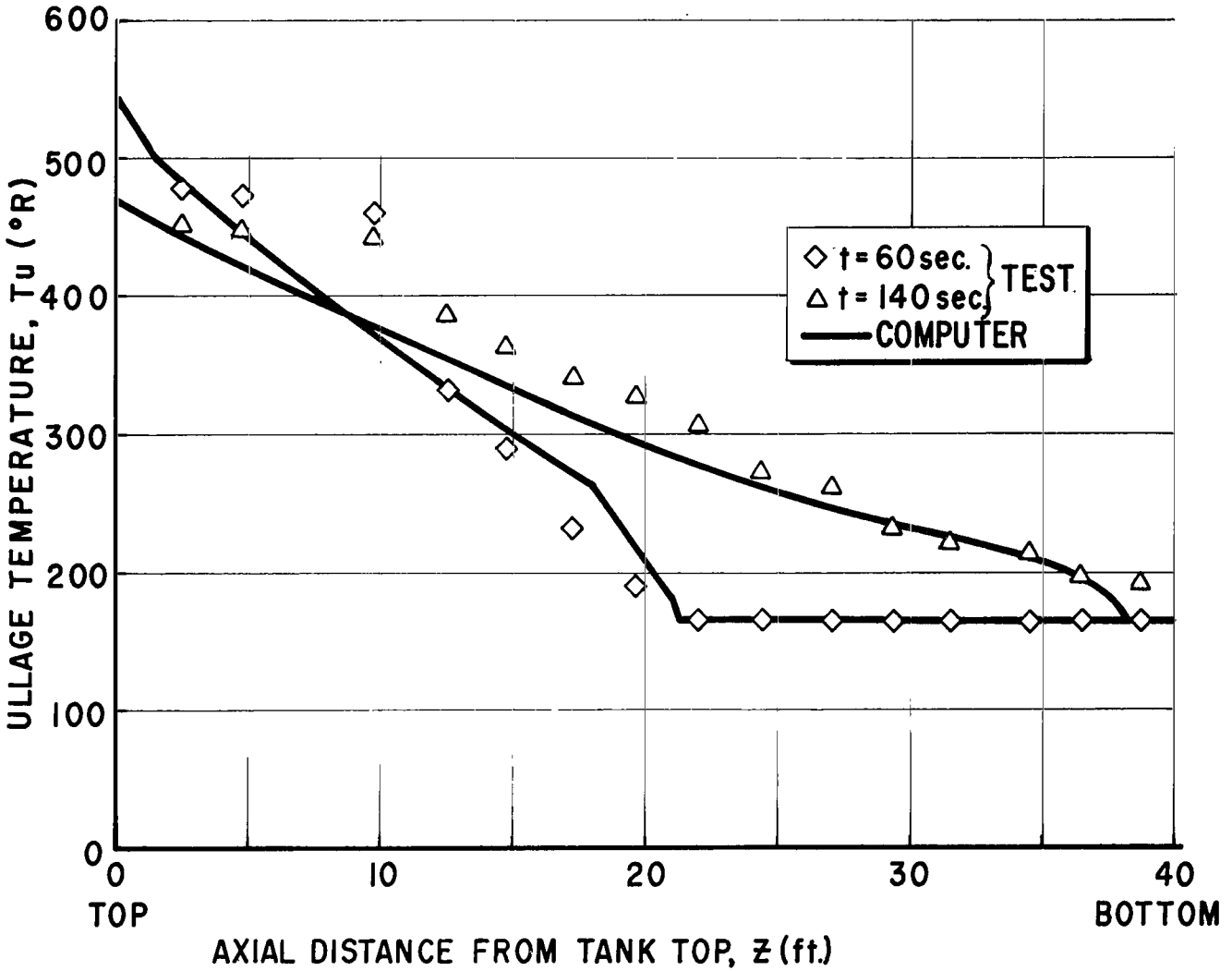

FIGURE 22b. COMPARISON BETWEEN EXPERIMENTAL AND COMPUTED ULLAGE TEMPERATURE GRADIENT, TANK CONFIGURATION C, TEST 130-7, OXYGEN AS PRESSURANT

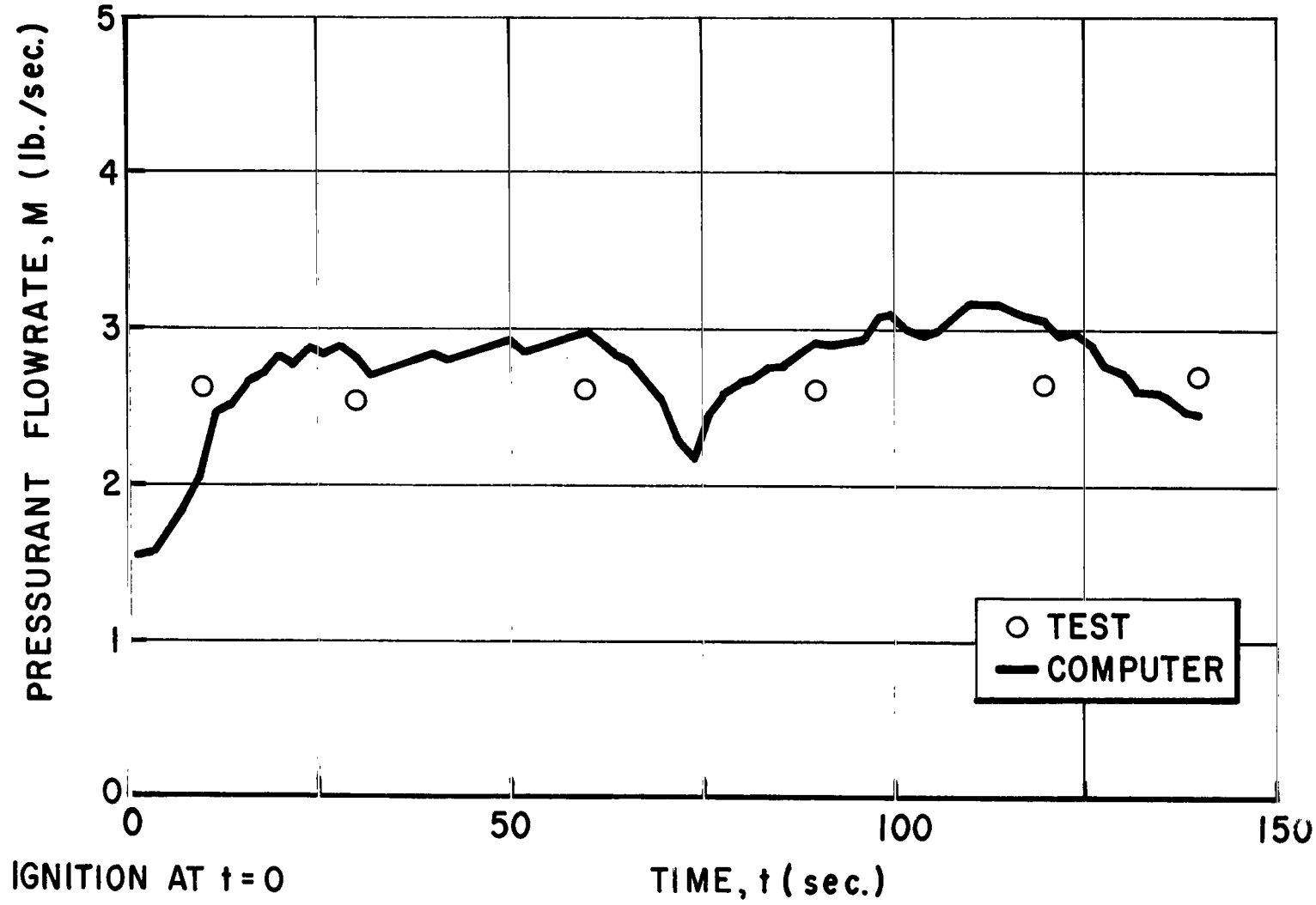

FIGURE 22c. COMPARISON BETWEEN EXPERIMENTAL AND COMPUTED PRESSURANT FLOWRATE, TANK CONFIGURATION C, TEST 130-7, OXYGEN AS PRESSURANT

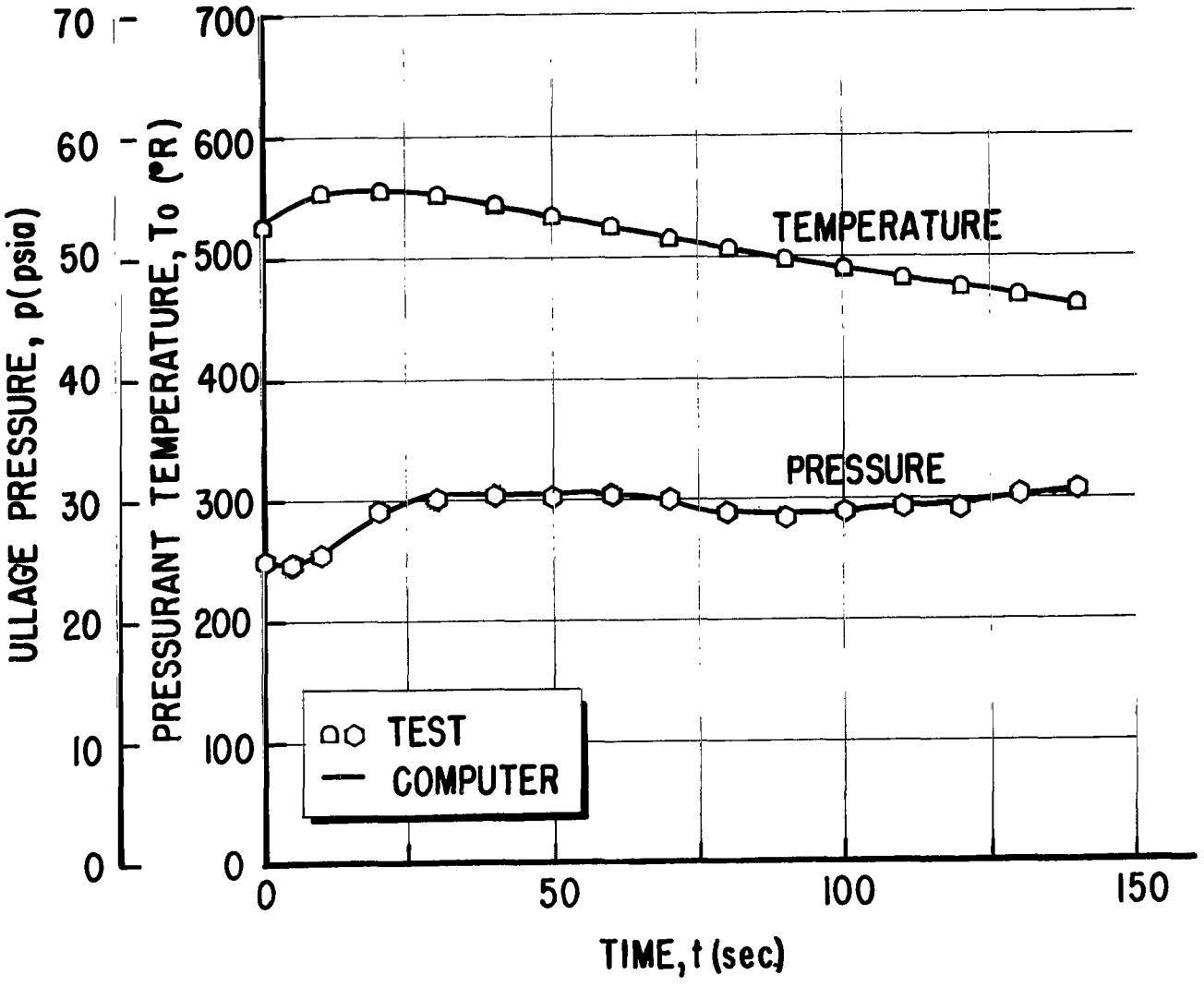

FIGURE 22d. ULLAGE PRESSURE AND PRESSURANT INLET TEMPERATURE HISTORIES, TANK CONFIGURATION C, TEST 130-7, OXYGEN AS PRESSURANT

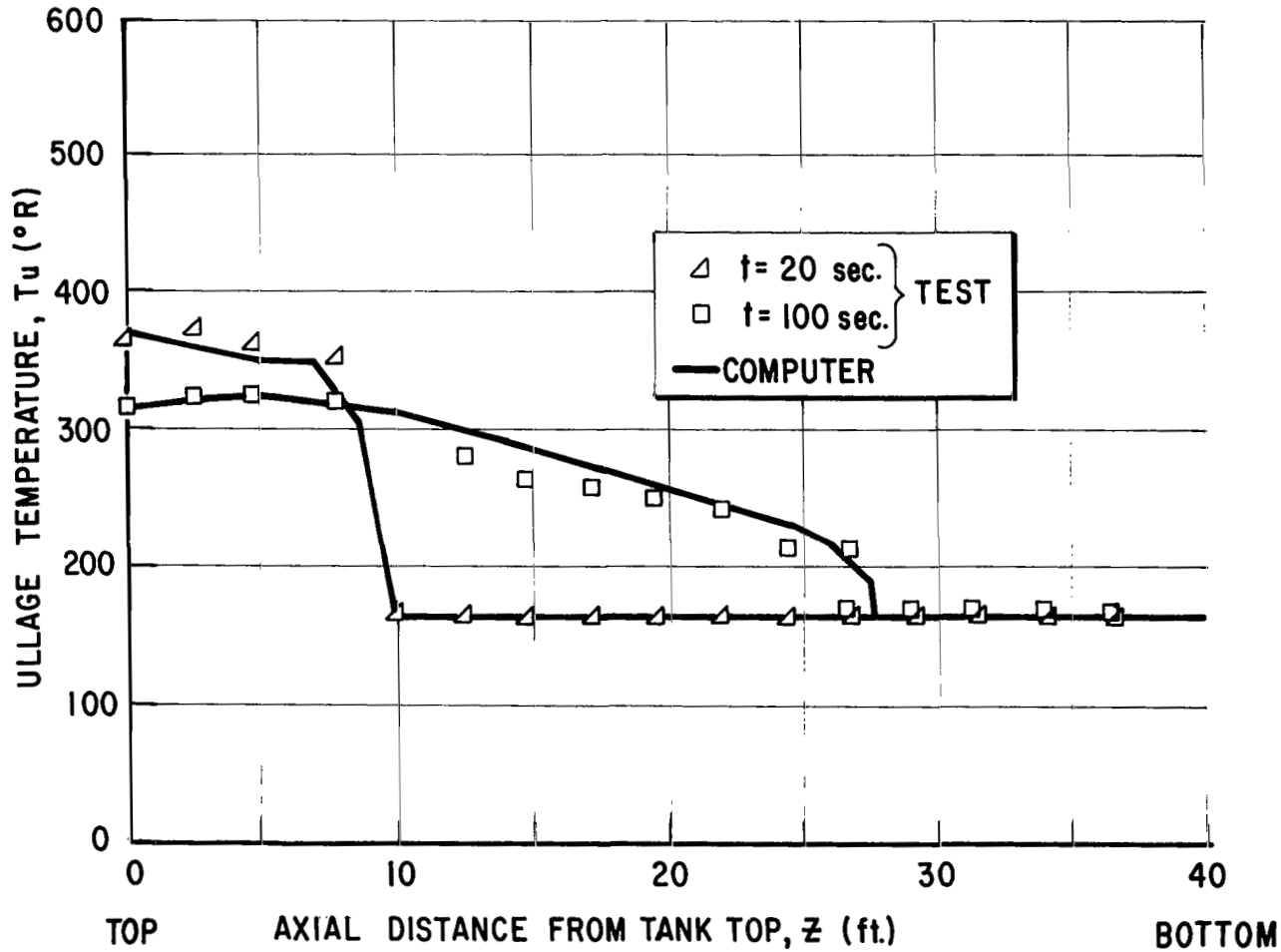

FIGURE 23a. COMPARISON BETWEEN EXPERIMENTAL AND COMPUTED ULLAGE TEMPERATURE GRADIENT, TANK CONFIGURATION C, TEST 130-9, OXYGEN AS PRESSURANT

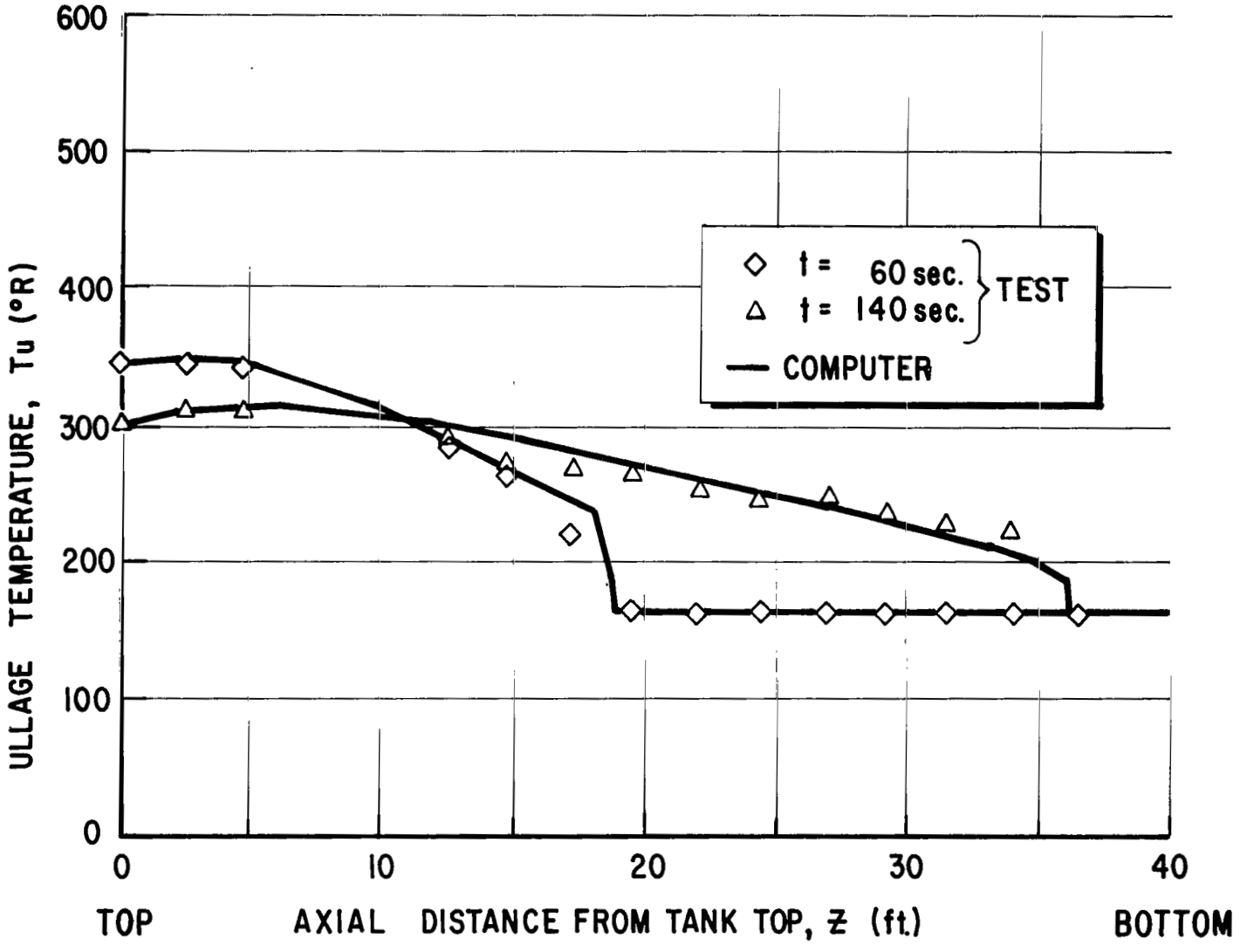

FIGURE 23b. COMPARISON BETWEEN EXPERIMENTAL AND COMPUTED PRESSURANT FLOWRATE, TANK CONFIGURATION C, TEST 130-9, OXYGEN AS PRESSURANT

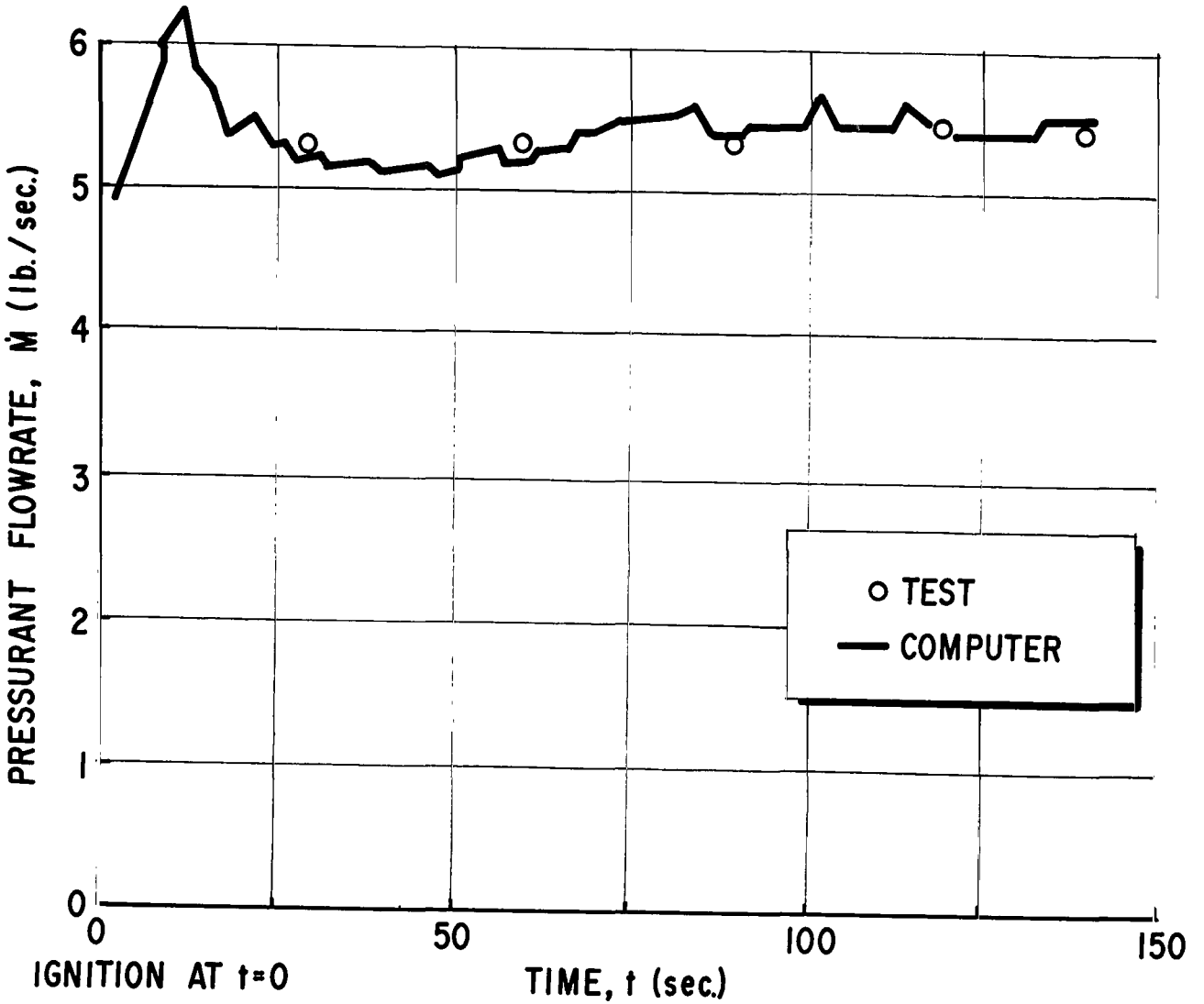

FIGURE 23c. COMPARISON BETWEEN EXPERIMENTAL AND COMPUTED PRESSURANT FLOWRATE, TANK CONFIGURATION C, TEST 130-9, OXYGEN AS PRESSURANT

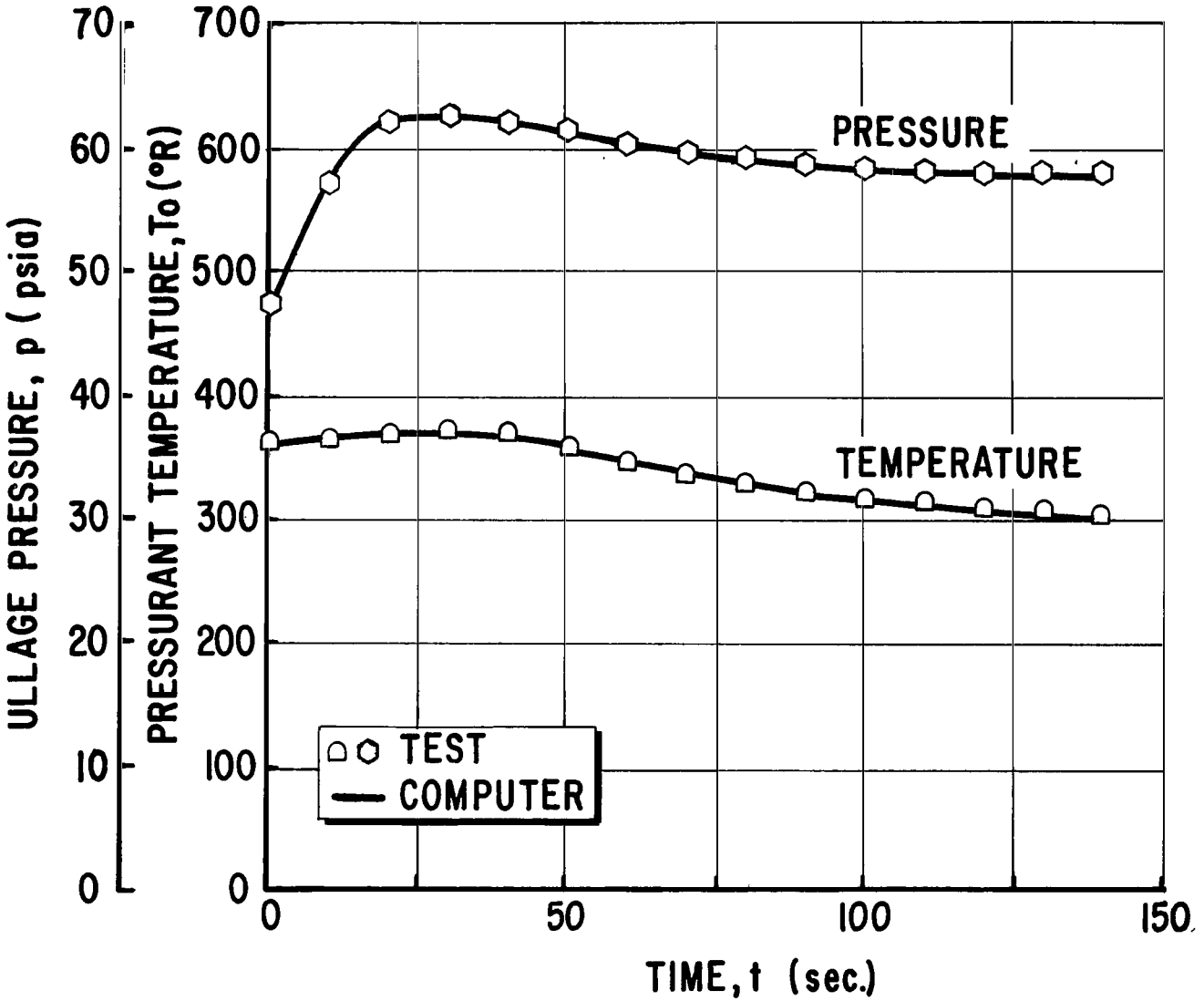

FIGURE 23d. ULLAGE PRESSURE AND PRESSURANT INLET TEMPERATURE HISTORIES, TANK CONFIGURATION C, TEST 130-9, OXYGEN AS PRESSURANT

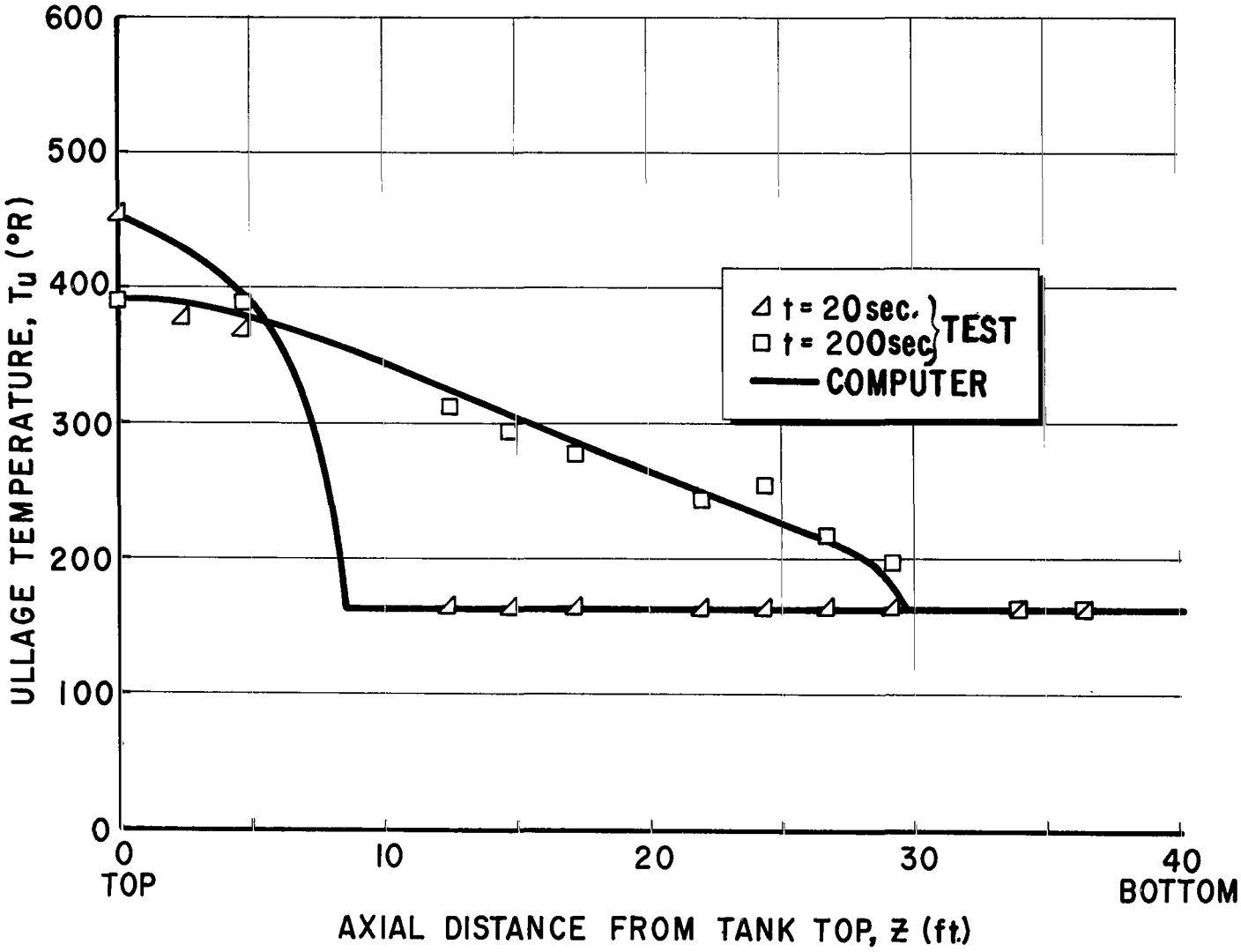

FIGURE 24a. COMPARISON BETWEEN EXPERIMENTAL AND COMPUTED ULLAGE TEMPERATURE GRADIENT, TANK CONFIGURATION C, TEST 130-10, OXYGEN AS PRESSURANT

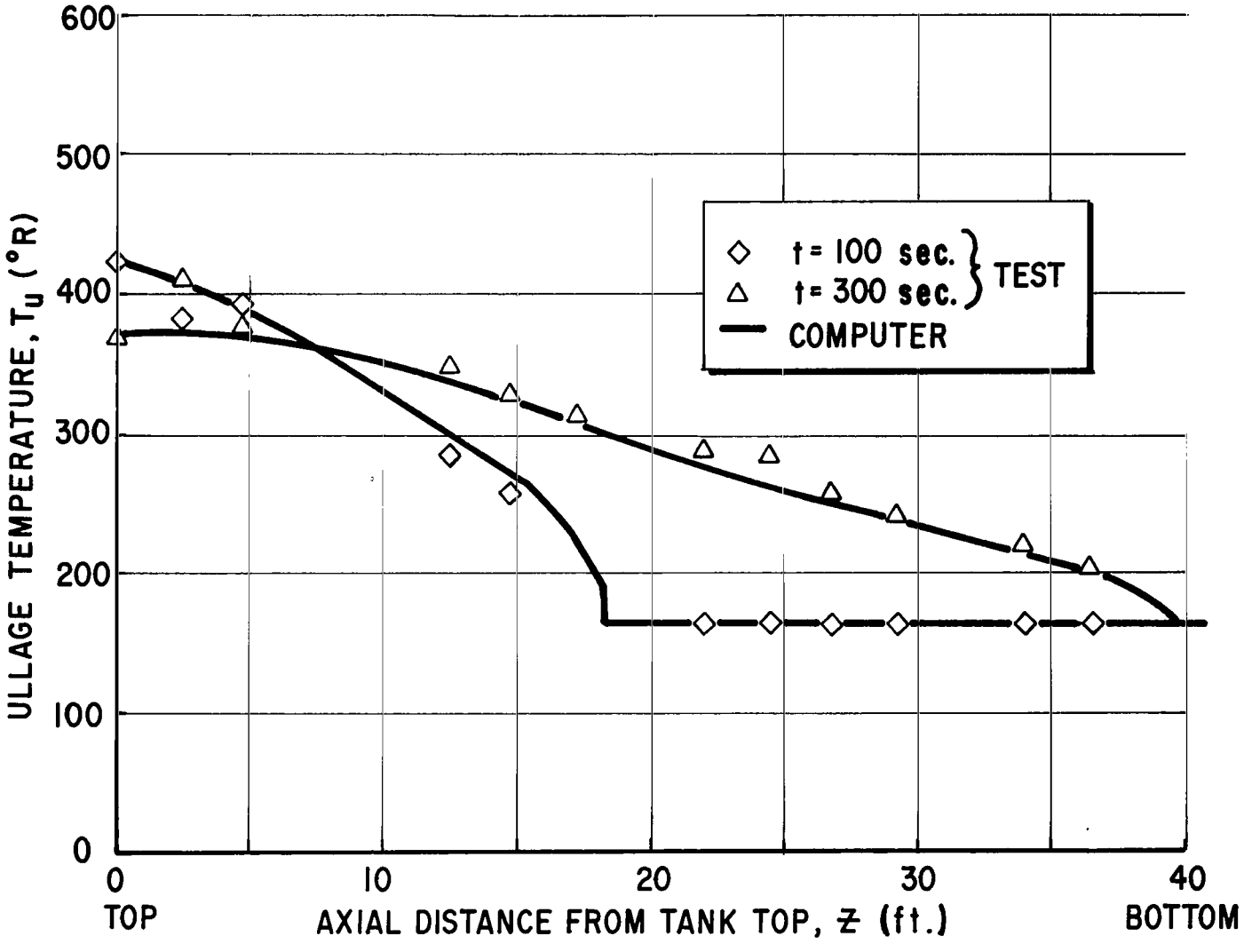

FIGURE 24b. COMPARISON BETWEEN EXPERIMENTAL AND COMPUTED ULLAGE TEMPERATURE GRADIENT, TANK CONFIGURATION C, TEST 130-10, OXYGEN AS PRESSURANT

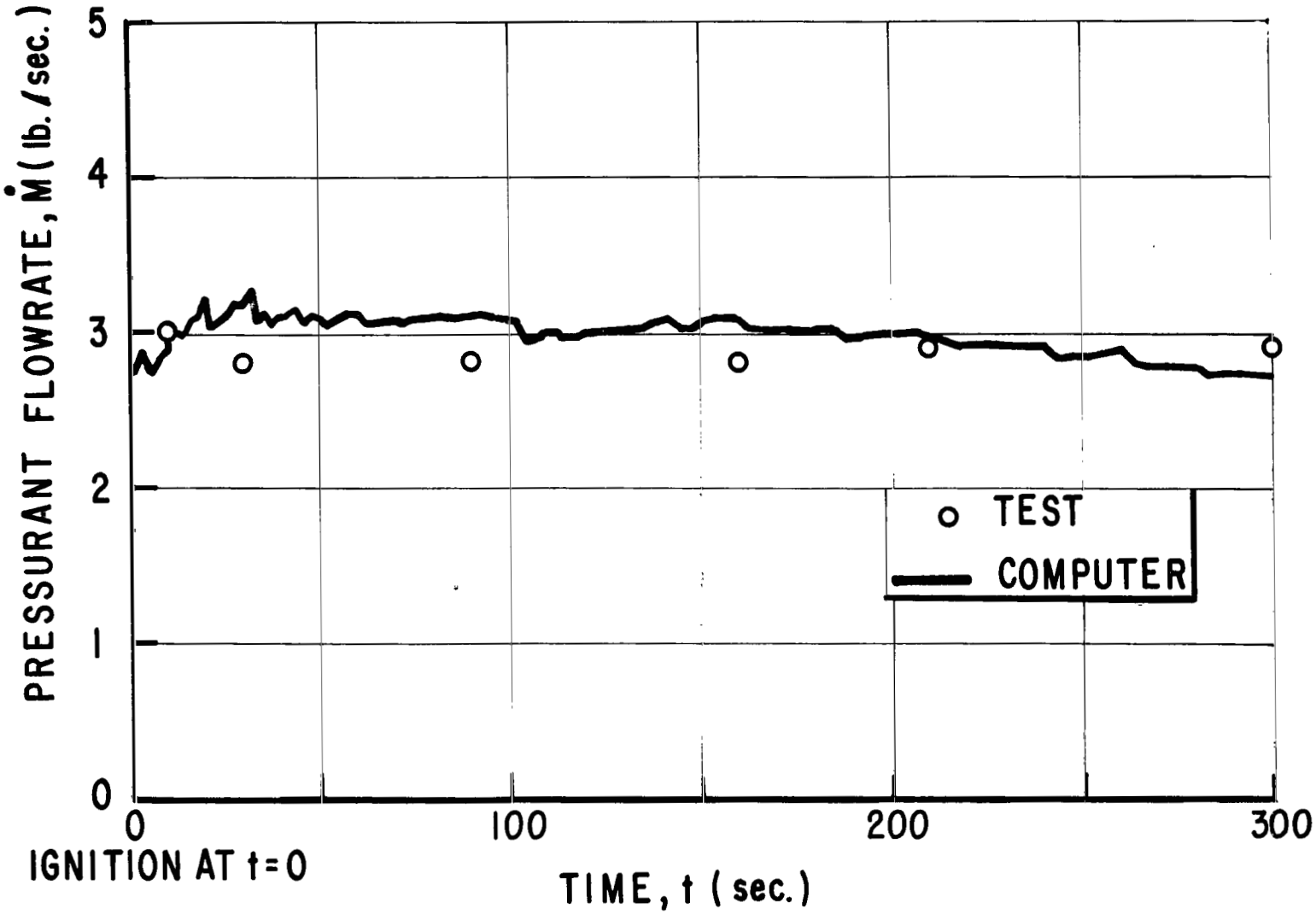

FIGURE 24c. COMPARISON BETWEEN EXPERIMENTAL AND COMPUTED PRESSURANT FLOWRATE, TANK CONFIGURATION C, TEST 130-10, OXYGEN AS PRESSURANT

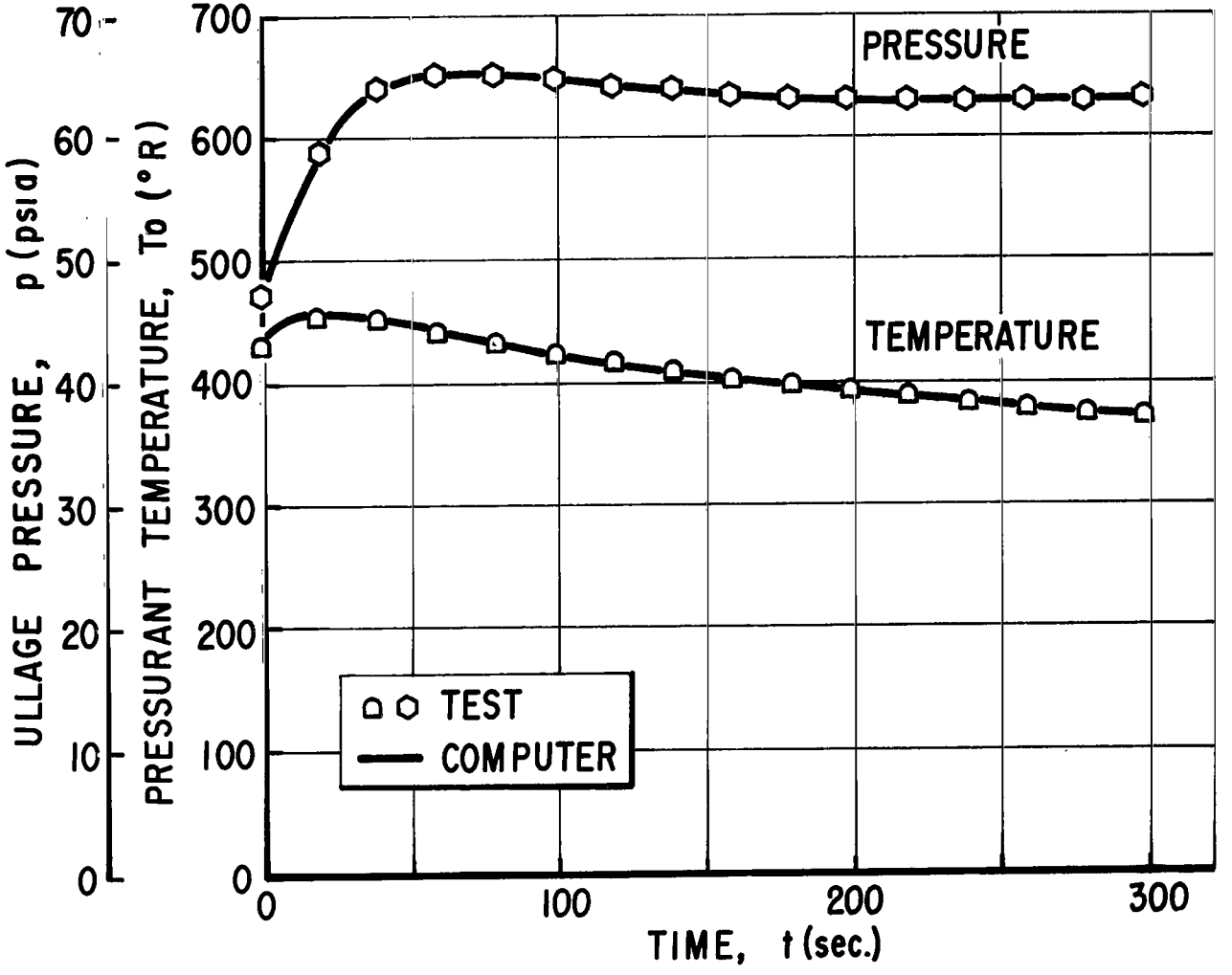

FIGURE 24d. ULLAGE PRESSURE AND PRESSURANT INLET HISTORIES, TANK CONFIGURATION C, TEST 130-10, OXYGEN AS PRESSURANT

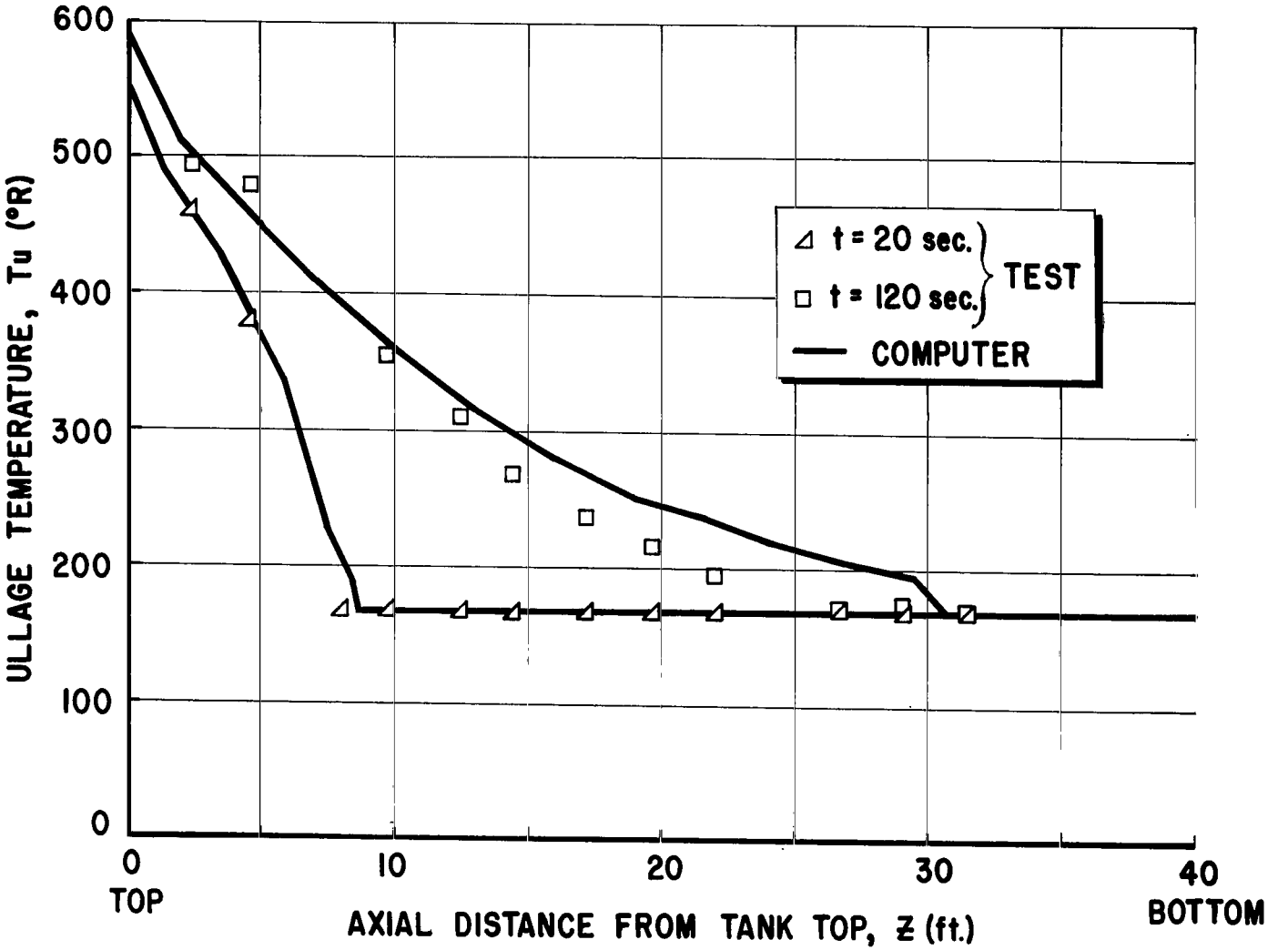

FIGURE 25a. COMPARISON BETWEEN EXPERIMENTAL AND COMPUTED ULLAGE TEMPERATURE GRADIENT, TANK CONFIGURATION C, TEST 130-15, HELIUM AS PRESSURANT

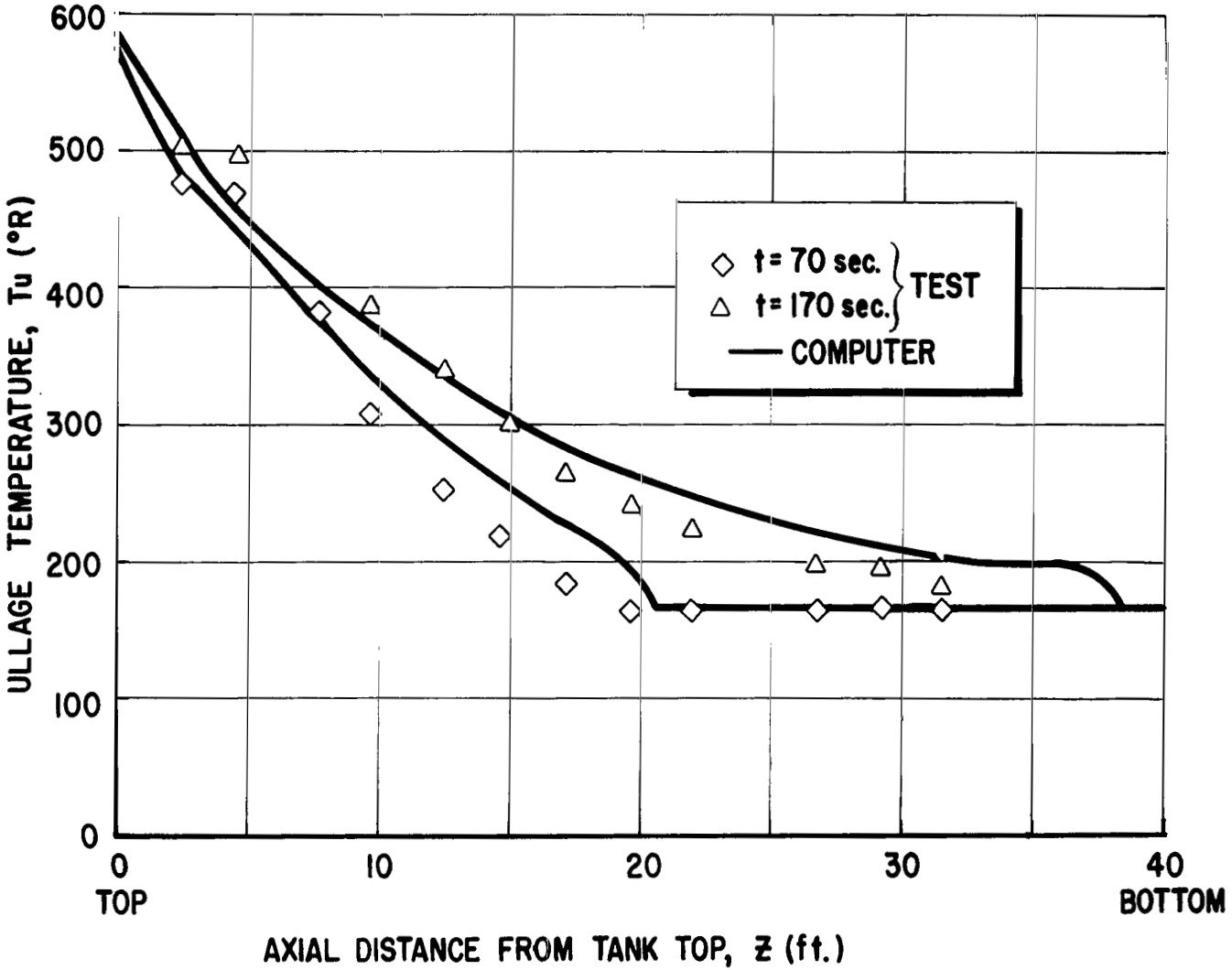

FIGURE 25b. COMPARISON BETWEEN EXPERIMENTAL AND COMPUTED ULLAGE TEMPERATURE GRADIENT, TANK CONFIGURATION C, TEST 130-15, HELIUM AS PRESSURANT

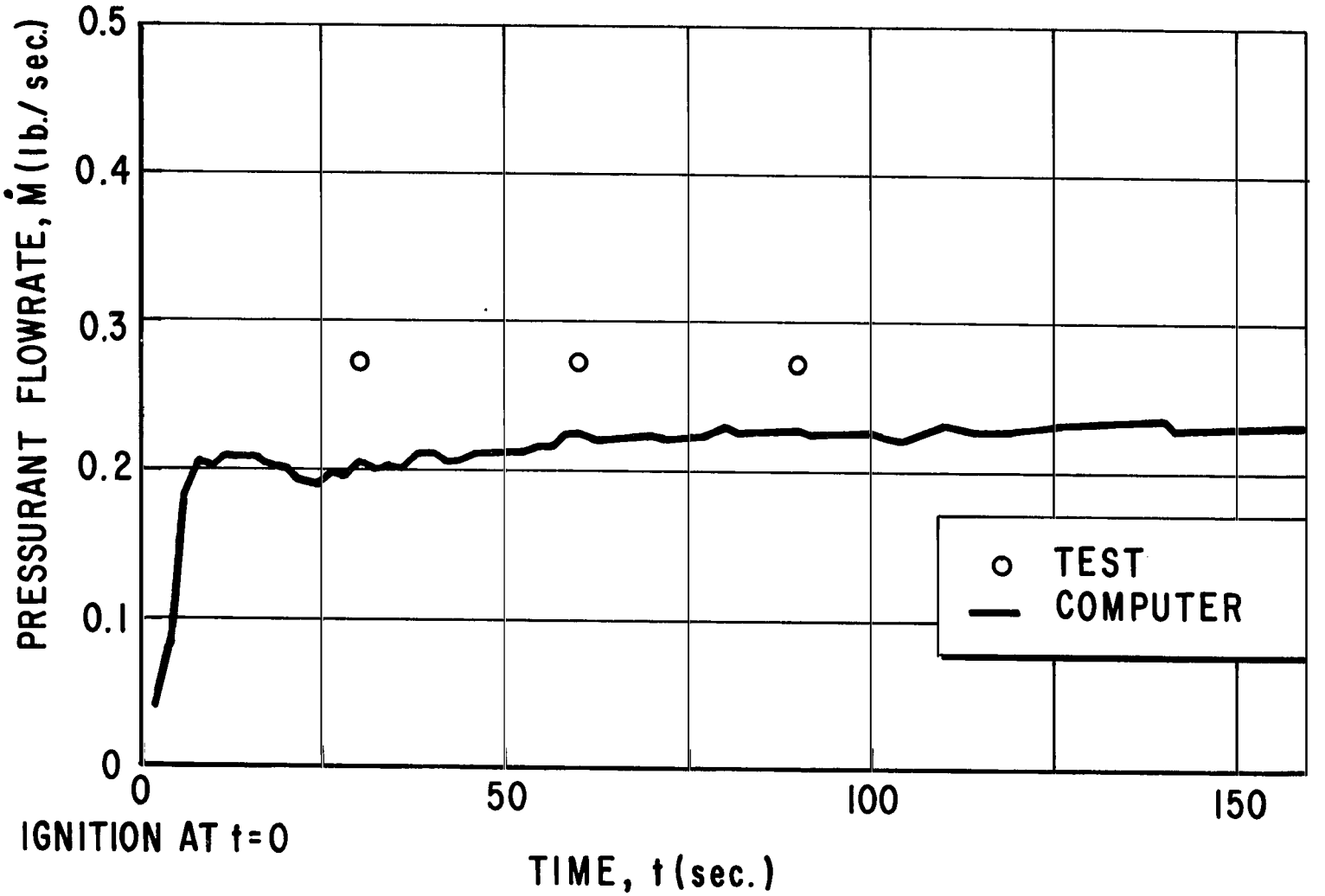

FIGURE 25c. COMPARISON BETWEEN EXPERIMENTAL AND COMPUTED PRESSURANT FLOWRATE, TANK CONFIGURATION C, TEST 130-15, HELIUM AS PRESSURANT

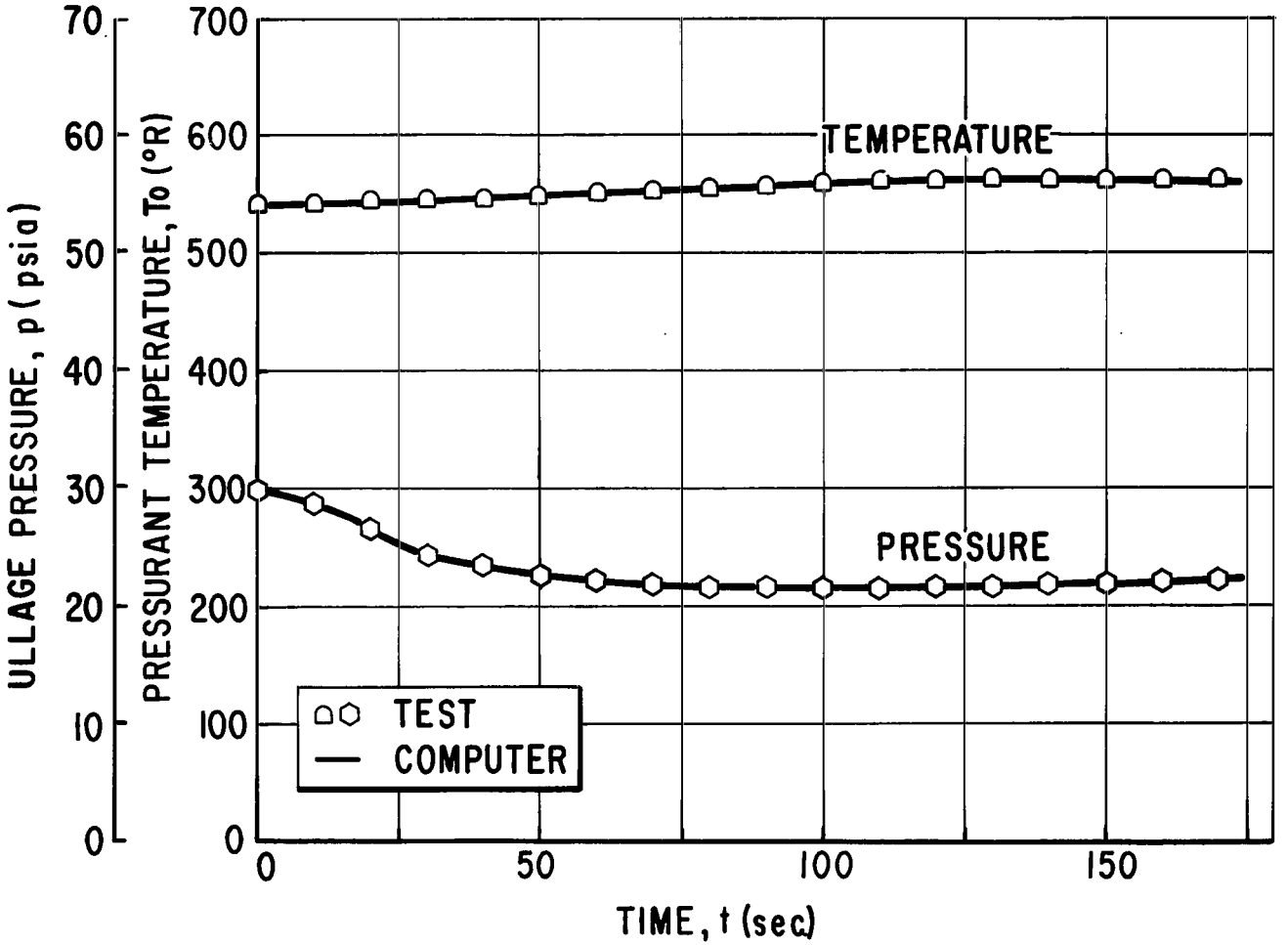

FIGURE 25d. ULLAGE PRESSURE AND PRESSURANT INLET TEMPERATURE HISTORIES, TANK CONFIGURATION C, TEST 130-15, HELIUM AS PRESSURANT

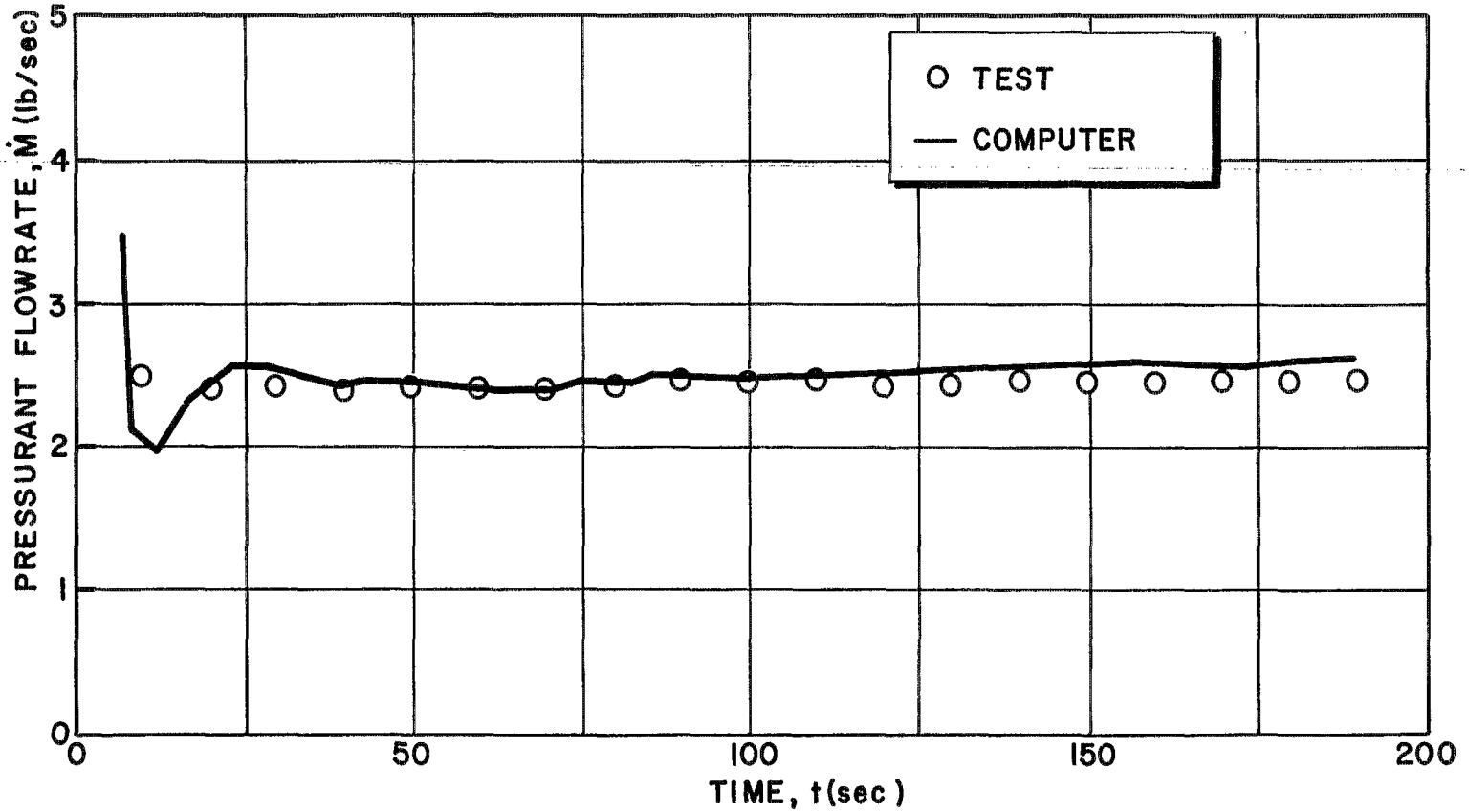

FIGURE 26a. COMPARISON BETWEEN EXPERIMENTAL AND COMPUTED PRESSURANT FLOWRATE, TANK CONFIGURATION D, TEST C 003-7a, OXYGEN AS PRESSURANT

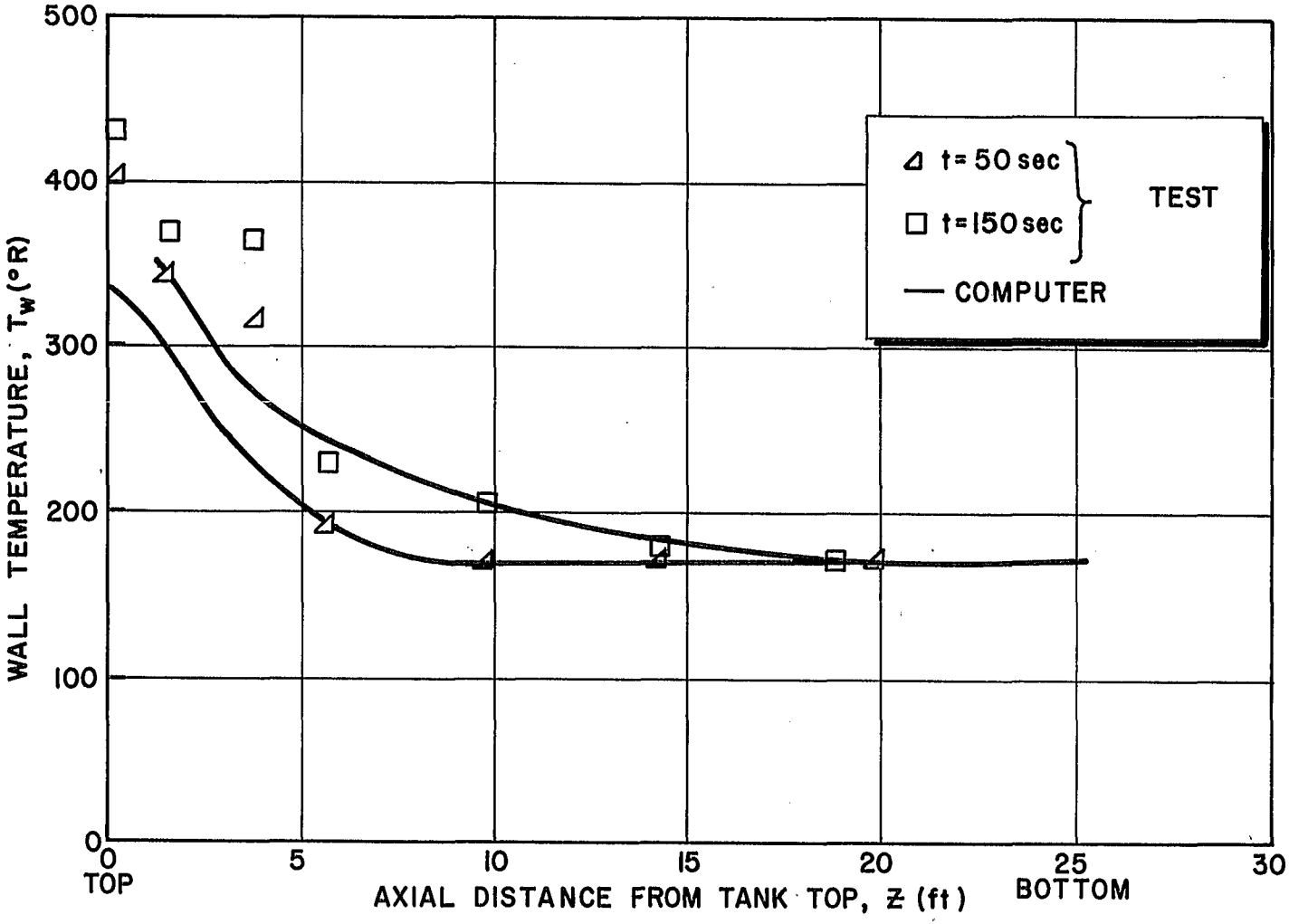

FIGURE 26b. COMPARISON BETWEEN EXPERIMENTAL AND COMPUTED TANK WALL TEMPERATURES, TANK CONFIGURATION D, TEST C007-7a, OXYGEN AS PRESSURANT

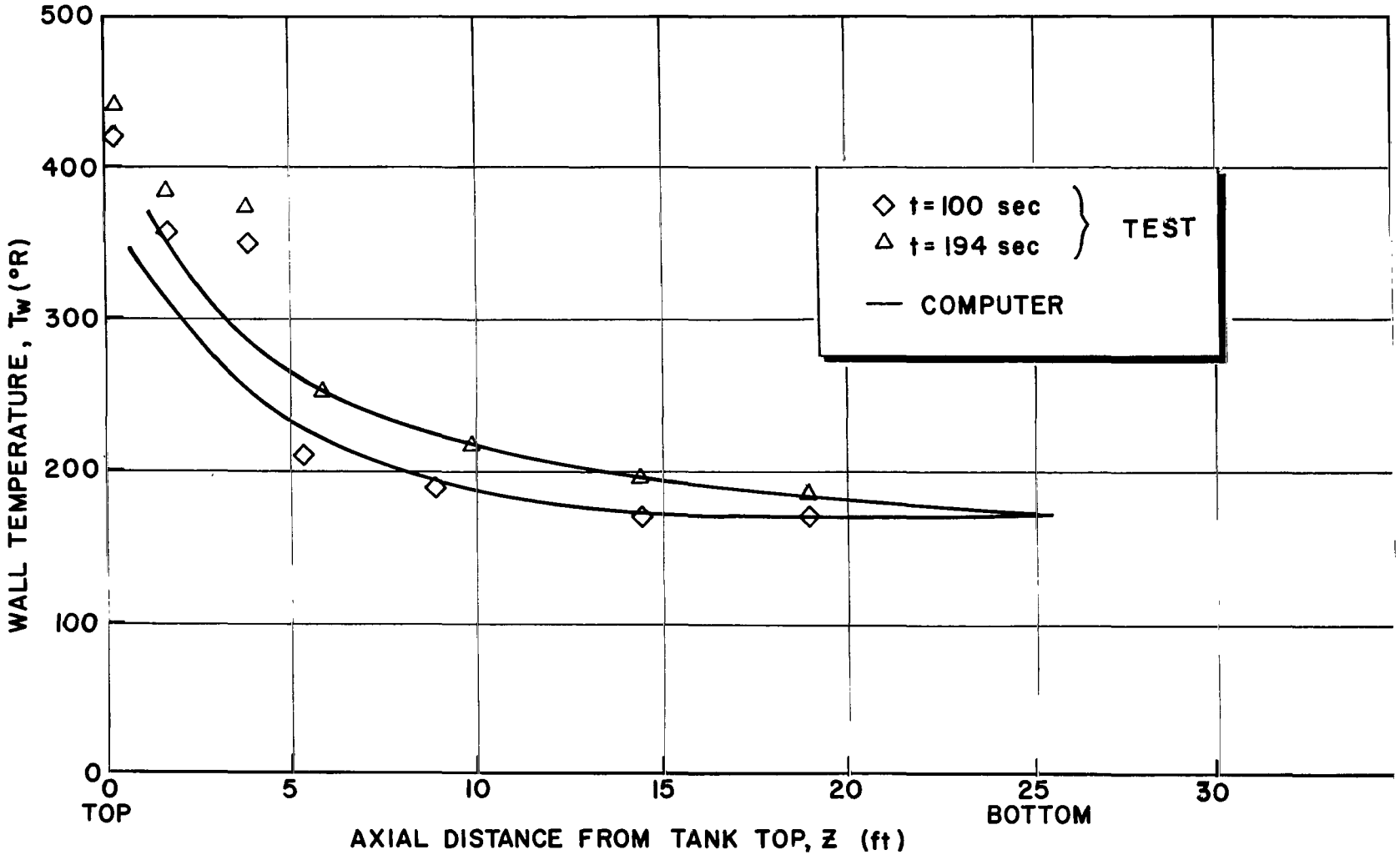

FIGURE 26c. COMPARISON BETWEEN EXPERIMENTAL AND COMPUTED TANK WALL TEMPERATURES, TANK CONFIGURATION D, TEST C003-7a, OXYGEN AS PRESSURANT

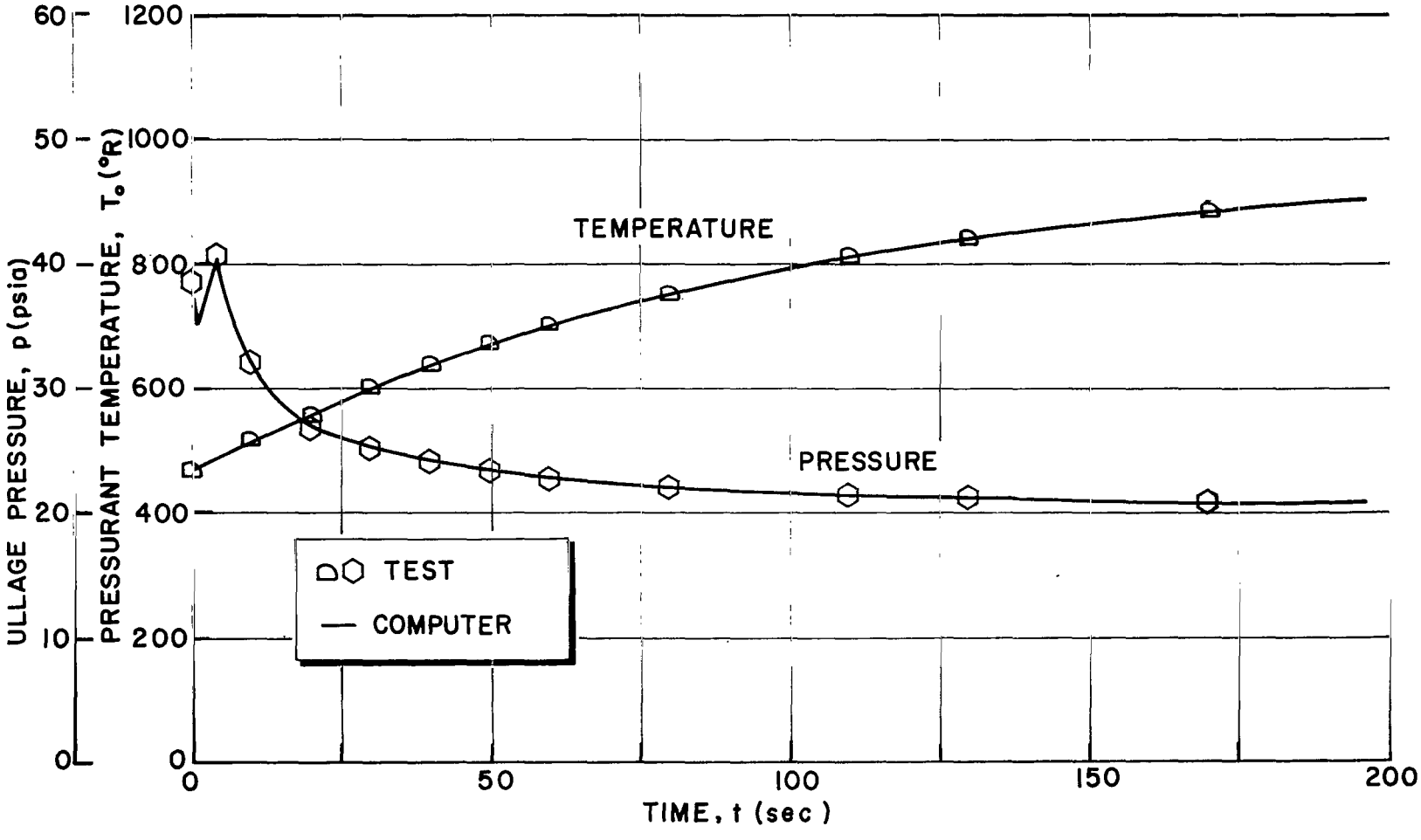

FIGURE 26d. ULLAGE PRESSURE AND PRESSURANT INLET TEMPERATURE HISTORIES, TANK CONFIGURATION D, TEST C003-7a, OXYGEN AS PRESSURANT

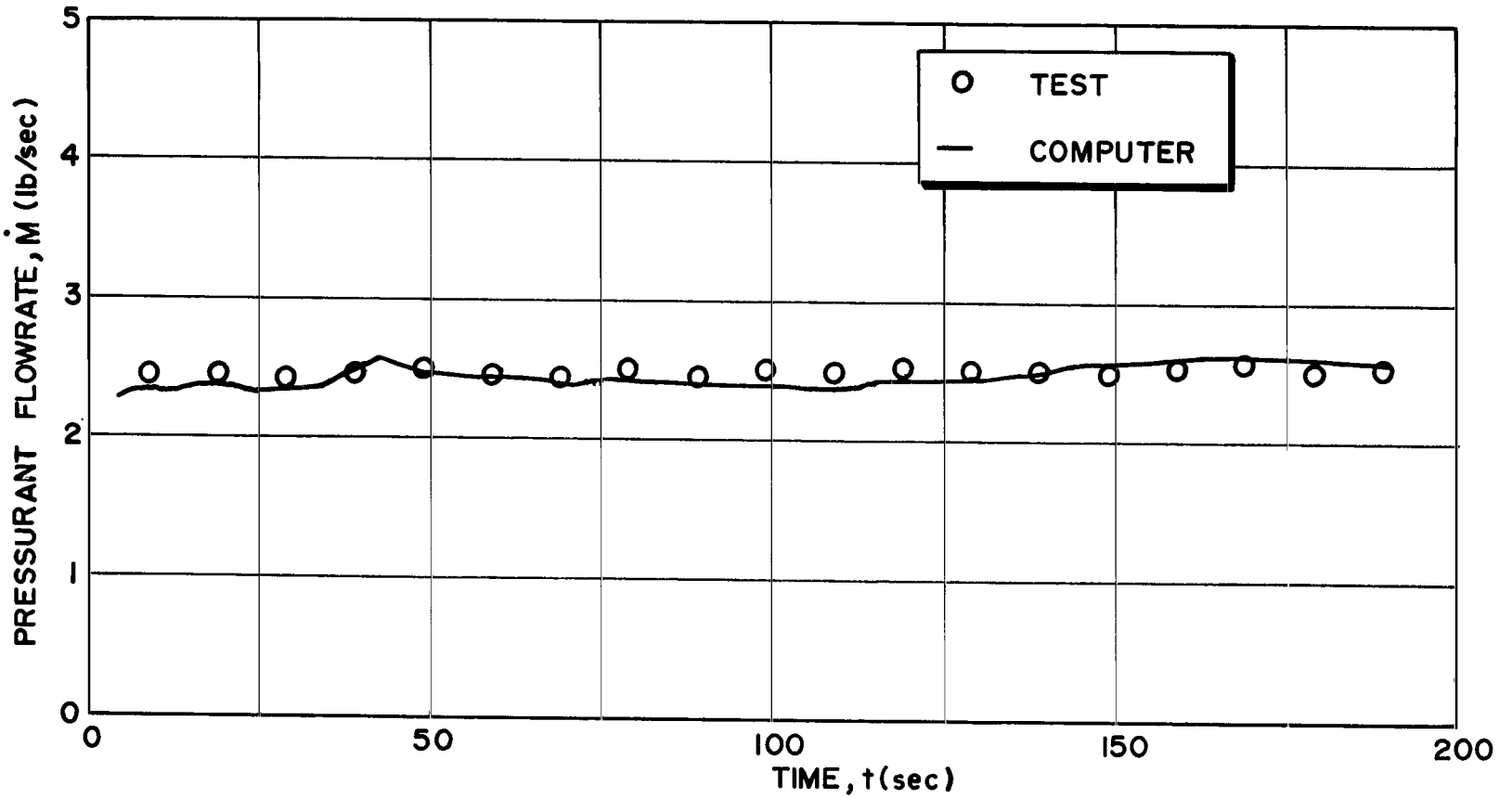

FIGURE 27a. COMPARISON BETWEEN EXPERIMENTAL AND COMPUTED PRESSURANT FLOWRATE, TANK CONFIGURATION D, TEST C003-12, OXYGEN AS PRESSURANT

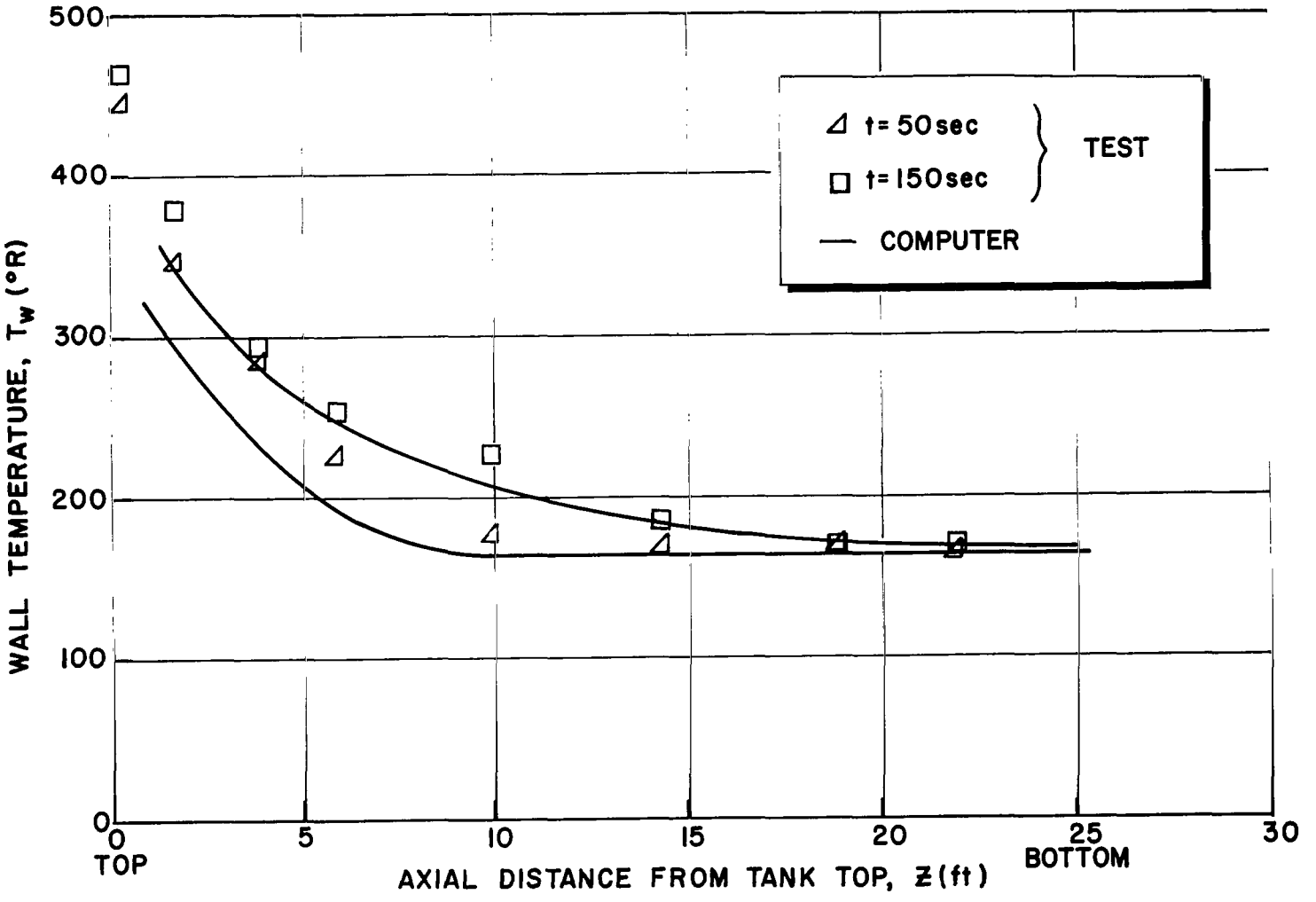

FIGURE 27b. COMPARISON BETWEEN EXPERIMENTAL AND COMPUTED TANK WALL TEMPERATURES, TANK CONFIGURATION D, TEST C003-12, OXYGEN AS PRESSURANT

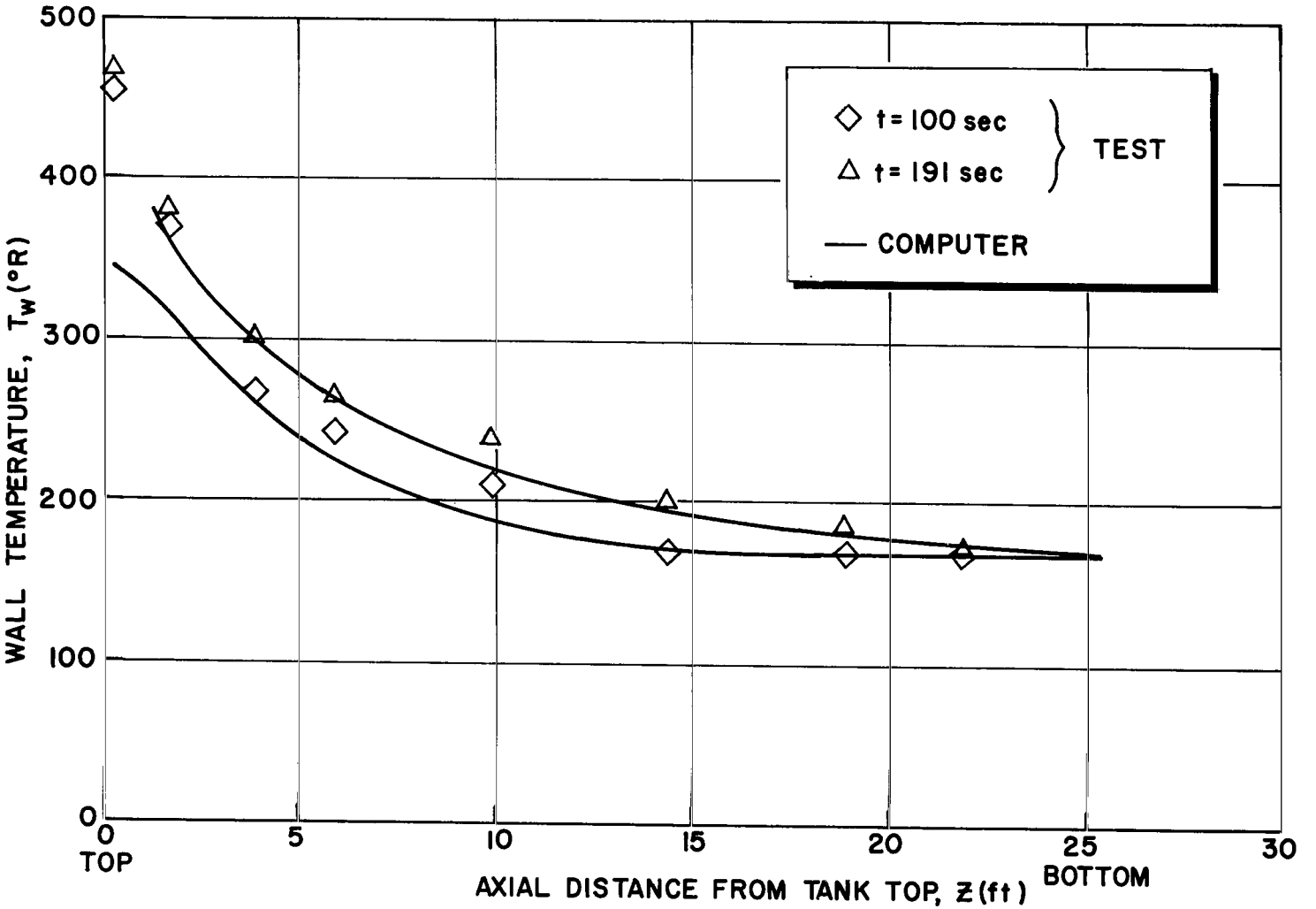

FIGURE 27c. COMPARISON BETWEEN EXPERIMENTAL AND COMPUTED TANK WALL TEMPERATURES, TANK CONFIGURATION D, TEST C003-12, OXYGEN AS PRESSURANT

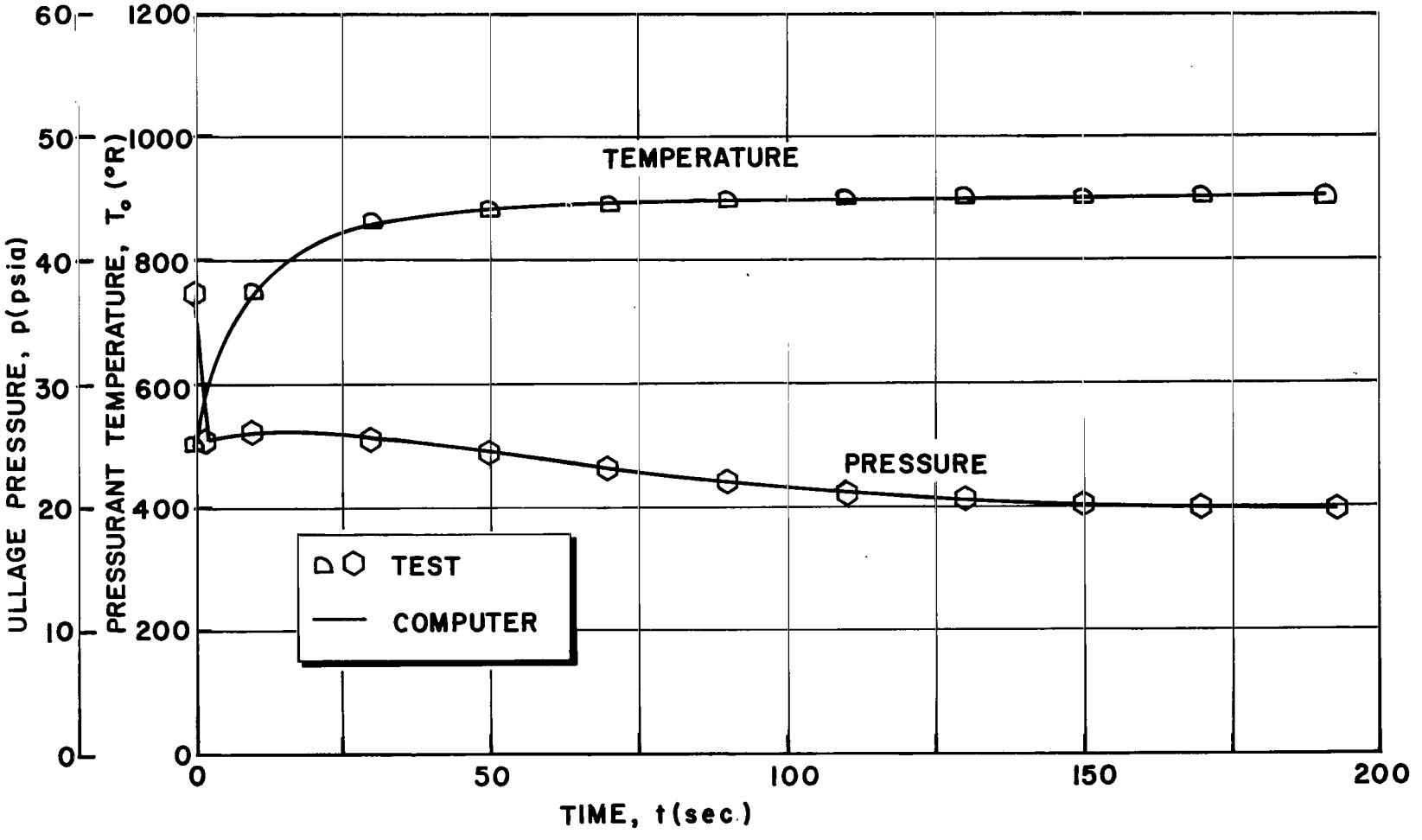

FIGURE 27d. ULLAGE PRESSURE AND PRESSURANT INLET TEMPERATURE HISTORIES, TANK CONFIGURATION D, TEST C003-12, OXYGEN AS PRESSURANT

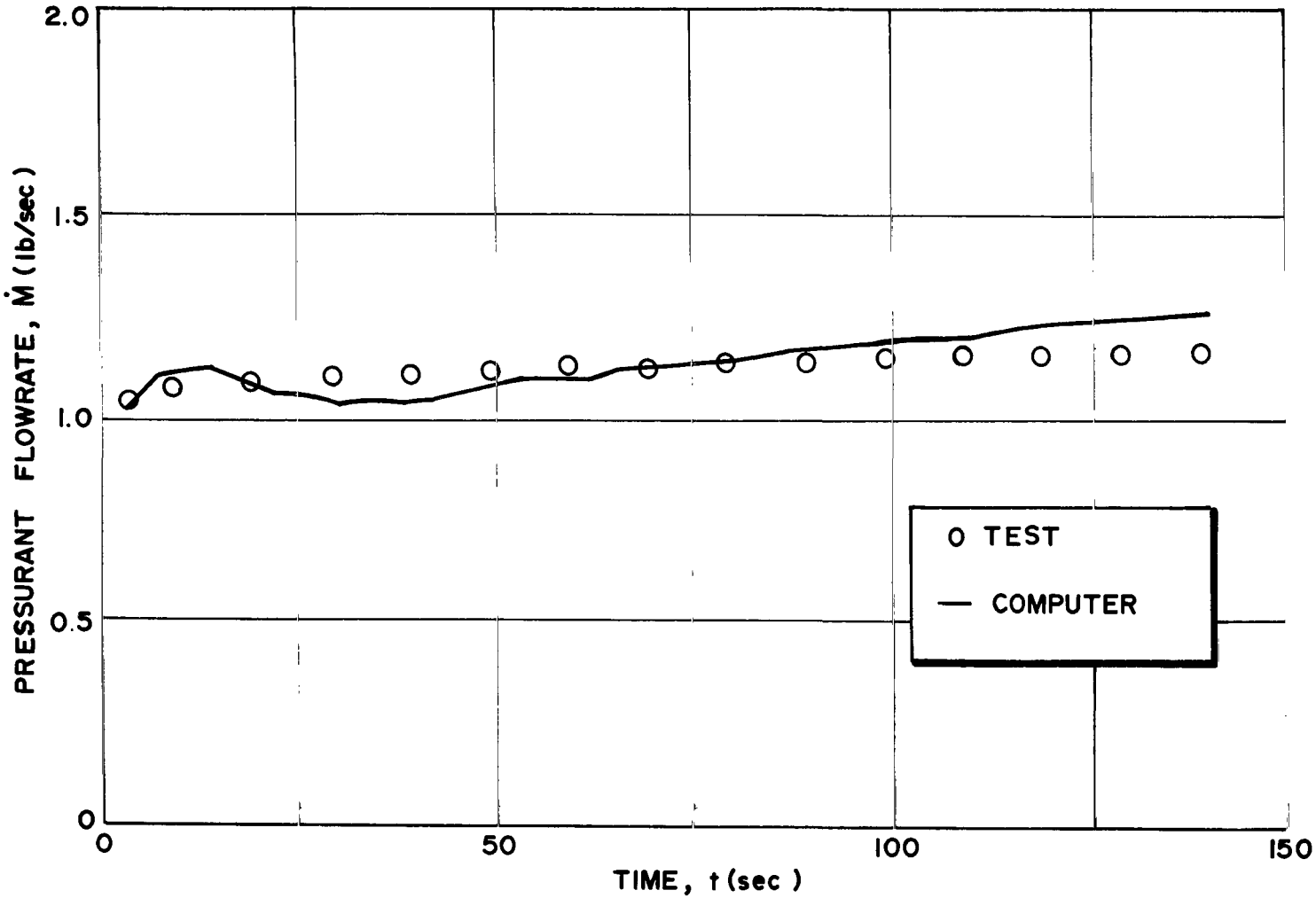

FIGURE 28a. COMPARISON BETWEEN EXPERIMENTAL AND COMPUTED PRESSURANT FLOWRATE, TANK CONFIGURATION D, TEST C003-10, HELIUM AS PRESSURANT

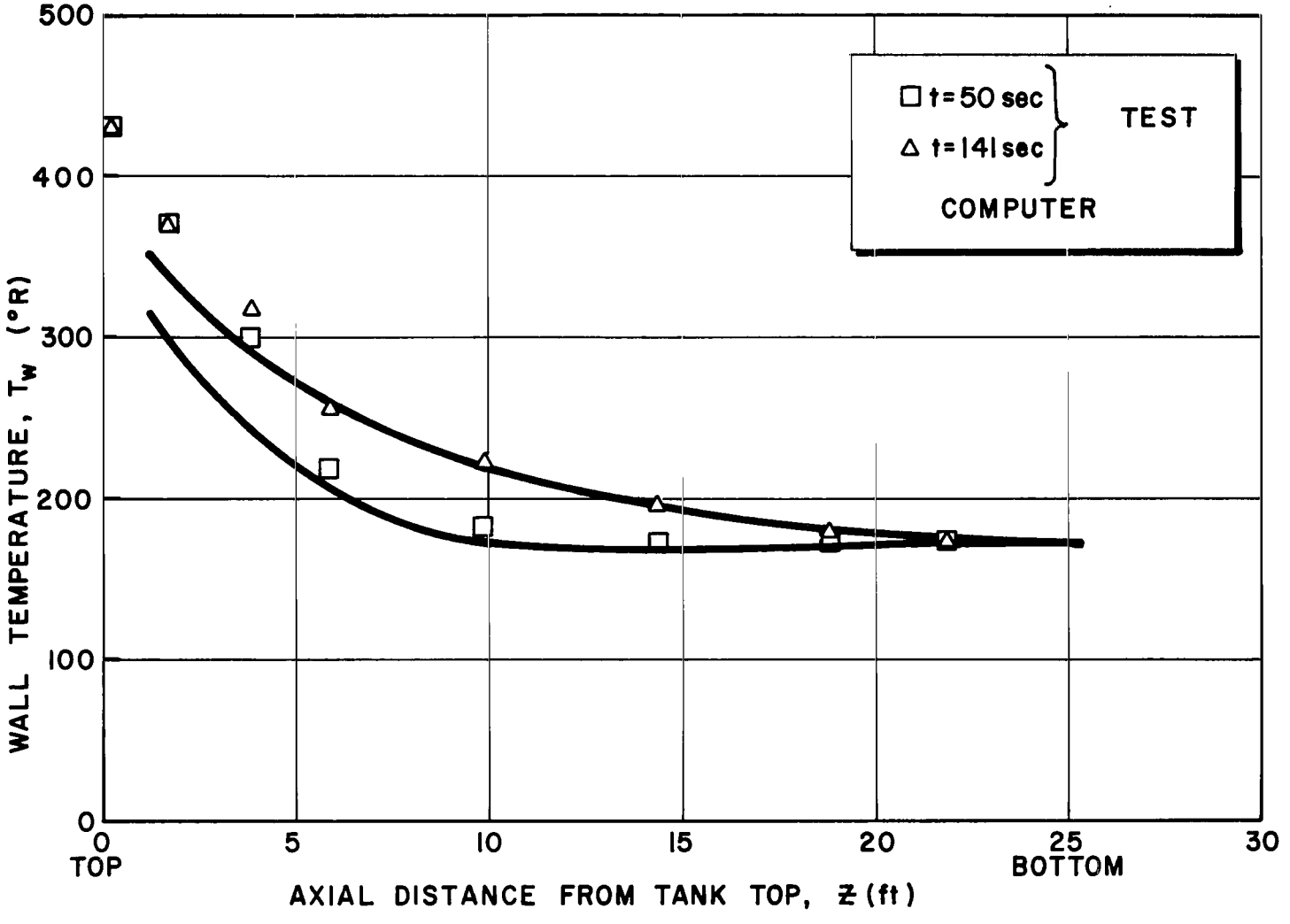

FIGURE 28b. COMPARISON BETWEEN EXPERIMENTAL AND COMPUTED TANK WALL TEMPERATURES, TANK CONFIGURATION D, TEST C003-10, HELIUM AS PRESSURANT

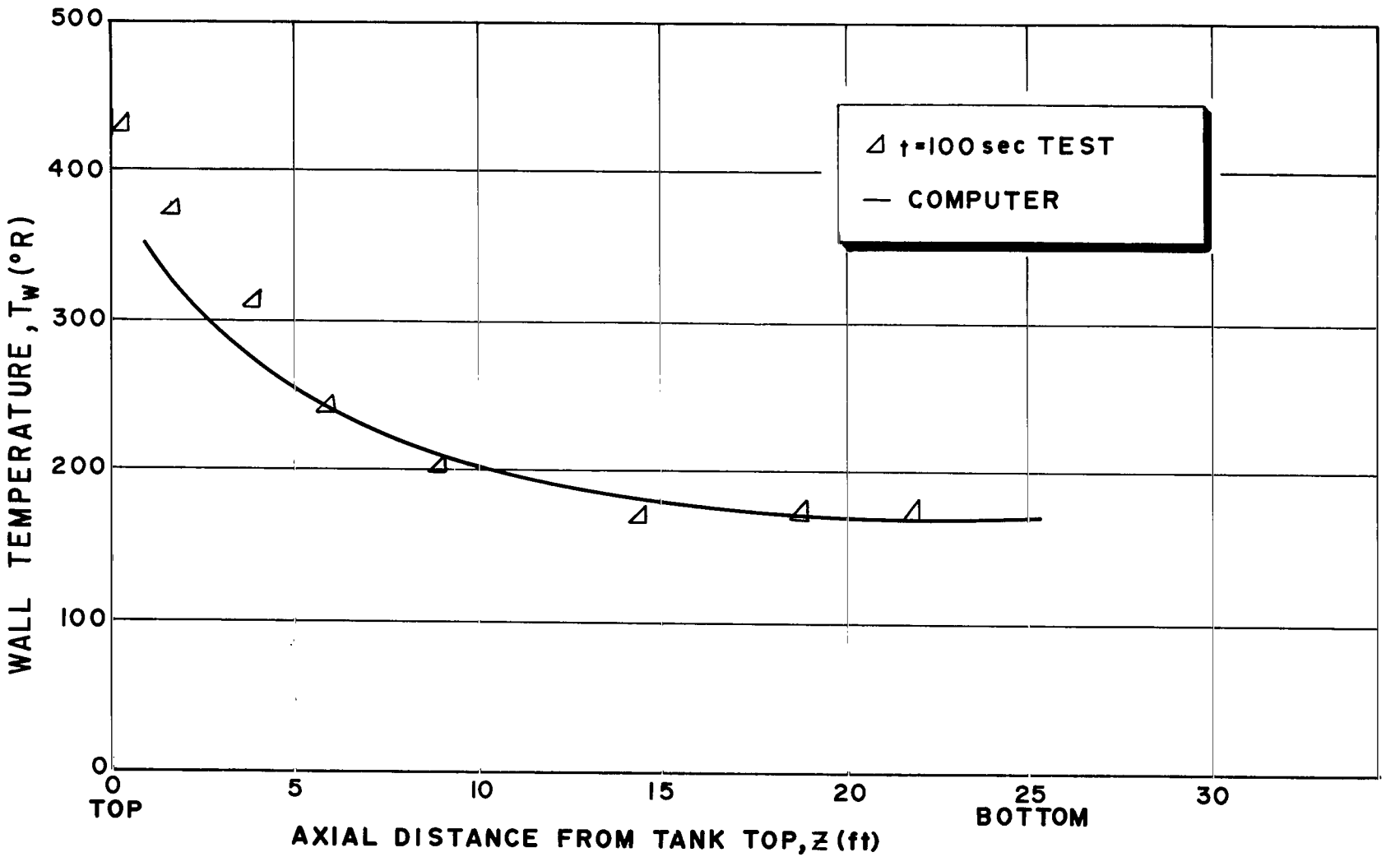

FIGURE 28c. COMPARISON BETWEEN EXPERIMENTAL AND COMPUTED TANK WALL TEMPERATURES, TANK CONFIGURATION D, TEST C003-10, HELIUM AS PRESSURANT

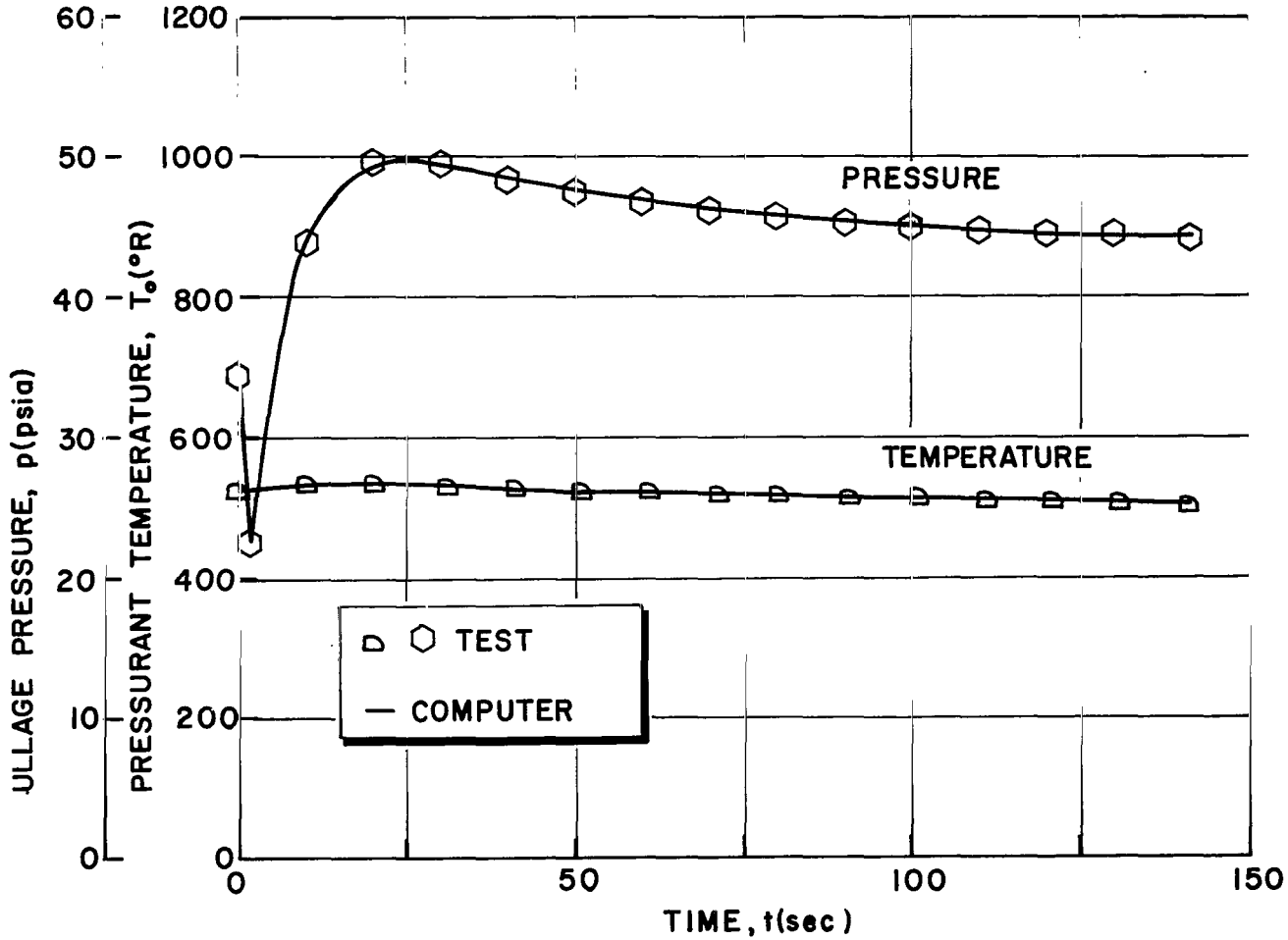

FIGURE 28d. ULLAGE PRESSURE AND PRESSURANT INLET TEMPERATURE HISTORIES, TANK CONFIGURATION D, TEST C003-10, HELIUM AS PRESSURANT

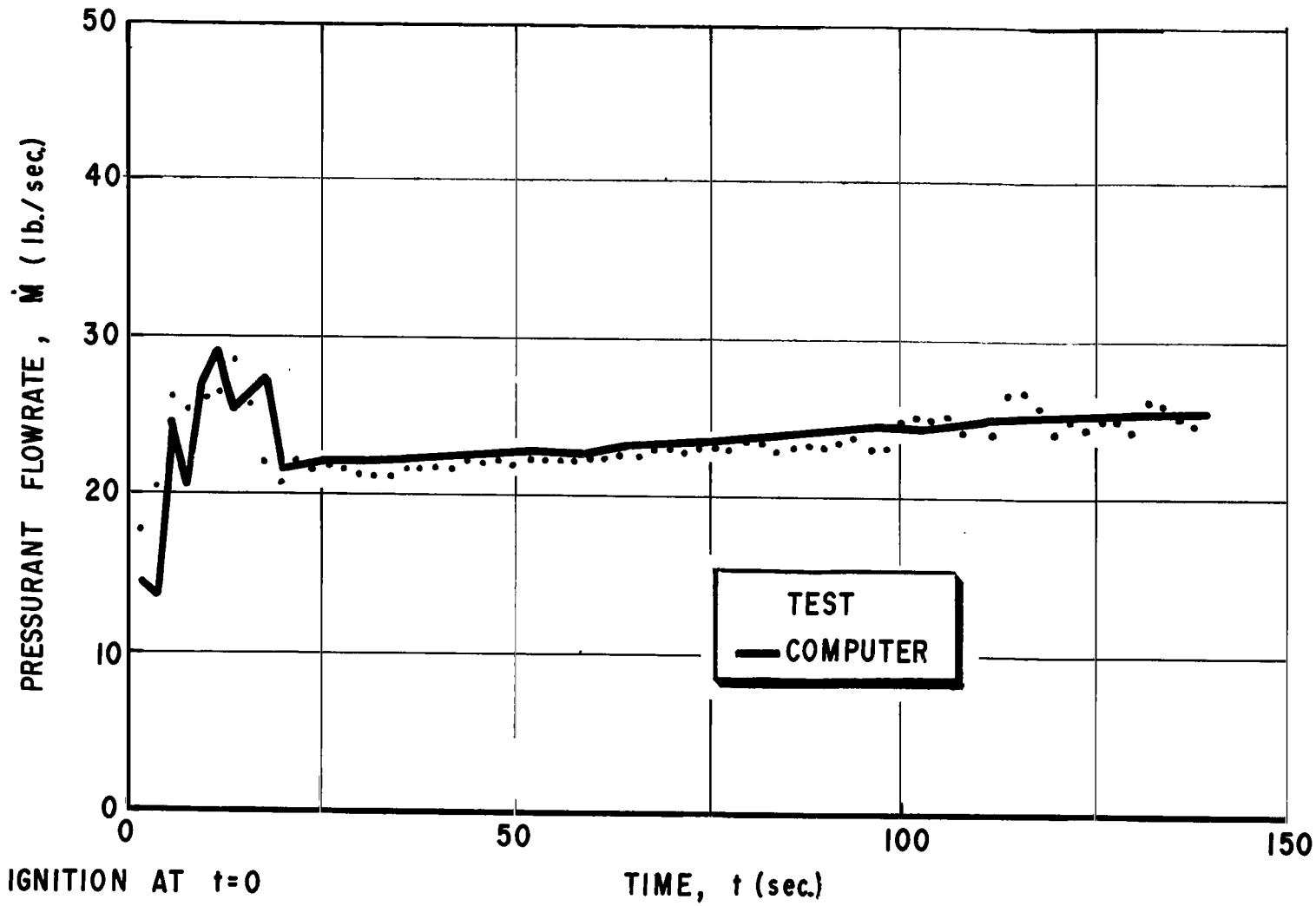

FIGURE 29a. COMPARISON BETWEEN EXPERIMENTAL AND COMPUTED PRESSURANT FLOWRATE, S-I STAGE LOX TANKS, SA-6 STATIC TEST, OXYGEN AS PRESSURANT

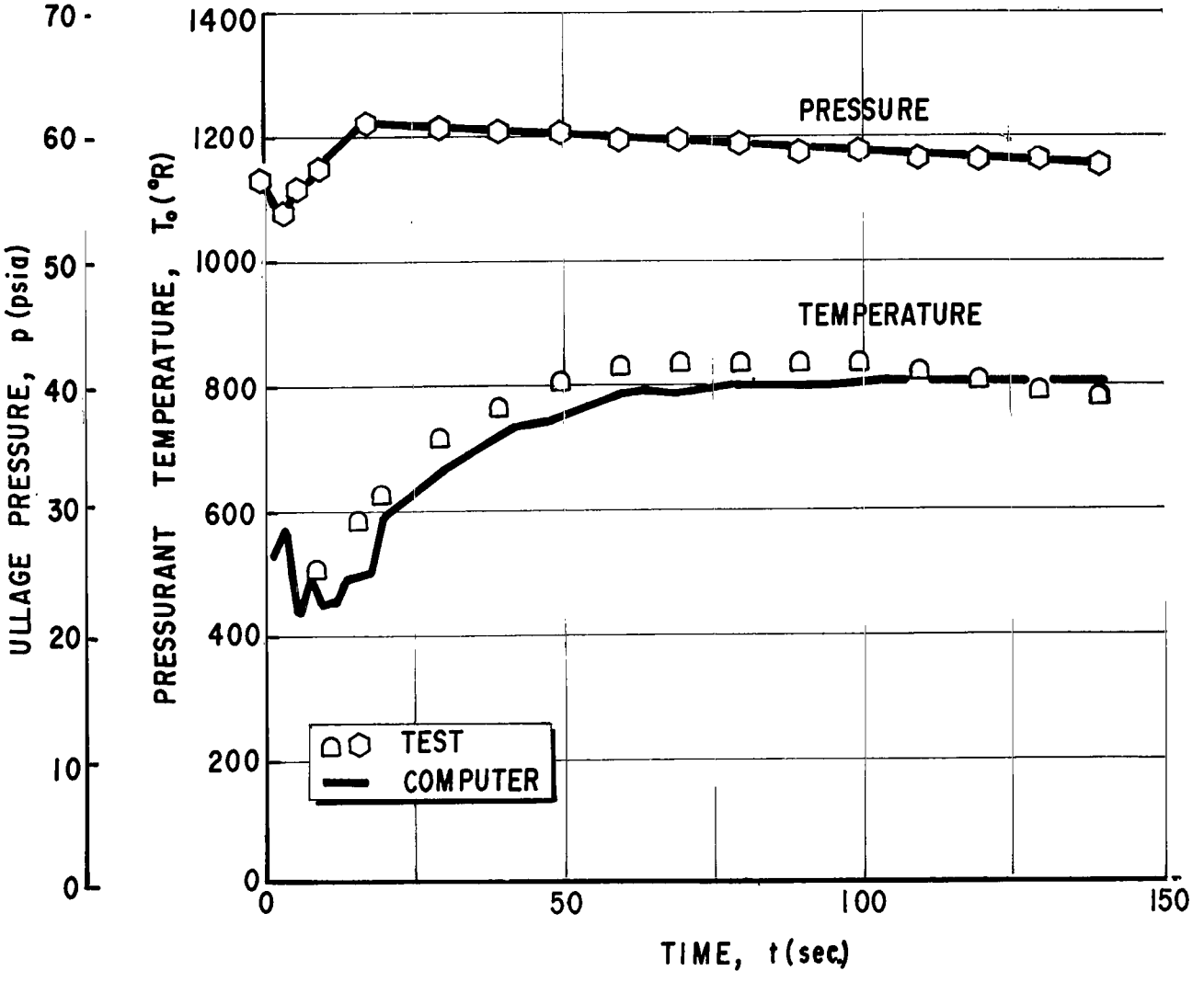

FIGURE 29b. ULLAGE PRESSURE AND PRESSURANT INLET TEMPERATURE HISTORIES, S-I STAGE LOX TANKS, SA-6 STATIC TEST, OXYGEN AS PRESSURANT

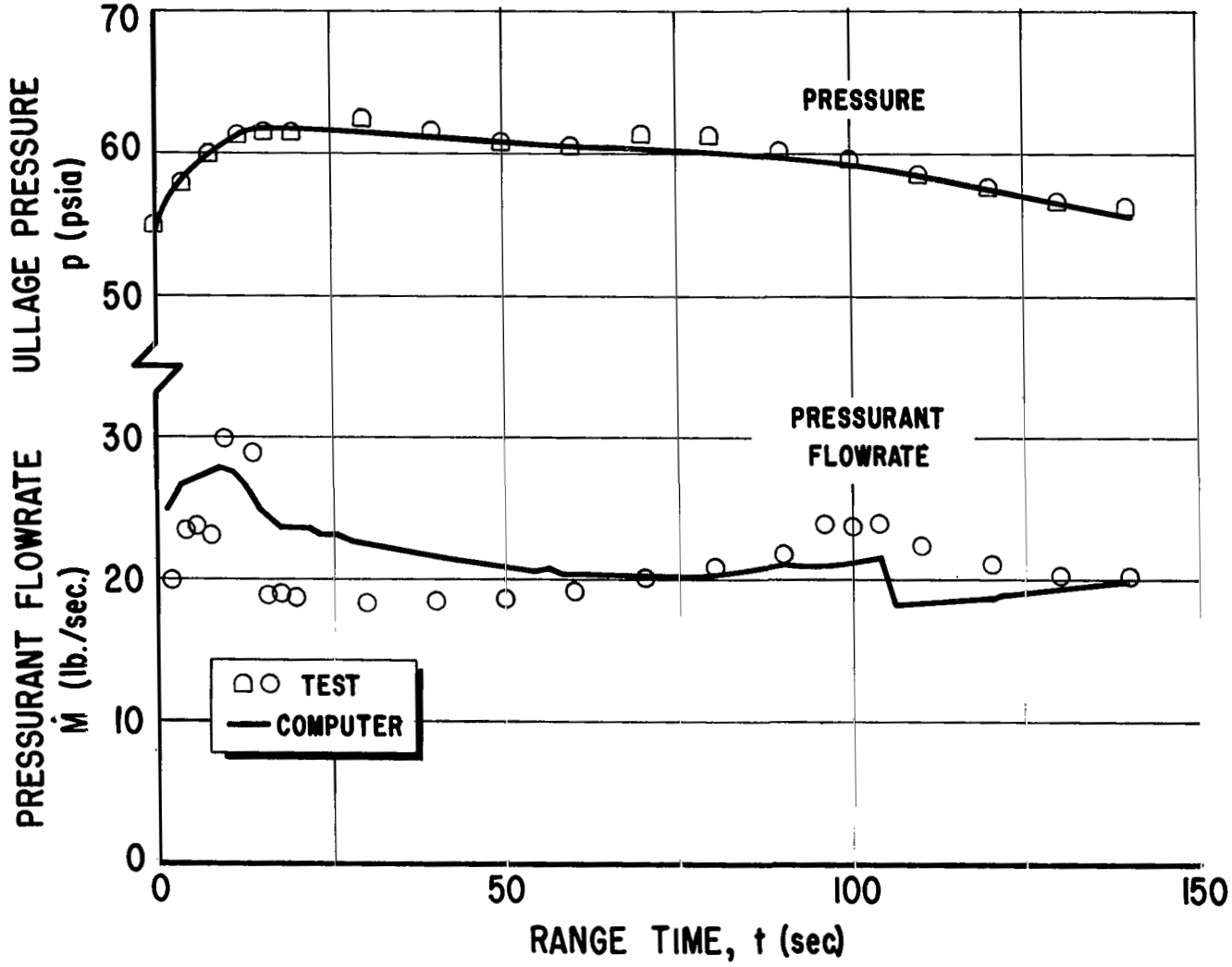

FIGURE 30. COMPARISON BETWEEN EXPERIMENTAL AND COMPUTED PRESSURANT FLOWRATE, S-I STAGE LOX TANKS, SA-5 FLIGHT TEST, OXYGEN AS PRESSURANT

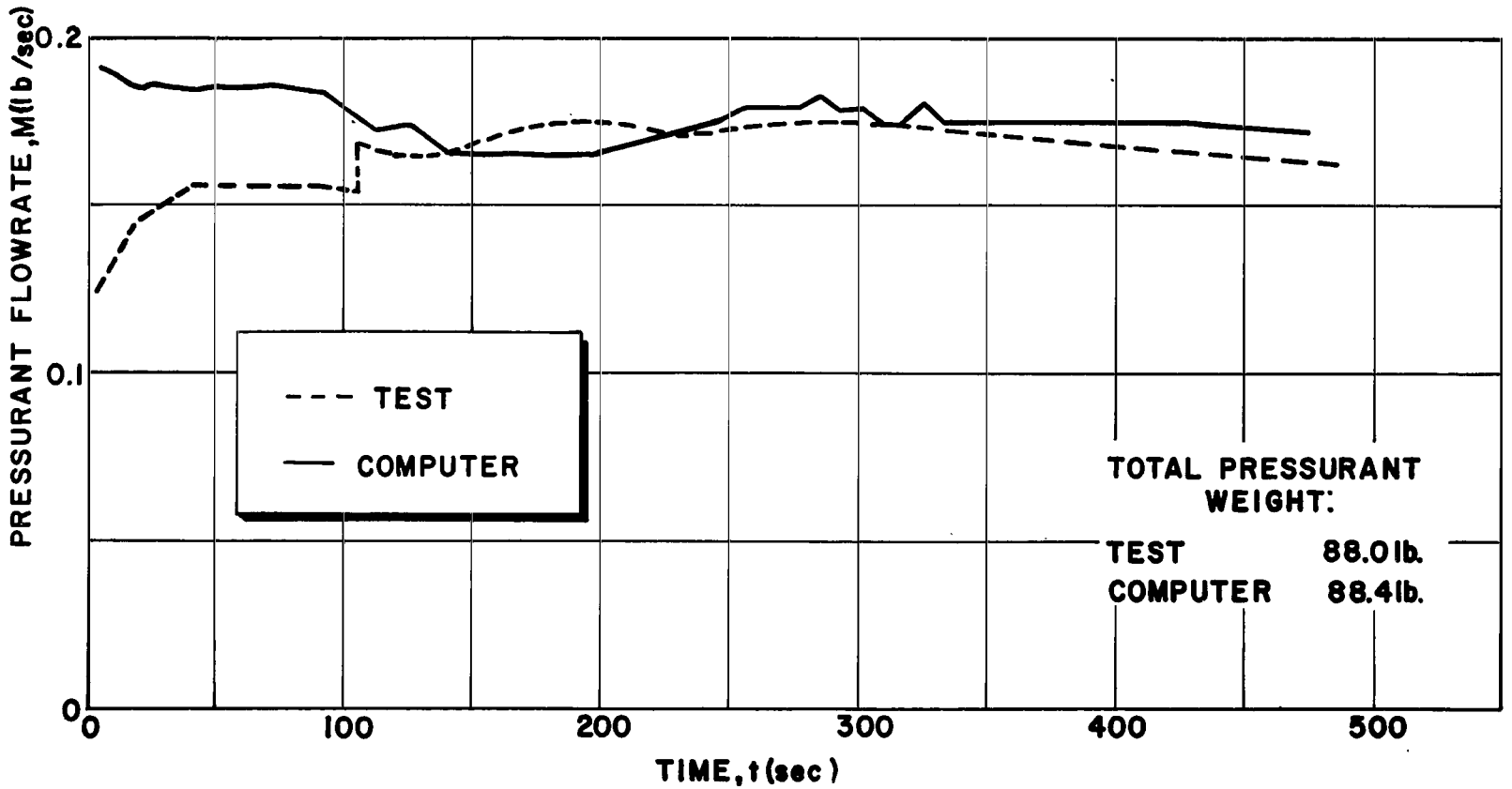

FIGURE 31a. COMPARISON BETWEEN EXPERIMENTAL AND COMPUTED PRESSURANT FLOWRATE, S-IV STAGE LOX TANK, HELIUM AS PRESSURANT

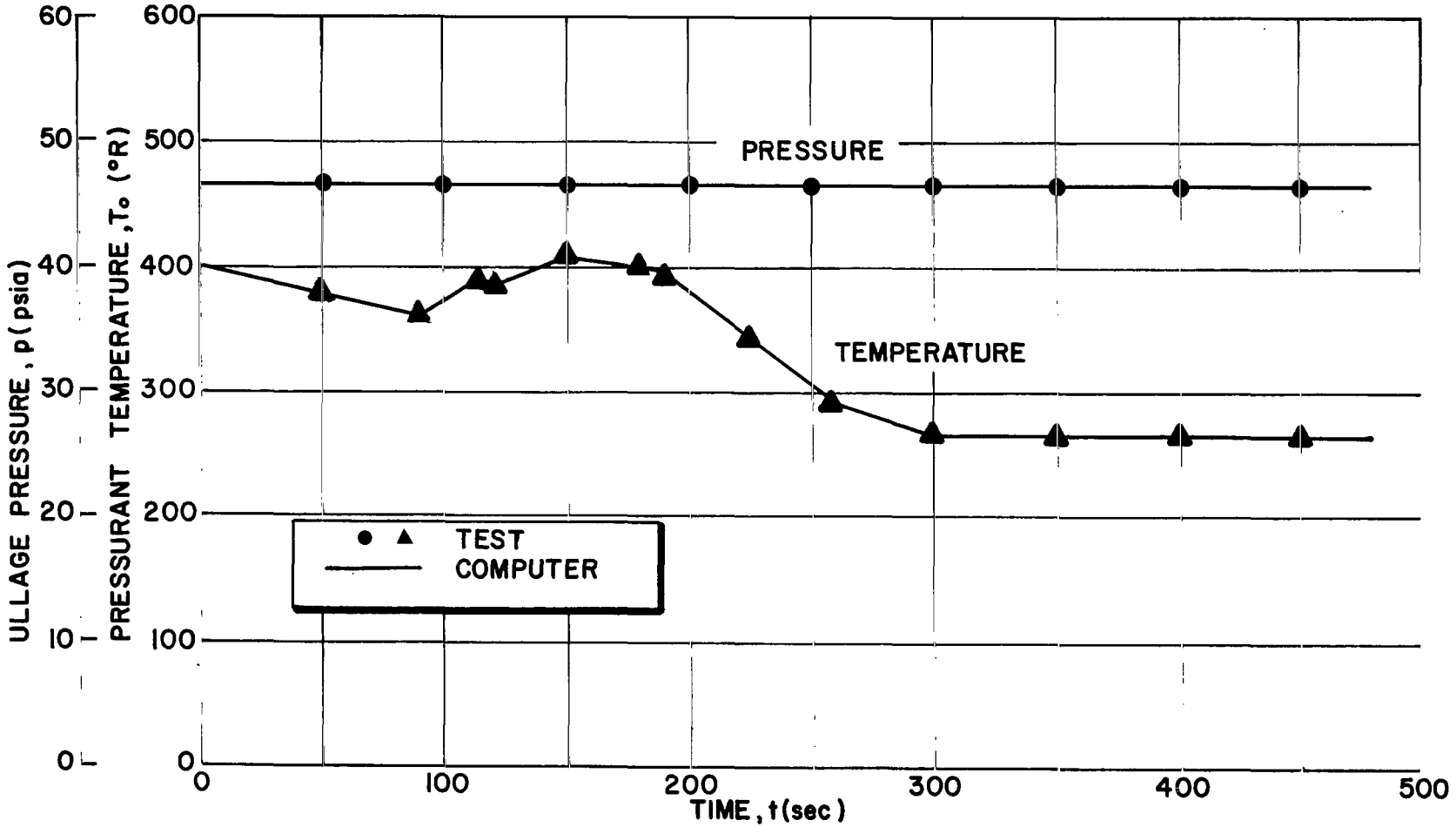

FIGURE 31b. ULLAGE PRESSURE AND PRESSURANT INLET TEMPERATURE HISTORIES, S-IV STAGE LOX TANK, HELIUM AS PRESSURANT

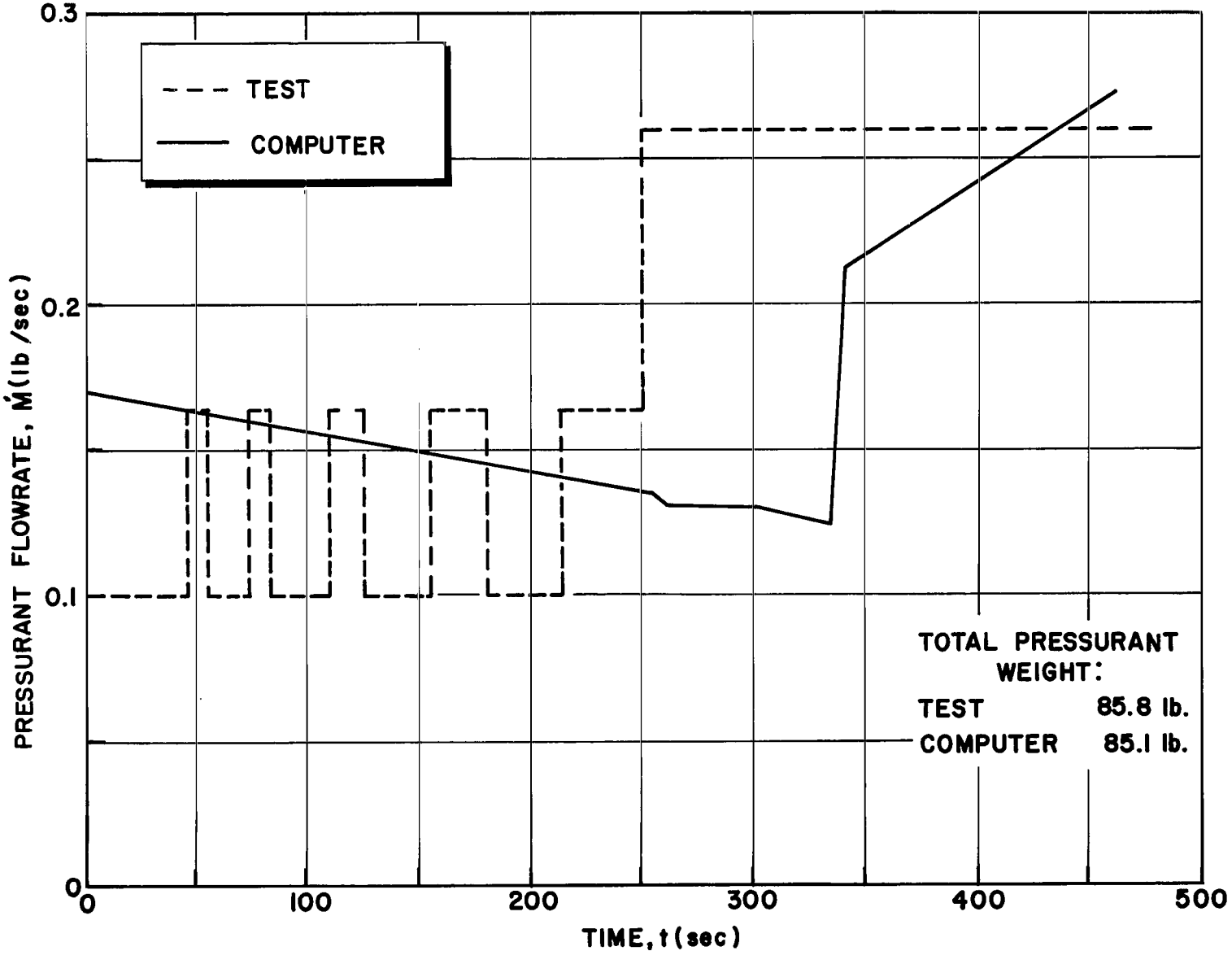

FIGURE 32a. COMPARISON BETWEEN EXPERIMENTAL AND COMPUTED PRESSURANT FLOWRATE, S-IV STAGE LH_2 TANK, HYDROGEN AS PRESSURANT

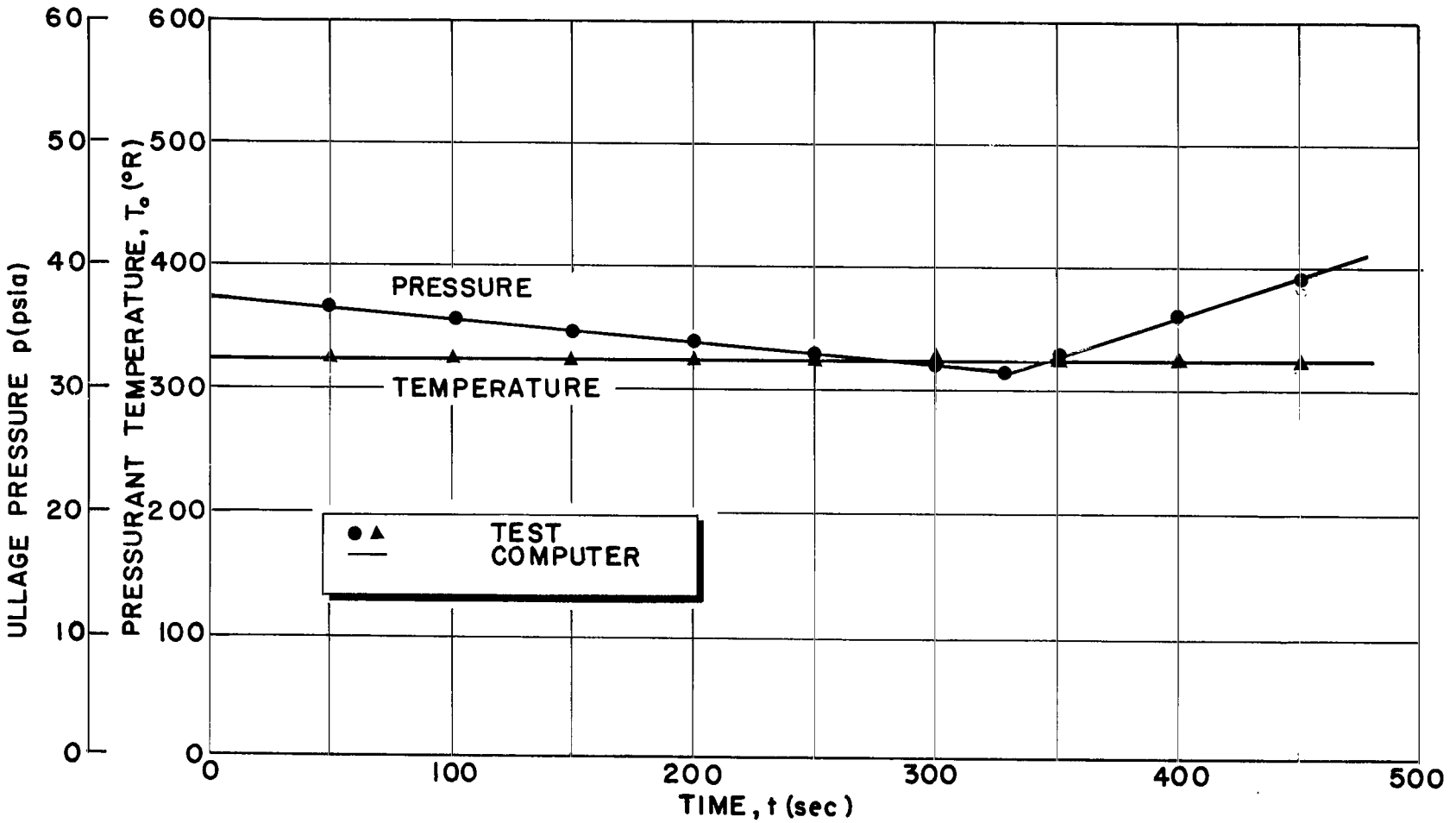

FIGURE 32b. ULLAGE PRESSURE AND PRESSURANT TEMPERATURE HISTORIES, S-IV STAGE LH_2 TANK, HYDROGEN AS PRESSURANT

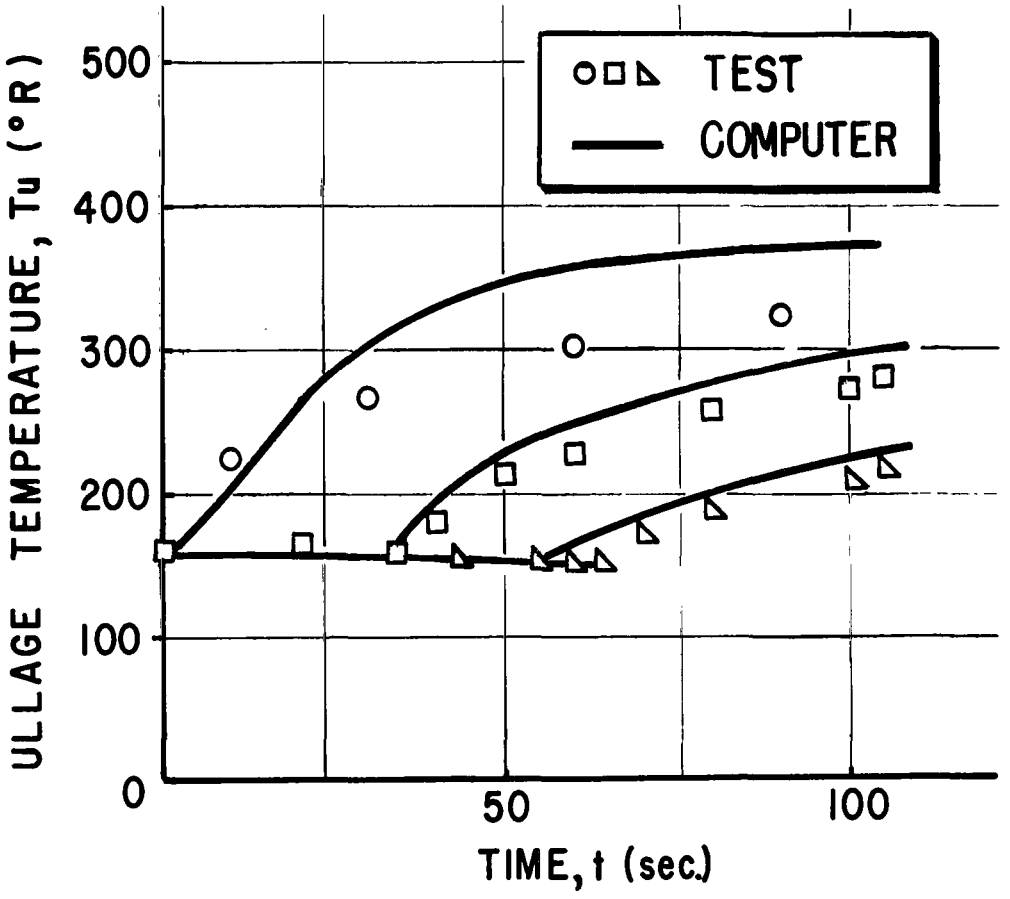

FIGURE 33. COMPARISON BETWEEN EXPERIMENTAL AND COMPUTED ULLAGE TEMPERATURE HISTORIES, TANK CONFIGURATION D, TEST 187260, NITROGEN AS PRESSURANT

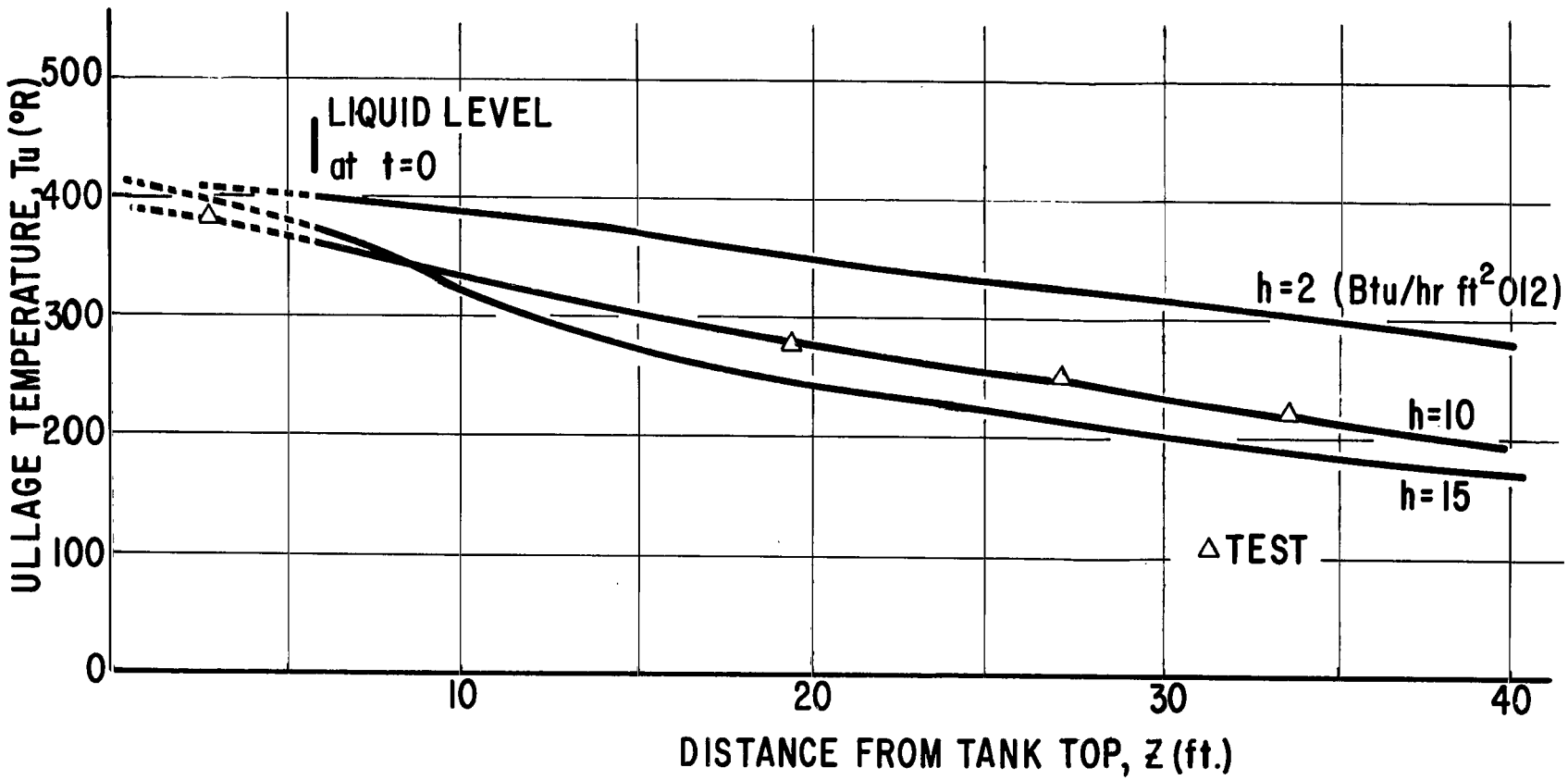

FIGURE 34. COMPARISON BETWEEN EXPERIMENTAL AND COMPUTED ULLAGE TEMPERATURE GRADIENT, TANK CONFIGURATION C, TEST 130-10, OXYGEN AS PRESSURANT

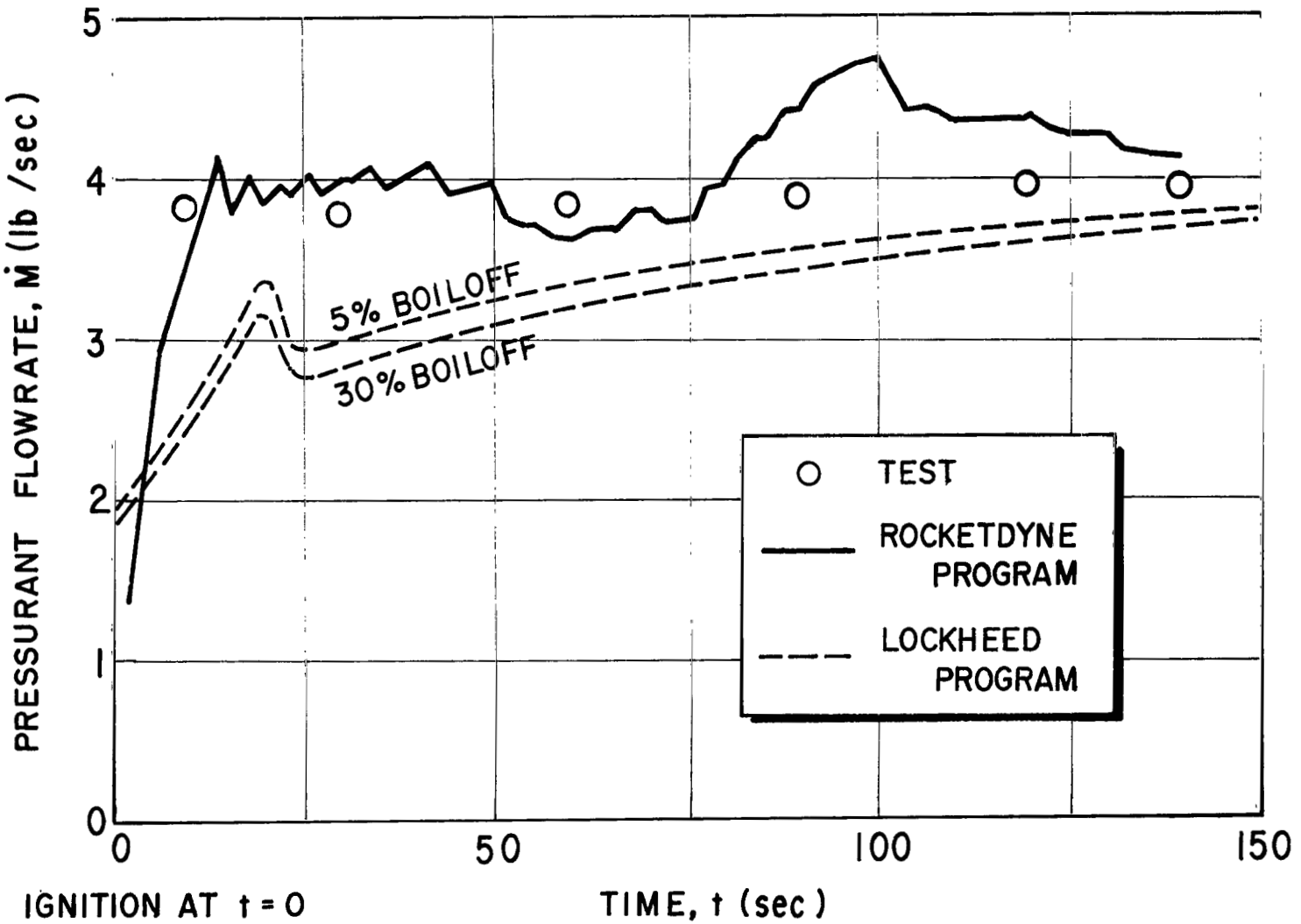

FIGURE 35. COMPARISON OF PRESSURANT FLOWRATE PREDICTIONS BY TWO COMPUTER PROGRAMS WITH EXPERIMENTAL RESULTS

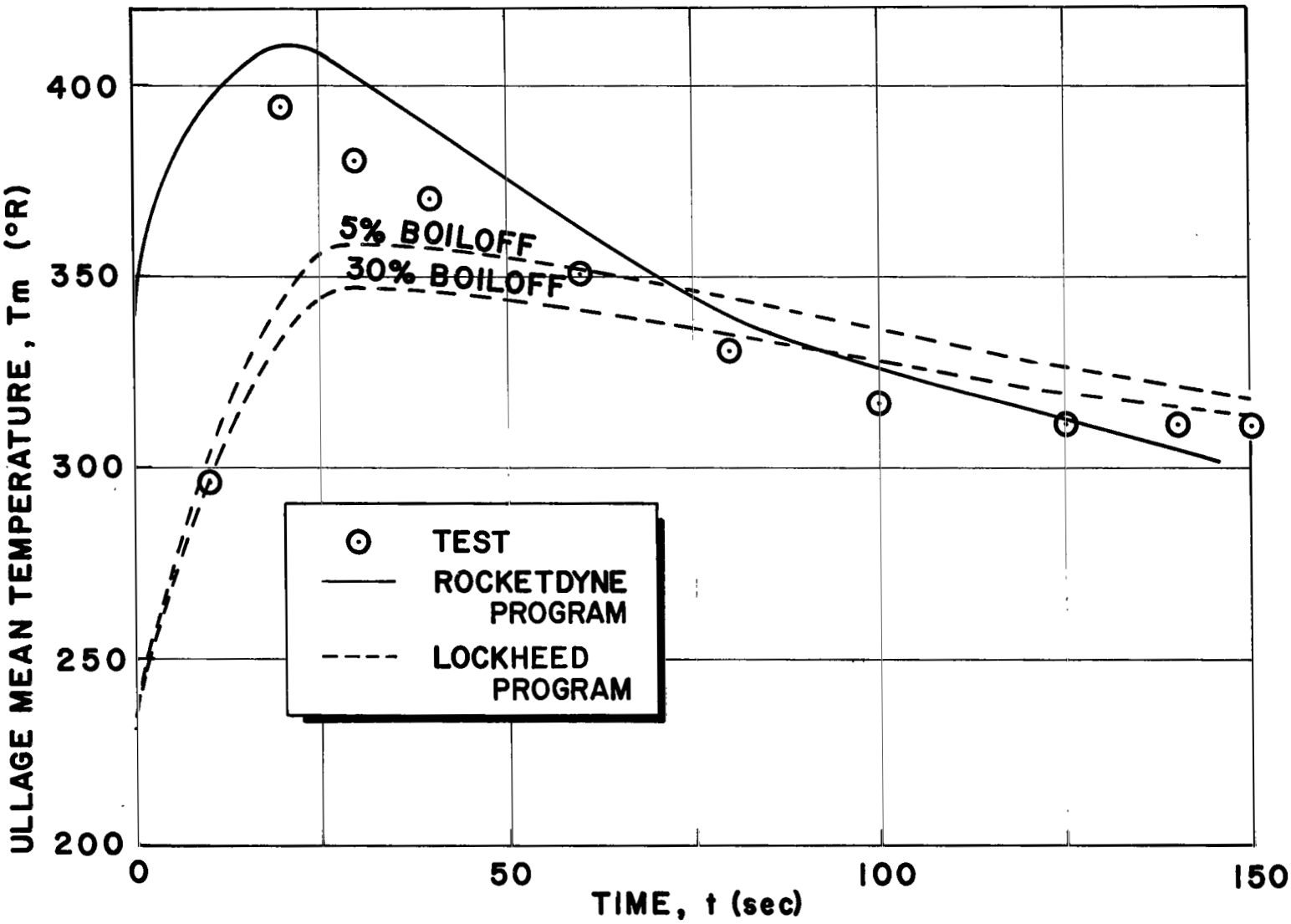

FIGURE 36. COMPARISON OF ULLAGE MEAN TEMPERATURE PREDICTION BY TWO COMPUTER PROGRAMS WITH EXPERIMENTAL RESULTS

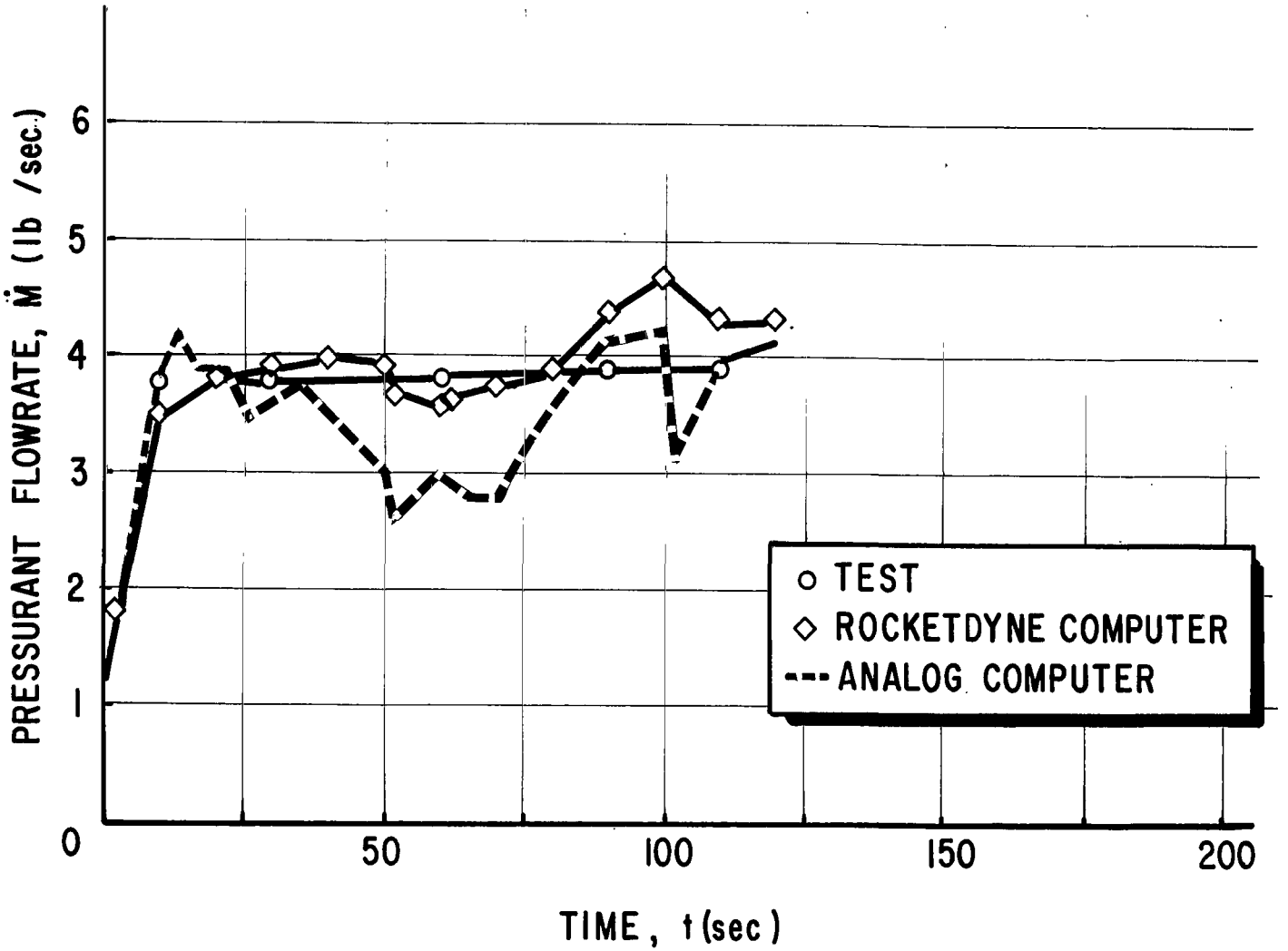

FIGURE 37. COMPARISON BETWEEN EXPERIMENTAL AND COMPUTED PRESSURANT FLOWRATE HISTORY, TANK CONFIGURATION C, TEST 130-6, OXYGEN AS PRESSURANT

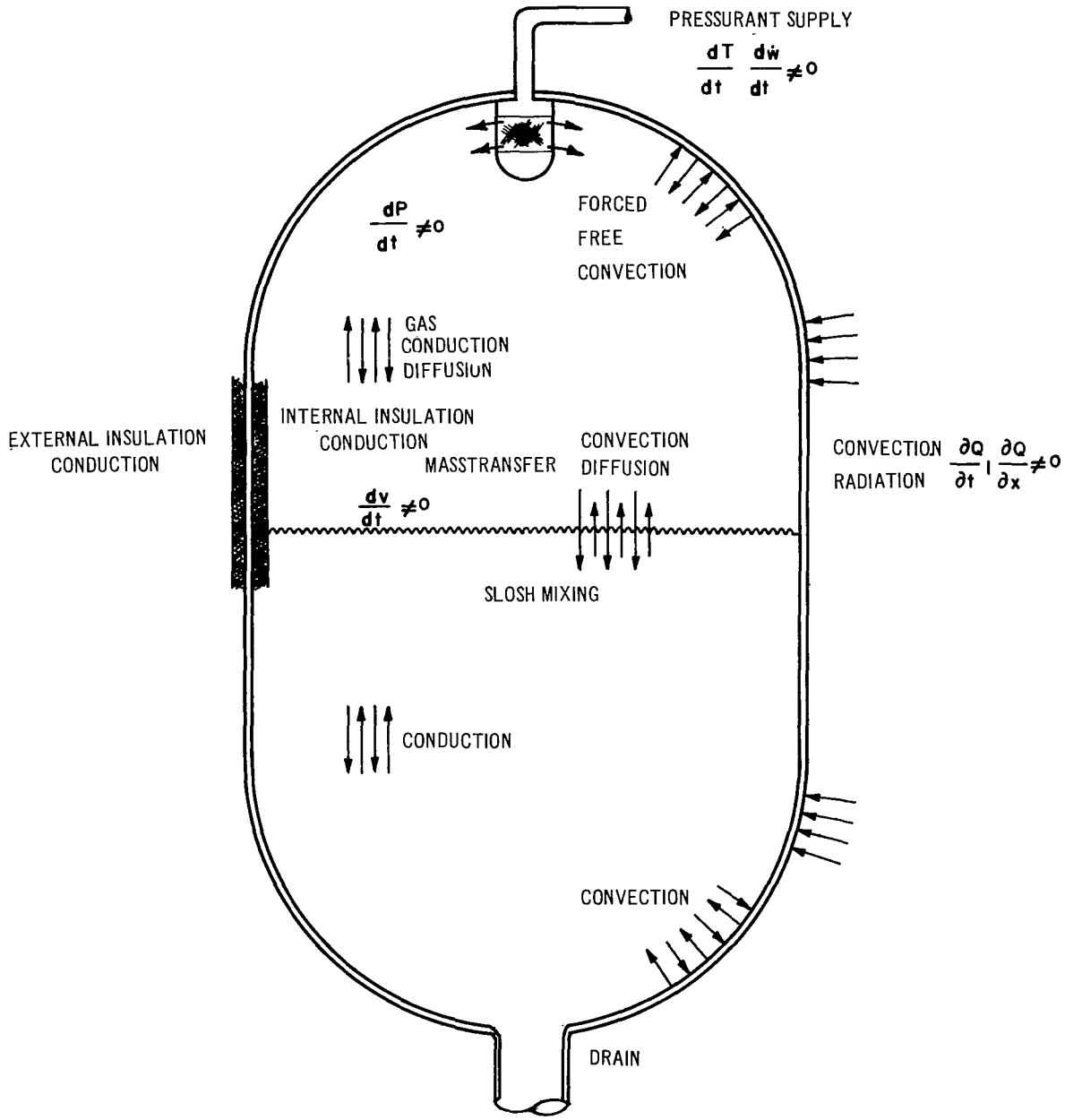

FIGURE 38. SCHEMATIC OF HEAT AND MASS TRANSFER CONDITIONS IN A PROPELLANT TANK

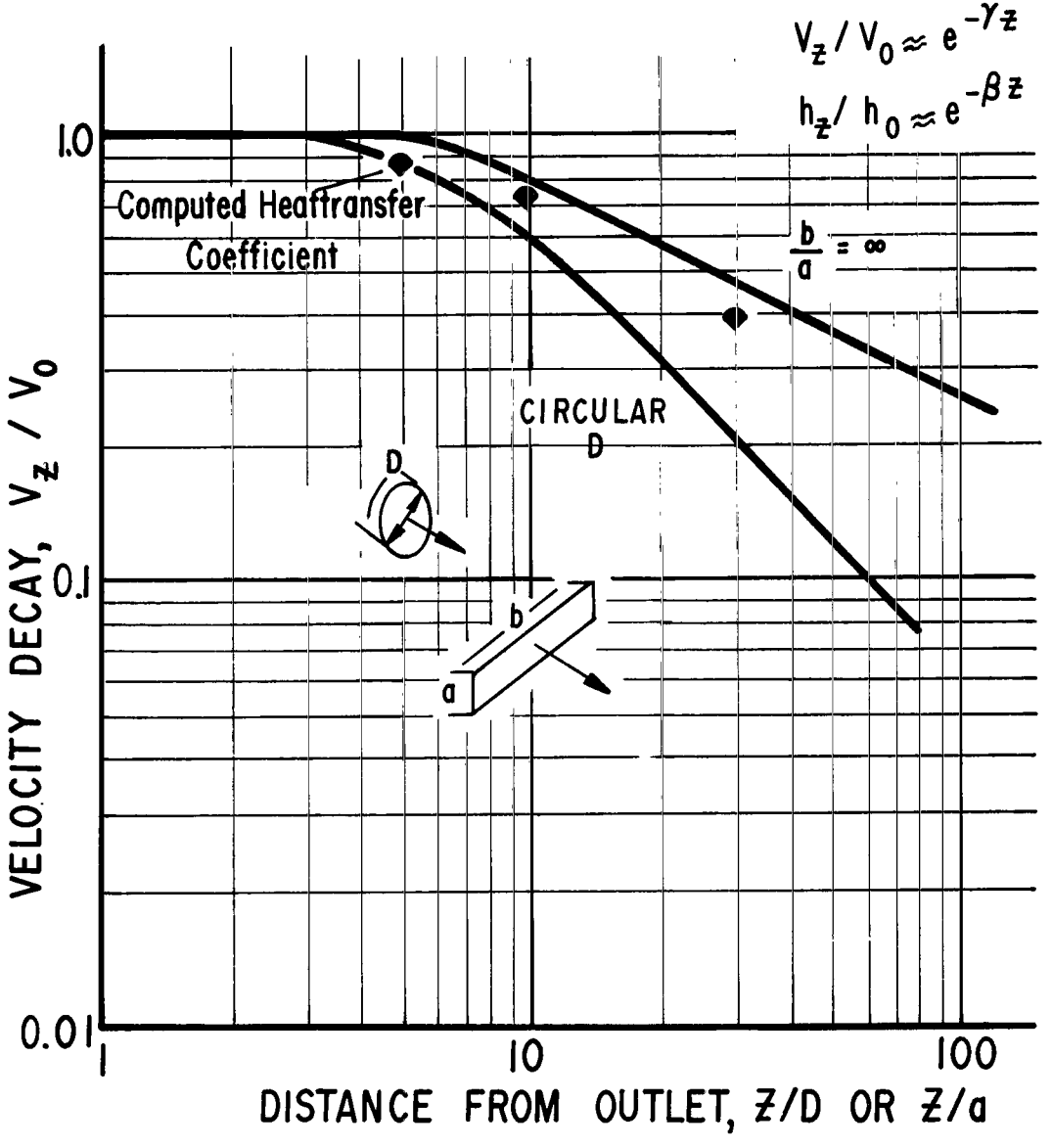

FIGURE 39. COMPARISON BETWEEN FREE JET VELOCITY DECAY AND FORCED HEAT TRANSFER COEFFICIENT DECAY

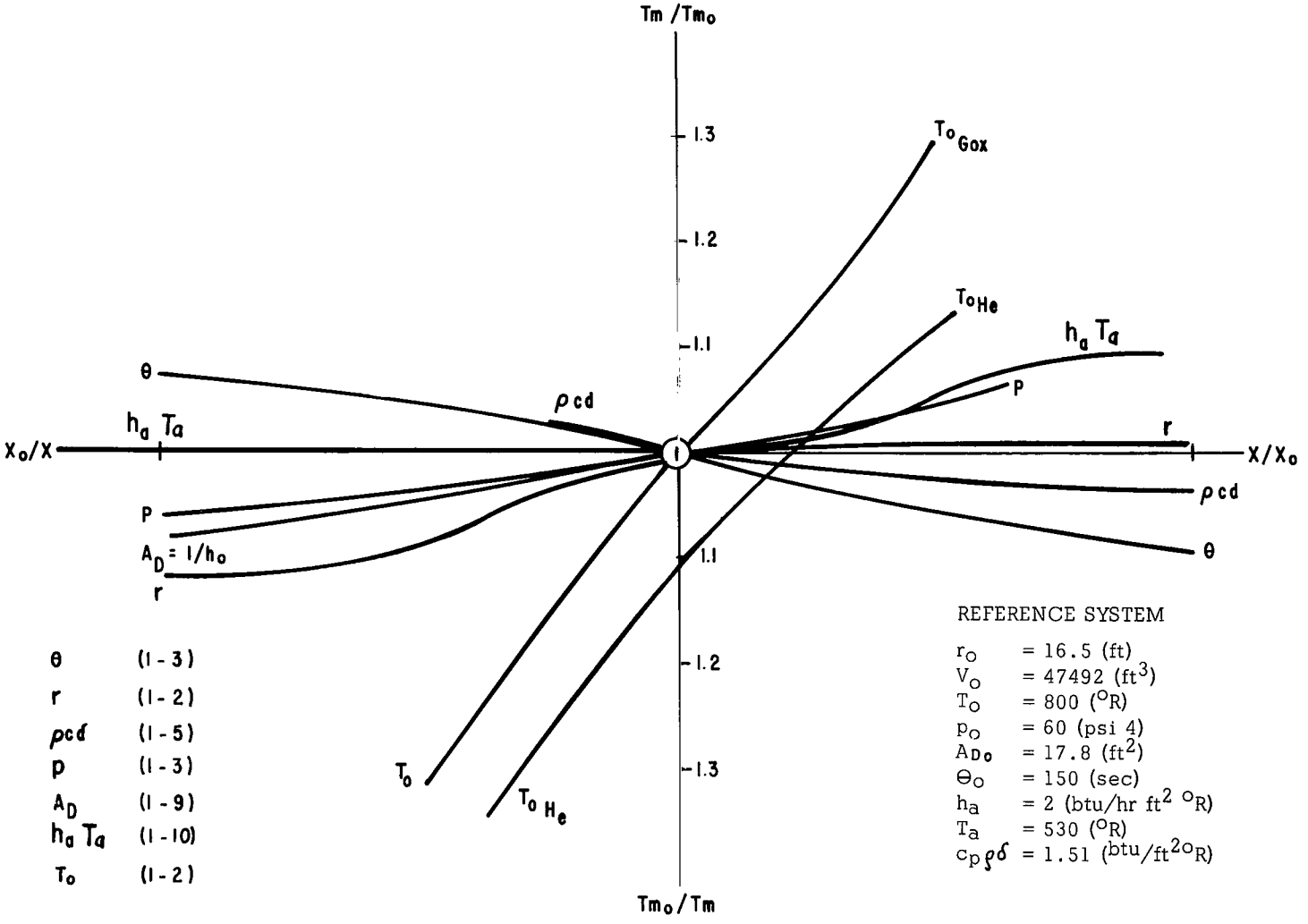

FIGURE 40. THE EFFECTS OF VARIOUS DESIGN PARAMETERS ON THE MEAN TEMPERATURE AT CUTOFF

REFERENCES

1. Clark, J. A. et al, Pressurization of Liquid Oxygen Containers, The University of Michigan under contract with the Department of the Army No. DA-20-018- or D-254, March 1961.

2. Coxe, E. and Tatum, John, Main Propellant Tank Pressurization System Study and Test Report, Lockheed-Georgia Company, Contract AF 04(611)6087.

3. Timmerhaus, K. D., Advances in Cryogenic Engineering, Volume 7 and Volume 8 (1962 and 1963).

4. Fortran Program for the Analysis of a Single Propellant Tank Pressurization System, Rocketdyne, Division of North American Aviation, Inc., R-3936-1, September 1963.

5. Platt, G. K., Nein, M. E., Vaniman, J., and Wood, C. C., Feedsystem Problems Associated with Cryogenic Propellant Engines, SAE National Aeronautical Meeting, Washington, D. C., 1963.

6. High Response Gas Temperature Probe for Pressurization Studies, NASA MSFC Memorandum R-P&VE-PTF-64-M-70, 1964.

7. Eckert, E. R. G., and Jackson, T. W., Analysis of Turbulent Free Convection Boundary.

8. Atmospheric Heat Transfer to Vertical Tanks Filled with Liquid Oxygen, A. D. Little, Inc., Special Report No. 50, Contract AF-04-(647)-130, November 1958.

9. Moses, J. L., and Nein, M. E., Evaluation of Propellant Sloshing on Pressurant Requirement for Large Scale Cryogenic Containers, presented at the 1962 Cryogenic Engineering Conference, Los Angeles, California.

10. Modification of Rocketdyne Tank Pressurization Computer Program, NASA MSFC Memorandum R-P&VE-PTF-64-M-83, 1964.

11. Liu, C. K., Sloshing and Pressure Decay in Pressurized Cryogenic Tanks of Launch Vehicles, NASA MSFC Internal Note MTP-P&VE-P-61-23, December 1961.

12. Schmidt, E., Experiments of Heat Transfer by Natural Convection, Chem. Ing. - Tech. 28/1956/No. 3, pages 175-180, October 1955.

13. MSFC Test Laboratory Reports CTL 2, 36, 34, 37, and CTL Flash Reports dated August 17, November 20, and December 11, 1962.

REFERENCES (Concluded)

14. SA-15 Static Test Report, Preliminary Summary Data, Confidential.

15. SA-5 Flight Data.

16. Results of Pressurization Tests on LN_2 Facility, NASA MSFC Memorandum R-P&VE-PE- M-526.

17. S-IV Stage Pressurization Data, NASA MSFC Memorandum R-P&VE-PTF-64-M-38, 1964.

18. Aerospace Applied Thermodynamic Manual, Society of Aeronautical Engineers, Section 2.

BIBLIOGRAPHY

J. E. Myers, C. O. Bennet: "Momentum, Heat and Mass Transfer," McGraw Hill, New York (1962).

R. B. Scott: "Cryogenic Engineering," D. Van Nostrand Company, Inc., Princeton (1959).

V. J. Johnson: "A Compendium of the Properties of Materials at Low Temperature (Phase I) Part I Properties of Fluids," National Bureau of Standards Cryogenic Laboratory (July 1960).

J. H. Hargis: "Thermophysical Properties of Oxygen and Hydrogen...." NASA MSFC Internal Note In R-P&VE-P-63-13 (October 1963).

"The aeronautical and space activities of the United States shall be conducted so as to contribute . . . to the expansion of human knowledge of phenomena in the atmosphere and space. The Administration shall provide for the widest practicable and appropriate dissemination of information concerning its activities and the results thereof."

—NATIONAL AERONAUTICS AND SPACE ACT OF 1958

NASA SCIENTIFIC AND TECHNICAL PUBLICATIONS

TECHNICAL REPORTS: Scientific and technical information considered important, complete, and a lasting contribution to existing knowledge.

TECHNICAL NOTES: Information less broad in scope but nevertheless of importance as a contribution to existing knowledge.

TECHNICAL MEMORANDUMS: Information receiving limited distribution because of preliminary data, security classification, or other reasons.

CONTRACTOR REPORTS: Technical information generated in connection with a NASA contract or grant and released under NASA auspices.

TECHNICAL TRANSLATIONS: Information published in a foreign language considered to merit NASA distribution in English.

TECHNICAL REPRINTS: Information derived from NASA activities and initially published in the form of journal articles.

SPECIAL PUBLICATIONS: Information derived from or of value to NASA activities but not necessarily reporting the results of individual NASA-programmed scientific efforts. Publications include conference proceedings, monographs, data compilations, handbooks, sourcebooks, and special bibliographies.

Details on the availability of these publications may be obtained from:

SCIENTIFIC AND TECHNICAL INFORMATION DIVISION

NATIONAL AERONAUTICS AND SPACE ADMINISTRATION

Washington, D.C. 20546